PHOTOCHEMICAL TREATMENT OF WASTEWATERS

Ardak Makhatova, Bachelor of Chemical Technology of Organic Compounds

Submitted in fulfillment of the requirements
for the degree of Masters of Science
in Chemical Engineering

School of Engineering
Department of Chemical Engineering
Nazarbayev University

53 Kabanbay Batyr Avenue,
Astana, Kazakhstan, 010000

Supervisors: Stavros G. Poulopoulos
Vassilis J. Inglezakis

December 2018

DECLARATION

I hereby, declare that this manuscript, entitled "*Photochemical treatment of wastewaters",* is the result of my own work except for quotations and citations which have been duly acknowledged.

I also declare that, to the best of my knowledge and belief, it has not been previously or concurrently submitted, in whole or in part, for any other degree or diploma at Nazarbayev University or any other national or international institution.

Name: Ardak Makhatova

Date: 13.12.2018

Abstract

In the present work, chemical/photochemical processes, specifically, Fenton and Fenton-like reactions were employed to treat a leachate from the municipal solid waste landfill of Astana (Kazakhstan). Each experiment lasted 120 minutes, and the treatment efficiency was assessed through total organic carbon (TOC), total inorganic carbon (TIC), total nitrogen (TN) and colour removal. An annular UV (254 nm) photoreactor operated in a batch recycle mode was used. The total volume of the solution was 250 mL, and the irradiated volume in the photoreactor was 56.8 mL. The effect of inorganic carbon, pH, initial H_2O_2 amount (0-9990 mg L^{-1}), Fe(II) (200-600 ppm) and Fe(III) (300-700 ppm) concentrations on total carbon and colour removal was studied. The landfill leachate had initial carbon concentration equal to 5868 mg L^{-1} and pH 8.16. The total carbon was by 40-45% inorganic, and nitrogen was 90% inorganic in the ammonium form. Preliminary experiments showed that inorganic carbon acting as hydroxyl radicals scavenger inhibited significantly the photo-Fenton treatment. Without the pretreatment steps only 7.7% TC removal was observed, while 29% TC (equal to TOC) removal was achieved when the inorganic carbon was removed at the pretreatment steps. Therefore, pretreatment process in two steps was applied: continuous air stripping for 24 hours at pH = 12 to remove ammonia and then pH adjustment to 5 to remove inorganic carbon. The pretreated leachate was further diluted with tap water in a ratio of 1/2.4 and sent for

chemical/photochemical treatment. The leachate used as feed to next processes had initial carbon concentration in the range of 1100-1300 mg L^{-1} (all carbon was organic) and pH 5.1-5.3. It was found that the most favourable concentrations of H_2O_2 and Fe(II) for carbon removal were 6660 mg L^{-1} and 400 ppm, respectively, while ammonia was not affected. The initial pH value was ranged in 2.2-5.3 and had also a considerable effect on total organic carbon and color removal. Specifically, the highest TOC removal (44.3%) was achieved when initial pH was adjusted at 3.01. Using classical Fenton process instead of photo-Fenton process led to TC removal around only 21%. Finally, the use of Fe(III) instead of Fe(II) was beneficial in terms of TOC and color removal achieved.

The second part of current work was devoted to the study of the photocatalytic efficiency of the synthesized Fe-doped TiO_2 catalysts with different iron contents (Fe/Ti weight ratio percentage = 0.5%, 1%, 2% and 4%). 4-tert-butylphenol was used as a target pollutant. The effectiveness of the catalysts was compared with TiO_2 catalyst (P-25). The work was also expanded by mineralization of 4-tert-butylphenol using UV/H_2O_2/catalyst process. The catalysts were characterized via ultraviolet-visible spectrophotometry (UV-Vis), scanning electron microscopy (SEM), X-ray powder diffraction (XRD) analyses, while their photocatalytic activities were attended via pH, TC, high-performance liquid chromatography (HPLC), UV-Vis, atomic absorption spectroscopy (AAS), ion chromatography (IC). Fe-doped TiO_2 catalyst with 4% Fe concentration demonstrated the highest photocatalytic efficiency.

Acknowledgements

I would like to express special thanks to my supervisor Professor Stavros G Poulopoulos for his support and guidance during this research and the entire master's program. Secondly, I would like to thank my co-supervisor, Professor Vassilis J Inglezakis, for all the advice and feedback during my work.

Finally, I would like to express my gratitude to Professor Timur Atabaev and his students from School of Science and Technology of our university for synthesizing Fe-doped TiO_2 catalysts for my experiments and helping in analyzing them.

Table of Contents

List of Abbreviations & Symbols

TC	Total carbon
TIC	Total inorganic carbon
TN	Total nitrogen
UV	Ultraviolet
AAS	Atomic absorption spectroscopy
SEM	Scanning electron microscope
XRD	X-ray powder diffraction
FT-IR	Fourier-transform infrared spectroscopy
IC	Ion chromatography
HPLC	High-performance liquid chromatography
EDS	Energy dispersive X-ray spectrometry
MSW	Municipal solid wastes
HSG	Hydrolytic sol-gel
NSG	Nonhydrolytic sol-gel
CEPT	Chemically enhanced primary treatment
TSS	Total suspended solids
BOD	Biochemical oxygen demand
COD	chemical oxygen demand
AOP	Advanced Oxidation Processes
POPs	Persistent Organic Pollutants
EDCs	Endocrine disrupting compounds
NOAEL	No-observed-adverse-effect-level
LD_{50}	Lethal Dose, 50%
ppm	Parts per million
ppb	Parts per billion
GCMS	Gas chromatography mass spectroscopy

List of Figures

List of Tables

Chapter 1 - Introduction

1.1 An overview of master thesis

Since water is the fundamental compound required for live, its quality is crucial for the welfare and existence of an individual human being and the society as a whole. Besides inventors, engineers and economists, many others show their interest in the study of issues related to water and its treatment due to the necessity of water in our life. The growth of world's population and water pollution by urban, agricultural, and industrial garbage have led to a decrease in water purity. As a result, water sources need some kind of treatment before using.

Progress in the processes of oxidative degradation of organic substances dissolved in water using catalytic and photochemical methods has been prompted by the latest evolution in the field of chemical water treatment. These methods are known as "advanced oxidation processes" (AOPs).

The efficiency of AOPs depends on the generation of reactive free radicals, such as hydroxyl radicals (•OH), which are the most common choice as they are highly reactive. The hydroxyl radicals for the AOPs can be obtained from the various photochemical technologies, such as photo-Fenton, UV light/H_2O_2, UV light/O_3, UV light/H_2O_2/O_3, UV light/TiO_2 and others. The application of AOPs to the real wastewater treatment has fascinated many researchers. AOPs have been applied for the treatment of the groundwater and water from sulphide fields, chemical, food, textile, pharmaceutical, paper and other manufacturing areas.

1.2 Thesis aims and structure

The main objective of the thesis is to study the degradation of organic contaminants in the landfill leachate using photo-Fenton and photo-Fenton-like processes. Landfill leachate is a highly concentrated wastewater produced in solid waste landfills. Untreated leachates can pollute soil, ground, and surface waters with various toxic organic compounds, inorganic salts, ammonia and heavy metals. The treatment efficiency of applied processes will be checked by total carbon and color removal. This work aims to test several series of experiments varying different parameters in order to determine the most favorable conditions for the decomposition of organic pollutants in the leachate.

The second part of this thesis is devoted to the study of the photocatalytic efficiency of Fe-doped TiO_2 catalysts with different concentrations of doping iron (Fe/Ti weight ratio = 0.5%, 1%, 2%, and 4%). 4-tert-butylphenol is used as a target pollutant. The effectiveness of the catalysts is compared with the commercial catalyst Degussa P-25. A combination of catalyst and hydrogen peroxide under ultraviolet light will also be studied.

The current thesis consists of five chapters, which are: 1) an introduction, 2) a literature review, 3) materials and methodology of the conducted experiments, 4) the obtained results and their discussion, 5) conclusion of the work presented in this thesis.

Chapter 2 - Literature review

This literature review focuses on wastewater treatment technologies, in particular, photochemical and photocatalytic methods, indicating their benefits and limitations.

2.1 Pollutants in wastewater

Wastewater can be characterized as a mixture of unwanted components, or "pollutants," in water [1]. Currently, wastewater management problems arise due to the extensive industrialization and increase in urbanized societies and population. Various substances contained in wastewater are toxic to plants, animals and people, and impact negatively on the environment [2]. The main pollutants in wastewater, which are organic substances, nutrients (nitrogen and phosphorus), hydrocarbons, heavy metals, and microbes, affect adversely both human health and the environment [3]. Organic waste can be carbohydrates, proteins or fats, and most organics in wastewater come from animals, plants or synthetic sources [2]. The main forms of nitrogen in wastewater are ammonia (NH_4^+ or NH_3), organic nitrogen, nitrate (NO_3^-) and nitrite (NO_2^-) [4], phosphorus is in the form of a soluble orthophosphate ion (PO_4^{3-}), organically-bound phosphate or other forms of phosphorus/oxygen. Ammonia in excess concentration is toxic to aquatic organisms [2]. Despite the fact that oil is one of the most important energy resources and raw materials of the chemical industry, an oil spill can lead to serious environmental issues and threaten fisheries, marine

life and human health [5]. Heavy metals in trace amounts, such as zinc, copper and iron, are important for the aquatic environment due to their role in several biochemical processes, however, they become harmful in high concentrations [6].

The proper treatment of wastewater is important for protecting both the environment and human health.

2.2 Conventional methods and stages of wastewater treatment

Conventional methods, which are physical, biological, chemical processes, or sometimes a combination of these processes, can be used to remove contaminants from wastewater. The main objective of wastewater remediation is the removal of organic compounds, solids, and nutrients from wastewater [7].

Chemical procedures of water treatment are those that include chemical oxidation or reduction, chemical precipitation, and other chemical reactions, which include the exchange of electrons between atoms. Stripping, sedimentation, flotation, adsorption, filtration, and other processes that remove dissolved and undissolved substances without the need to change their chemical structures are physical processing methods. The use of living organisms and organic, or in some cases, inorganic, matter as food, which totally changes the physical and chemical characteristics of the substances, represents a biological method of water treatment [8].

A more suitable water treatment process for each specific case can be used based on the basic properties of the contaminants. For example, the technology of

physical treatment works well when the basic properties of the removed substances (dissolved inorganic cations and anions) are taken as a basis [8].

Depending on the degree of treatment in order of increasing the level of treatment, the following steps of wastewater remediation can be distinguished, such as preliminary, primary, secondary and tertiary wastewater treatment [9]. The preliminary treatment removes coarse solids and other large substances that are often found in untreated effluent [9]. Primary treatment removes organic and inorganic solids through physical sedimentation and flotation processes. During primary processing, 65% oil and fat, 50-70% of the total suspended solids (SS) and about 25-50% of the biochemical oxygen demand (BOD) are removed. During primary sedimentation, part of the organic phosphorus and nitrogen, and heavy metals related with solids are also removed, but the colloidal and dissolved components are not removed [9]. The precipitation increased by adding of chemicals is called chemically enhanced primary treatment (CEPT). Coagulation of particles occurs when adding chemicals. As a result, an increase in particle size increases the sedimentation efficiency [10].

Secondary treatment process removes residual organic matter, suspended solids after primary treatment, and consists of biological wastewater treatment using microorganisms in a controlled environment [9]. Secondary treatment removes more than 85% of both total solids and BOD [11]. Solids are removed in approximately the following ratio: 30% suspended, 65% dissolved and 6% colloidal solids [9].

Tertiary methods, which are granular and membrane filtration, chemical precipitation, and carbon adsorption [10], are used when it is necessary to decrease the amount of dissolved phosphate and nitrate or to remove more than 85% of the total solids and BOD [11]. More than 99% of all contaminants from wastewater can be removed with tertiary treatment, thereby producing water with a quality similar to drinking water. Tertiary treatment is used only under special cases, as it is expensive, doubling the secondary treatment cost [11].

Wastewater may have organic compounds that are resistant to conventional treatment methods, therefore, these methods are considered inefficient to achieve full mineralization of pollutants [7].

2.3 Advanced Oxidation Processes

Advanced Oxidation Process (AOP) is a chemical treatment method, which is highly recommended for the removal of problematic organic compounds [7].

The efficiency of AOPs depends on the generation of reactive free radicals [12], which are atoms or molecules capable of independent existence and possessing one or several unpaired electrons [13]. Hydroxyl radical plays a central role in AOP for effluent treatment among a number of radicals [14].

The hydroxyl radical •OH has sufficient characteristics to attack almost all organic compounds and reacts 106-1012 times faster than the other oxidizing agents, such as ozone [15].

The hydroxyl radical has the second largest thermodynamic potential of oxidation after fluorine, as shown in *Table 2.1* [16].

Table 2.1: The redox potential of oxidants [16]

Oxidant	Redox potential, V vs NHE
F_2	3.03
HO•	2.80
O•	2.42
O_3	2.07
HO_2•	1.70
H_2O_2	1.78
HOCl	1.49
Cl_2	1.36

The hydroxyl radical is an powerful oxidizing agent and a highly reactive, non-selective reagent, which is easy to obtain (*Figure 2.1*) [17].

Figure 2.1: Characteristics of the hydroxyl radical [17]

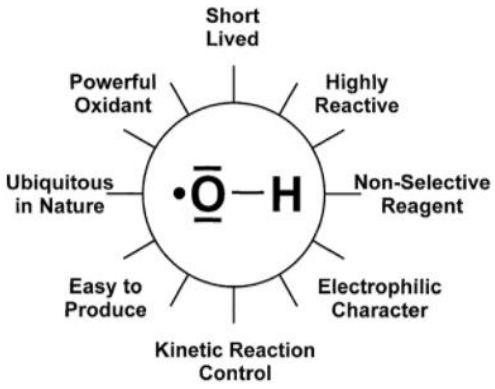

AOPs reduce the concentration of a contaminant from a few hundred ppm to less than 5 ppb, since an attack by the hydroxyl radical results in the complete destruction of the organic substances [18].

Equation 2.1 is the oxidation process by •OH radical of organic matter (R-H) by removing protons. Organic radicals (•R), which are highly reactive, are produced and can be further oxidized [19].

$$R - H + HO^{\bullet} \rightarrow H_2O + R^{\bullet} \rightarrow further\ oxidation \qquad (2.1)$$

2.3.1 Classification of AOPs

The hydroxyl radicals can be obtained by several methods, which include:

- Non-photochemical methods that do not use light energy: ozonation at elevated pH (>8.5), O_3/H_2O_2, O_3/catalyst, and Fenton system (H_2O_2/Fe^{2+});
- Photochemical methods: H_2O_2/UV, O_3/UV, O_3/H_2O_2/UV, photo-Fenton/Fenton-like systems, and photocatalytic oxidation [18].

In many cases the classical oxidation by ozone or hydrogen peroxide does not completely mineralize organics to carbon dioxide and water [20], although it is theoretically assumed that it should occur using AOP [21]. Sometimes the oxidation intermediates remaining in the solution may be as toxic as or even more toxic than the parent compound [18].

In recent decades, photochemical methods of water treatment have been developed. The most obvious goal of photochemical process is to achieve water quality standards that do not affect the human health, environment, and comply with government regulations [17].

Photochemical processes contain chemical reactions that occur when exposed to either UV-Vis radiation, or the Sun or another source, and the reaction kinetics can be enhanced by adding H_2O_2, O_3, semiconductor or metal salts [22].

Sandip Sharma et al. [15] claim that the photochemical technologies grant the following benefits for the water and wastewater treatment:

- An increase of the reaction rate in contrast to the similar method without the light;

- Prevention of extreme pH modification;
- Allowing the application of diversity of oxidants;
- Creation of useful additions to the organoleptic qualities of purified water.

The design of the reactor (geometry, lamp type, UV lamp power, emission spectrum of UV lamp, turbulence, hydrodynamics, etc.) and physicochemical properties of the medium, such as pH, turbidity, transmission of UV radiations, can drastically change the rate of production of free radicals and productivity of photochemical process [15,23].

There are several drawbacks associated with the use of photochemical AOPs: high initial capital costs compared to other technologies, and the need to pretreat the wastewater to improve its optical properties. The lamps (or quartz sleeves containing the lamps) can foul significantly by formation of ultraviolet absorbing films, which leads to a sharp decrease in the intensity of the UV irradiation that the medium receives. Therefore, there are additional costs due to the need to periodically replace the UV lamps. Nevertheless, the high cost of energy sources, such as ultraviolet light, or reagents (ozone and hydrogen peroxide) is the major issue of photochemical AOPs, limiting their industrial use [17].

2.3.2 Photolysis of hydrogen peroxide (H_2O_2/UV)

UV/H_2O_2 is an alternative way to destroy toxic organic substances, since this process can occur in nature itself [24].

Photolytic dissociation of H_2O_2 in water by ultraviolet irradiation at a wavelength of 254 nm leads to the formation of hydroxyl radicals [7]. The following reactions describe the UV/H_2O_2 process [25]:

$$H_2O_2 + h\nu \rightarrow 2HO^{\bullet} \quad (2.2)$$

$$H_2O_2 + HO^{\bullet} \rightarrow HO_2^{\bullet} + H_2O \quad (2.3)$$

$$H_2O_2 + HO_2^{\bullet} \rightarrow HO^{\bullet} + H_2O + O_2 \quad (2.4)$$

$$2HO^{\bullet} \rightarrow H_2O_2 \quad (2.5)$$

$$2HO_2^{\bullet} \rightarrow H_2O_2 + O_2 \quad (2.6)$$

$$HO^{\bullet} + HO_2^{\bullet} \rightarrow H_2O + O_2 \quad (2.7)$$

According to Stasinakis A.S. [26], the rate limiting reaction is described by *Equation 2.2*. Theoretically, in the process of UV/H_2O_2, a higher initial concentration of hydrogen peroxide leads to a higher concentration of hydroxyl radicals (*Equation 2.2*), therefore, more of the target compound decomposes. However, there is a limiting concentration of hydrogen peroxide, since an overdose of H_2O_2 will lead to a reaction with •OH radical and the formation of the perhydroxyl radical HO_2•, which is the undesired product (*Equation 2.3*) [26].

The initial concentration of H_2O_2, the pH of the wastewater, the presence of bicarbonate and the reaction time are factors that mainly influence UV/H_2O_2 process [26]. Andreozzi et al. [27] revealed that the photolysis rate of aqueous H_2O_2 is pH dependent and increases in alkaline medium at pH > 10. This can be explained by the fact that the HO_2-anion, which is a result of the ionization of H_2O_2, can absorb UV radiation and produce free radicals (HO_2• and •OH) [28].

UV/H_2O_2 process has some disadvantages. Hydrogen peroxide weakly absorbs UV radiation, thus it can be considered that most of the light input is used unreasonably. The bromate formation for this system can interfere with the process, but a decrease in pH and an increase in the peroxide to ozone ratio can decrease this problem [7].

The decomposition of pollutants can be accelerated by adding H_2O_2 to UV/O_3 process due to an increase in the rate of formation of •OH radicals [29]. Kusic et al. [29] conducted a comparative study of the processes of UV, UV/O_3, UV/H_2O_2 and UV/ H_2O_2/O_3 for the degradation of organic contaminants, and found that the $UV/H_2O_2/O_3$ process has the highest degree of mineralization. The degree of removal obtained after a 1-hour treatment of the organic dye C.I. Reactive Red 45 was in the following order: UV < UV/H_2O_2 < UV/O_3 < UV/ H_2O_2/O_3 [29].

2.3.3 Fenton's Reagent, Fenton-like and photo-Fenton processes

The Fenton method is the oldest and most used chemical AOP, in which the Fenton's reagent that is a mixture of a soluble iron(II) salt (catalyst) and hydrogen peroxide (oxidant) is used to destroy Persistent Organic Pollutants (POPs) [27,30].

Fenton reaction is considered as convenient and economical process [31]. The production of the hydroxyl radical is a key step in the conventional or free radical Fenton chain reaction. The conventional Fenton mechanism in the absence of organic substances involves the following reactions [32]:

$$Fe^{2+} + H_2O_2 \rightarrow Fe^{3+} + OH^{\bullet} + OH^{-} \quad (2.8)$$

$$Fe^{3+} + H_2O_2 \rightarrow Fe^{2+} + HO_2^{\bullet} + H^{+} \quad (2.9)$$

$$OH^{\bullet} + H_2O_2 \rightarrow HO_2^{\bullet} + H_2O \quad (2.10)$$

$$OH^{\bullet} + Fe^{2+} \rightarrow Fe^{3+} + OH^{-} \quad (2.11)$$

$$Fe^{3+} + HO_2^{\bullet} \rightarrow Fe^{2+} + O_2H^{+} \quad (2.12)$$

$$Fe^{2+} + HO_2^{\bullet} + H^{+} \rightarrow Fe^{3+} + H_2O_2 \quad (2.13)$$

$$2HO_2^{\bullet} \rightarrow H_2O_2 + O_2 \quad (2.14)$$

The reaction (*2.8*) occurs in acidic conditions. A small amount of ferrous ions (Fe^{2+}) is needed, as this ion is regenerated from *Equation 2.9* between ferric ions (Fe^{3+}) and hydrogen peroxide, which is called Fenton-like reaction [33]. The rate of Fenton-like reaction (*Equation 2.9*) is much slower than the Fenton's reaction (*Equation 2.8*) [34], and this could be due to the lower reactivity of Fe^{3+} towards H_2O_2 [35].

The effectiveness of the Fenton's reagent is highly dependent on pH, temperature, hydrogen peroxide and catalyst concentrations that control the regeneration ability of Fe^{2+} from Fe^{3+} formed in the process and the oxidation rate of organic substances by produced •OH [28]. The most favorable pH values for Fenton reactions are 2.80-3.20 [36]. The ferrous ions are unstable and can be transformed to ferric ions, forming complexes with hydroxyl, at pH above 4. Additionally, H_2O_2 loses its oxidizing ability under alkaline conditions due to its decomposition to oxygen and water [37]. Therefore, the pH regulation of wastewater is usually required prior to treatment with Fenton processes.

Neyens and Baeyens [19] investigated the relation between the reaction temperature and the H_2O_2 concentration at pH 3. A high concentration of hydrogen peroxide and a long reaction time at low temperatures (<40 °C) were needed to achieve a satisfactory sludge dewaterability, while at a reaction temperature of 80–90 °C, very low hydrogen peroxide concentrations were required for satisfactory sludge dewaterability.

Phosphate, sulfate, bromide, chloride and fluoride ions inhibit the Fenton oxidation of organic matter. This inhibition may be associated with iron deposition, scavenging of HO•, or formation of a less reactive complex from dissolved Fe(III) [31].

The Fenton process has the following benefits for water/wastewater treatment [38]:

- No need for power supply;
- Easy-to-use and inexpensive chemicals;
- A simple and flexible operation that can be easily implemented in existing plants.

The following negatives of the Fenton process can be noted [30]:

- Significant amounts of chemicals are required to acidify wastewater at pH 2-4 before the treatment and/or to neutralize the treated solutions before the disposal;
- Iron sludge accumulates and must be removed at the end of the treatment;

- Relatively high costs and risks because of the H_2O_2 transportation and storage;
- Total mineralization is impossible due to the formation of Fe(III)-carboxylic acid complexes, which cannot be effectively destroyed by using the bulk •OH.

Some actions may be taken to minimize these drawbacks. For example, the amount of added H_2O_2 can be reduced by optimizing its concentration. Solid iron-containing catalysts, such as iron-modified clays, zeolites, iron oxides, mesoporous molecular sieves, alumina, ion-exchange resins, or iron-exchanged Nafion membranes, easily separated from the treated solutions, can be used to prevent iron sludge [31]. Iron hydroxide is found as a by-product in the iron sludge [39]. The sludge disposal should be included in the valuation of this process. Chemical coagulation was found to be an effective method for removing COD, as well as flocs [40], which were discovered during a number of studies [39].

The classical Fenton reaction (*Equation 2.8*) under UV irradiation is called photo-Fenton process (*Equation 2.15*), which enhances the catalytic reduction of Fe^{3+} into Fe^{2+} in H_2O_2 aqueous solutions, thereby increasing the generation of •OH radicals:

$$Fe^{3+} + H_2O + h\nu \rightarrow Fe^{2+} + H^+ + OH^{\bullet} \quad (2.15)$$

The predominant form of Fe^{3+} at pH 2.8–3.5 is the $[Fe(OH)]^{2+}$ ion, which is of great importance for the photo-Fenton process [31]. Specifically, the large accumulation of Fe^{3+} species in the classical Fenton reaction (*Equation 2.8*) slows

down the treatment efficiency. This disadvantage is eliminated in the photo-Fenton process, as the reductive photolysis of $[Fe(OH)]^{2+}$ (*Equation 2.16*) regenerates the Fe^{2+} ions that catalyze the Fenton reaction (*Equation 2.8*) and provide additional •OH radicals [41]:

$$Fe(OH)^{2+} + h\nu \rightarrow Fe^{2+} + OH^{\bullet} \quad (2.16)$$

Ultraviolet irradiation in the photo-Fenton process can directly decompose H_2O_2 molecules into hydroxyl radicals, as in the H_2O_2/UV process (*Equation 2.2*) [28].

Several UV regions can be used by the photo-Fenton process as a source of light energy, specifically UVA (λ = 315–400 nm), UVB (λ = 285–315 nm), and UVC (λ < 285 nm). The intensity and wavelength of UV radiation significantly affect the rate of degradation of organic contaminants. The disadvantage of the photo-Fenton process is a cost of using UV light [28]. An alternative method is to use sunlight (λ > 300 nm) as a free and renewable source of energy in the so-called solar photo-Fenton process [42].

Various AOPs have been shown as possible technologies for treating real wastewaters. Bandala et al. [43] applied the photo-Fenton process to colored real wastewater, and the results demonstrated that COD concentrations could be reduced by 62.6%. The solar photo-Fenton process was used by Sirtori et al. [44] as a final stage for biological treatment of a pharmaceutical wastewater. The complete degradation of nalidixic acid and the reduction of toxicity were found,

which confirms the benefit of using the photo-Fenton process for complete biological treatment.

Moraes et al. [45] studied the application of photo-Fenton process for the removal of hydrocarbons from saline wastewater. It was observed that the initial concentration of Fe^{2+} and salinity significantly affect the degradation process, whereas the effect of hydrogen peroxide concentration was insignificant. The removal of hydrocarbons was higher than 81% in all experimental conditions.

The classical photo-Fenton process was also applied for the treatment of landfill leachates [46–48]. Primo et al. [46] studied several oxidation processes and their efficiency of removing organic substances in the treatment of landfill leachates and recommended using the photo-Fenton process as the most effective AOP, since it was noted that the removal efficiency decreased in the following sequence: photo-Fenton > Fenton-like > Fenton > H_2O_2/UV > UV alone.

More efforts are still required in the studies with real wastewaters, since most of the work is still on a laboratory scale.

2.3.4 Photocatalytic process: TiO_2 and Fe-doped TiO_2 photocatalysts

Titanium dioxide has high stability to light illumination, high activity, low cost and non-toxicity among many semiconductor photocatalysts [49]. Titanium dioxide can exist in three crystallographic forms: anatase and rutile forms, which are used most in photocatalysis studies, occur naturally and can be easily synthesized in the laboratory, and brookite, which is found in nature and is very

difficult to synthesize. Anatase is more active photocatalyst compared to rutile [50].

Anatase has an energy bandgap of 3.2 eV and can be activated using UV radiation with a wavelength up to 387.5 nm [18].

Degussa P25 is a titanium dioxide photocatalyst, which is a mixture of 70% anatase, 30% rutile. Better degradation efficiency can be obtained with its use compared to other photocatalysts [49]. Degussa P25 has a high specific surface area equal to 50 $m^2 g^{-1}$ [50], while anatase has 10 $m^2 g^{-1}$, rutile 20 $m^2 g^{-1}$of surface area. Given the fact that the main factor influencing the photocatalytic activity is the surface area, and the photocatalytic activity increases with increasing the surface area, it can be argued that Degussa P25 is more effective. The large surface area is due to the small particle size, which gives more active sites. Therefore, the adsorption rate, the adsorbability of the organic contaminants on the surface, the photocatalytic activity of catalyst increased as the particle size of the catalyst reduced [51].

The mechanism of the semiconductor photocatalytic reaction is shown in *Figure 2.2.* When a photocatalytic surface is illuminated with light of a corresponding wavelength (<380 nm) and energy equal to or greater than the bandgap energy of semiconductor, electrons from the valence band are excited to the conduction band, which leads to the generation of electron-hole pairs: a positive hole in the valence band and electron in the conduction band [52].

Figure 2.2: The principal illustration of photocatalytic process [52]

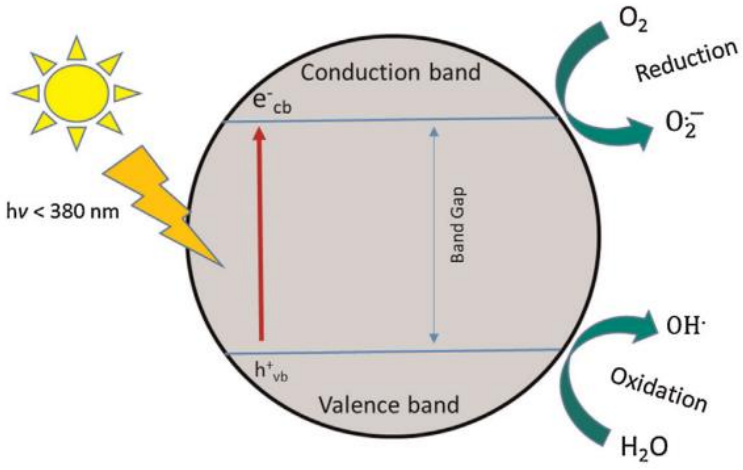

A titanium peroxide semiconductor absorbs ultraviolet light and generates hydroxyl radicals in TiO_2/UV process. In particular, electrons in the conduction band (e^-_{cb}) and holes in the valence band (hv^+_{vb}) are first obtained with UV illumination of TiO_2 (*Equation 2.17*). Anions of superoxide radical are formed by the interaction of band electrons with surface adsorbed molecular oxygen (*Equation 2.18*), and a hydroxyl radical is obtained by the interaction of band holes with water (*Equation 2.19*) [53]:

$$TiO_2 + hv \rightarrow e^-_{cb} + hv^+_{vb} \quad (2.17)$$

$$e^-_{cb} + O_2 \rightarrow O_2^{-\bullet} \quad (2.18)$$

$$hv^+_{vb} + H_2O \rightarrow OH^\bullet + H^+ \quad (2.19)$$

Oxidative degradation of organic compounds can occur through their reactions with hydroxyl and peroxide radicals, valence band holes, and reductive splitting through their reactions with electrons [26].

The main factors that affect the TiO_2/UV process are reactor design, temperature, pH of the solution, initial organic concentration, light intensity

amount of catalyst, UV irradiation time, and presence of ionic particles. Ionic species can affect the degradation process by adsorbing pollutants, absorbing ultraviolet light and reacting with hydroxyl radicals [54].

Laoufi et al. [55] studied the oxidation of phenol in wastewater using photocatalysis with titanium dioxide, and after 4 hours of irradiation, approximately 99% of the phenol was removed. Increasing the intensity of light from 15 W to 400 W and increasing the amount of TiO_2 from 0.1 to 1 g L^{-1} improved the degradation of phenol.

The amount of energy transferred into the medium can be reduced by using an excessive amount of catalyst as a result of the opacity resulting from the catalyst particles [54].

Herrmann J.M. found a slight temperature effect for temperatures between 20 and 80 °C and a decrease in the reaction rate at temperatures above 80 °C [56].

The pH of the solution affects the rate of photocatalytic oxidation. The reaction rate increases at lower pH for weakly acidic contaminants [57], and at higher pH for contaminants that hydrolyze in alkaline medium [58].

At the same time, Wei and Wan [59] noticed that a pH of less than 2 does not favour photocatalytic oxidation of phenol. The rate of phenol decomposition increases with increasing pH and reaches its maximum at pH ~ 6.5. The rate of phenol oxidation decreases quickly with a further increase in the pH value, and then increases again when the pH value is above 11.

The TiO_2/UV process is widely used for wastewater treatment. The benefits of this process are as follows: work under ambient conditions, the absence of mass transfer limitations when using nanoparticles as photocatalysts, highly oxidizing photogenerated holes, cheap and readily available TiO_2 and the possible use of solar irradiation [26]. TiO_2 can oxidize various organic substances to harmless substances, such as CO_2 and H_2O [60].

An increasing number of studies are focused on improving the efficiency of photocatalysts in order to expand the absorption spectrum to visible light, slow down the recombination rate between electrons and holes and increase the efficiency of interfacial charge transfer. This is done by doping metals, metal ions, non-metal atoms (N, S, I, C), semiconducting oxides into TiO_2 [61]. Thus, the photocatalytic performance under visible light illumination can be increased, and electrical power and expenses may be notably reduced.

The photocatalytic activity of Fe-doped TiO_2 nanoparticles has been studied by many researchers [62–68]. Choi et al. [62] studied the effects of doping 21 metal ions into TiO_2 and found that doping with Fe^{3+} at 0.1-0.5 % significantly increases the photoreactivity for both oxidation and reduction.

Zhu et al. [63] prepared Fe-doped nanocrystalline TiO_2 (Fe/TiO_2) through a nonhydrolytic sol-gel method. Fe/TiO_2 showed a higher activity than either undoped TiO_2 or Fe/TiO_2 obtained by conventional hydrolytic sol-gel method during the photodegradation of methylene blue under visible light irradiation. The positive effect of Fe-doping on the photocatalytic activity can be explained by the

formation of intermediate energy levels, which make it easy to activate Fe/TiO_2 in the visible region. The most favourable Fe-content in Fe/TiO_2 is defined as 0.1% (Fe/Ti molar ratio) [63].

Vargas et al. [64] synthesized 0.05% and 0.1% Fe-doped TiO_2 (Fe/Ti molar ratio) using the sol-gel method in combination with the solvothermal technology at 200°C and calcined in the temperature range of 350-620°C. The photoactivity under the ultraviolet and visible light irradiation was tested using degradation of the non-biodegradable dye Cbacron Yellow LS-R and phenol. The samples containing only anatase and processed at a temperature of 200°C to 500°C demonstrated enhanced photocatalytic activity under UV irradiation. UV photocatalytic activity was significantly lower in samples calcined at 620 °C due to the loss of their surface area and the presence of other phases. The synthesized samples had removal efficiencies similar to the commercial photocatalyst Degussa P25.

Zhu et al. [65] prepared Fe^{3+}-doped anatase nanosized TiO_2 photocatalysts by combining the sol–gel method with hydrothermal treatment. Fe^{3+}-doped TiO_2 showed photoactivity under visible irradiation, since its absorption was expanded to more than 500 nm. The photocatalytic activity of the prepared samples was verified by photodegradation of the active yellow XRG. 0.40% Fe-TiO_2 showed a higher photoactivity than undoped TiO_2 and P25 under UV irradiation, whereas 0.15% Fe-TiO_2 was more effective than TiO_2 and P25 when irradiated with visible light. Much more oxygen vacancies in the crystal lattice and on TiO_2 surface were

introduced by doping with Fe^{3+}, and they stimulated H_2O adsorption, the formation of surface hydroxyl groups and photocatalytic activity.

2.4 Landfill leachate

Due to its economic advantages, sanitary landfilling is currently widely used practice for the disposal of municipal solid wastes (MSW) in most countries [69]. Landfill leachate is a wastewater generated due to percolation of rain-water and moisture through waste in landfills and characterized by a high organic content [70]. Chlorinated organic and inorganic salts, heavy metals and high level of ammonia-nitrogen are also contained in leachates [69].

Approximately 125 m^3 of greenhouse gases with 65% of methane and 34% of carbon dioxide are produced by one ton of the landfilled MSW [71]. Untreated leachates can penetrate ground water or mix with surface water, leading to contamination of soil, groundwater and surface water [32].

Impact on human health, which arises from the leachate, can be not only from drinking water, but can also occur through the food chain, aquatic plants and fish that live the media contaminated by leachate. Minamata disease and Itai-Itai disease caused by chronic mercury and cadmium poisoning, respectively, are the classic examples of exposure to bioconcentrated toxicants. The pollutants in both cases are concentrated in fishes from coastal waters containing industrial waste [72]. The danger of landfill leachate was confirmed by toxicity analysis conducted using various test organisms (Daphnia similes, Brachydanio rerio, etc.) [69]. It is necessary to treat the leachate to prevent the methane emission and the pollution

of ground and surface water, as the leachate has a negative impact on human health and environment [71]. Usually for this purpose organic material and ammonia are removed from the leachate [69].

Biologically refractory organic components, ammonia and heavy metals are the three main problems associated with the treatment and removal of the leachate [32]. Ammonia at concentrations up to about 2000 mg L^{-1} can remain in water over time and be toxic to biological processes for treating the leachate [32].

The landfill leachate is usually characterized by such parameters as pH, chemical oxygen demand (COD), biological oxygen demand (BOD), total organic carbon (TOC), the ratio BOD/COD, ammonium nitrogen (NH_3-N), total Kjeldahl nitrogen (TKN), suspended solids (SS) and heavy metals [69].

The composition of landfill leachates depends on the age of the landfill [73]. Volatile fatty acids (VFA), such as acetic acid, propionic acid and butyric acid, are the major products of the anaerobic fermentation process that occur rapidly in young landfill leachates [74]. The acidogenic phase takes place in the young leachates, which results in the release of large amounts of free VFA [75], whereas in the mature (stabilized) leachate there is the methanogenic phase, where the growth of methanogenic microorganisms in the waste and transformation of the VFA to biogas (CH_4, CO_2) occur [76]. Young leachate contain large quantities of biodegradable organic compounds [74]. As leachate matures, refractory (non-biodegradable) substances, like humic and fulvic acids, dominate the organic

fraction of the leachate [76]. The characterization of young and mature leachates is presented in *Table 2.2*.

Table 2.2: Characteristics of young and mature leachates

Parameters	Young leachate	Mature leachate	Reference
Age (years)	<5	>10	[71]
	<1-2	>10	[32]
Composition	Low molecular weight compounds, such as VFAs (acetic acid, propionic acid and butyric acid)	High molecular weight compounds, such as humic acid and fulvic acid	[71]
pH	4.5-6.5	7.5-9.0	
NH_3-N (mg L^{-1})	500-2000	400-5000	
BOD (mg L^{-1})	4000-13000	20-1000	
COD (mg L^{-1})	6000-60000	5000-20000	
	3000-60000	100-500	[32]
BOD_5/COD	0.4-0.7	<0.1	[71]
	>0.6	<0.3	[32]
COD/TOC	>2.8	<2.0	[71]
TKN (g L^{-1})	0.1-2	NA	
Heavy metals (mg L^{-1})	>2	<2	

Biological processes can be not effective for leachates with high content of toxic components or low BOD_5/COD ratio [32]. Young landfill leachate can be treated by biological processes, as it is characterized by high ratio of BOD_5/COD [77]. Mature leachate has low BOD_5/COD ratio and relatively high NH_3-N [69]. Physicochemical treatment can be applied for pretreatment or full treatment of less biodegradable leachate [32].

Various advanced oxidation processes (AOPs) have been studied to treat landfill leachate [78]. Fenton process can significantly improve leachate quality in terms of organic content, color and odor. Moreover, toxic organic matter can

be removed, and biodegradability of organic substances can be increased by Fenton treatment [32].

2.5 Photodegradation of 4-tert-butylphenol in aqueous solution

Endocrine disrupting compounds (EDCs) are a serious concern for water quality, since they are contaminants with androgenic or estrogenic activity at very low concentrations [79].

4-tert-butylphenol (4-t-BP) is an alkylphenol and one of the EDCs with a poor biological degradability [80] and highly estrogenic effect [81–83]. *Table 2.3* summarizes some physical properties and toxicity data of 4-tert-butylphenol.

Table 2.3: Summary of physical properties and toxicity data of 4-tert-butylphenol [84]

Property	Species	Results
Physical properties		
Melting point		99.3°C
Boiling point		237 °C (at 1,013 hPa)
Density		0.92 g/m^3 at 110°C
Vapour pressure		130 Pa at 60°C
Water solubility		610 mg/l at 25°C
Toxicology		
Acute oral toxicology	Rat	LD_{50} = 4000 mg/kg
Acute inhalation toxicology	Rat	No lethal effects in saturated air
Acute dermal toxicology	Rabbit	LD_{50} = 2318 mg/kg
Skin irritation	Rabbit	Irritating
Eye irritation	Rabbit	Irritating
Repeated dose toxicity	Rat	NOAEL = 200 mg/kg/day
Carcinogenicity	Rat	Promoting forestomach tumor
Toxicity to reproduction	Rat	NOAEL = 200 mg/kg/day
Experience with human exposure		Depigmentation on skin

4-t-BP is widely used as a raw material for the production of phosphate esters, oil field chemicals, fragrances, demulsifiers [85], polymerization inhibitors

and stabilizing agents in the chemical industry [80]. It is spread in the aquatic environment, including sea and river waters and sediments, effluent samples from sewage and wastewater treatment plants [86]. Removal of 4-tert-butylphenol from the aquatic media is essential for the protection of the environment [87] and human health [80], since it is a serious water contaminant because it persists in the environment [88], has acute and chronic toxicity [89] and estrogenic activity [90].

Heterogeneous photocatalysis has the potential for the decomposition of organic pollutants in water, but the photocatalytic degradation of 4-tert-butylphenol is practically not investigated [88]. Biological processes could be applied for degradation of 4-t-BP [86,87], but they took a relatively long time. Physicochemical treatments, such as advanced oxidation processes, were more efficient for the decomposition of 4-t-BP. However, the path of photodegradation of 4-t-BP in aqueous solution is not completely clear [91].

Various researchers have discovered the following by-products during 4-t-BP photodegradation: 2,4-di-tert-butylphenol [92], 4-tert-butylphenol dimer [91,92], 4-tert-butylcatechol [86,91], isobutyl acetate [88], butyl acetate [88], ethylbenzene [88], 3,3-dimethyl-2-butanone [86], pyruvic acid [86], 6-tert-butyl-3-methylanisole [91] and benzene-1,4-diol [91] (*Figure 2.3*).

Xiao et al. [88] observed isobutyl acetate, butyl acetate, ethylbenzene after a photocatalytic reaction due to the destruction of aromatic structures, followed by the reaction with oxygen-containing oxidizing components. This result differs

from the study of Toyama et al. [86], in which 3,3-dimethyl-2-butanone was a typical intermediate. According to Toyama et al. [86], 4-tert-butylphenol was initially hydroxylated to 4-tert-butylcatechol, which decomposed to form 3,3-dimethyl-2-butanone and pyruvic acid. The results of these two studies [86,88] may vary due to different oxidation processes and decomposition methods.

Figure 2.3: By-products of 4-tert-butylphenol photodegradation

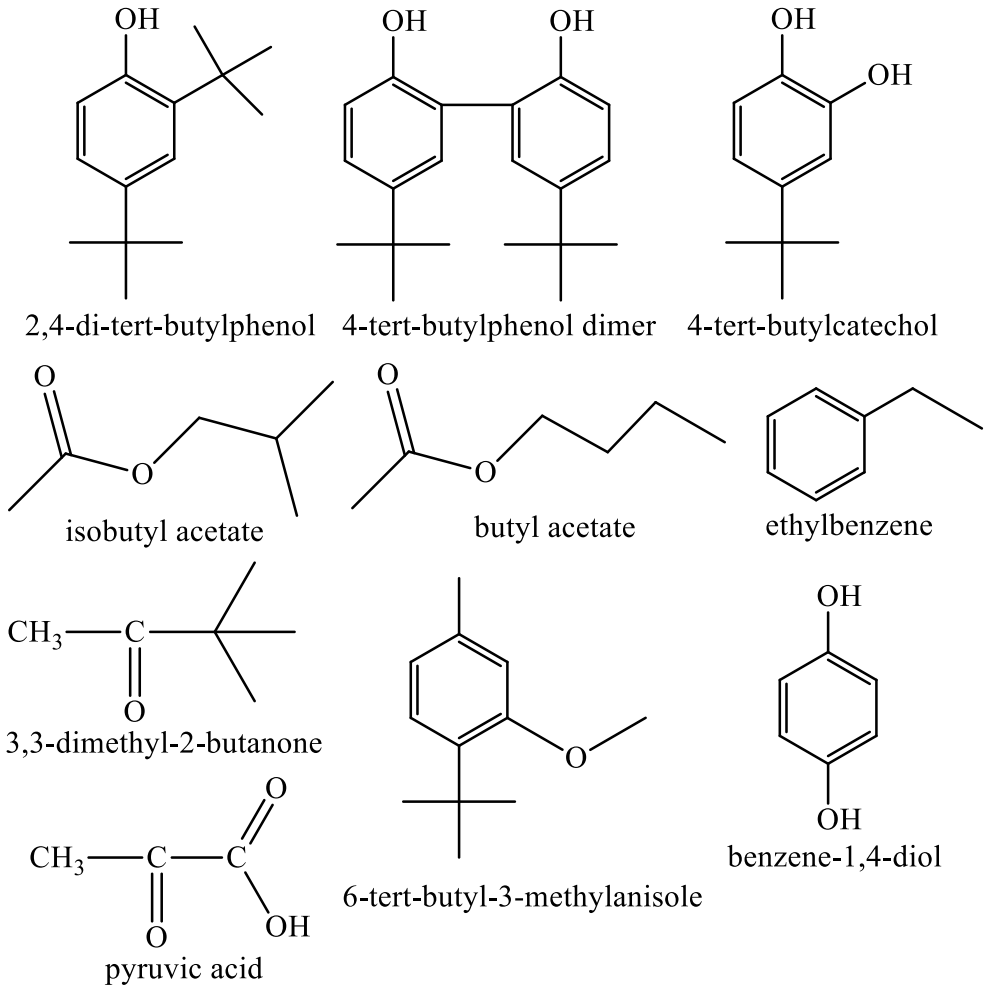

Wu et al. [91] found some byproducts (2-nonen-1-ol, 2-decen-1-ol, 2-dodecenal) from the breakdown of the benzene ring during the decomposition of 4-t-BP in the presence of H_2O_2 under UV irradiation of 254 nm. *Figure 2.4* shows the route of 4-t-BP oxidation with HO• [91].

Figure 2.4: The pathway for 4-t-BP oxidation by HO• [91]

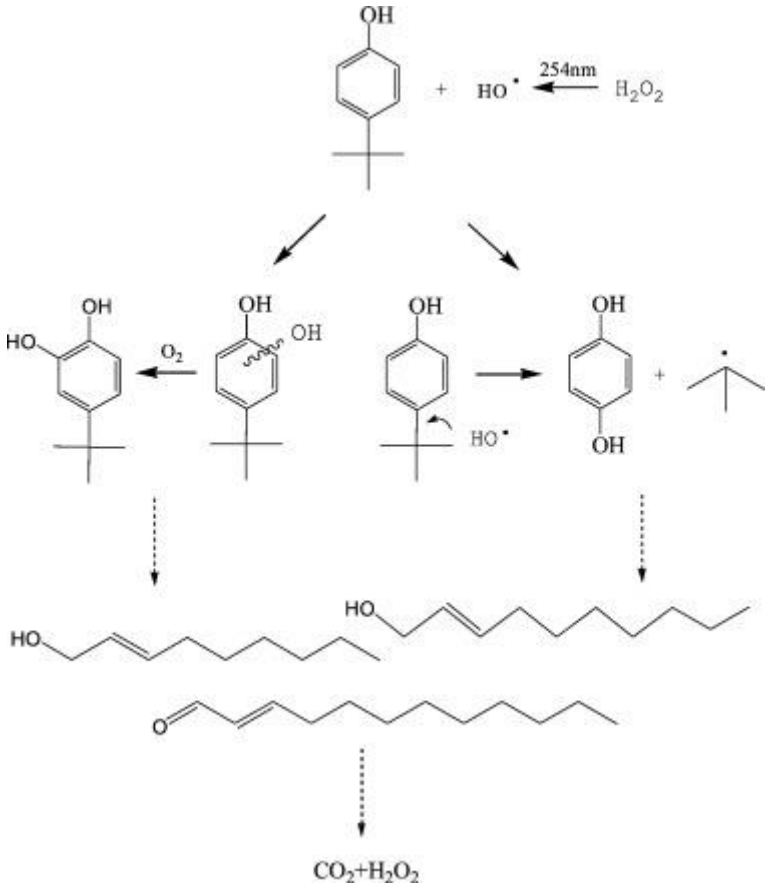

Chapter 3 – Materials and Methods

3.1 Scope of the study

Based on the literature review, it can be said that currently research on landfill leachate treatment and photocatalytic activity of synthesized Fe-doped TiO_2 with different iron contents is not enough. 4-tert-butylphenol was used as a model pollutant for studies with catalysts. The photocatalytic treatment of 4-tert-butylphenol in aqueous solution has not been fully studied. The current work focuses on the treatment of real landfill leachate and wastewater containing 4-tert-butylphenol using advanced oxidation processes. The main purpose was to increase the removal efficiency of organic carbon.

Firstly, photo-Fenton and photo-Fenton-like processes were used to treat a leachate from the municipal solid waste landfill of Astana (Kazakhstan), and the efficiency of these processes was compared with the Fenton process. Secondly, the photodegradation of 4-tert-butylphenol in aqueous solution was studied using Fe-doped TiO_2 catalysts, and the effectiveness of the catalysts was compared with TiO_2 catalyst (P-25). The work was also expanded by mineralization of 4-tert-butylphenol using UV/H_2O_2/catalyst process. This work can help to expand knowledge on advanced oxidation processes of wastewater treatment.

3.2 Methodology

35 experiments were conducted using Fenton's reagent, Fenton-like and photo-Fenton processes for landfill leachate treatment, and the work included the following steps:

- Analysis of the effect of inorganic carbon on total carbon and colour removal;
- Investigation of the UV/H_2O_2 process;
- Study of the pH effect on total carbon and colour removal;
- Identification of the most favourable initial concentrations of ferrous (200-600 ppm) and ferric (300-700 ppm) ions and hydrogen peroxide dosage (0-9990 mg L^{-1}) on total carbon and colour removal;
- Comparison of the photochemical treatment of leachate with Fenton and Fenton-like processes.

22 experiments were carried out to examine the efficiency of the synthesized Fe-doped TiO_2 catalysts with different iron contents (Fe/Ti weight ratio percentage = 0.5%, 1%, 2% and 4%) to remove 4-tert-butylphenol under ultraviolet light. The combination of catalysts, hydrogen peroxide and UV irradiation was also investigated on degradation of 4-tert-butylphenol. The performance of the synthesized catalysts on the mineralization of 4-tert-butylphenol was compared with TiO_2 catalyst (P-25). Each separate experiment was repeated two times and the average was taken using the standard error of the mean.

3.3 Materials

In the experiments with landfill leachate, two chemicals were used to adjust the pH: hydrochloric acid (37% w/w, Sigma-Aldrich) to decrease the pH of the solution and sodium hydroxide solution (10 M) to increase the pH to the required value. NaOH solution was prepared from sodium hydroxide (pellets) purchased from Fisher Chemical. Ammonium iron (II) sulfate hexahydrate ($(NH_4)_2Fe(SO_4)_2$, 99% w/w) and iron (III) chloride anhydrous ($FeCl_3$, ≥97% w/w) were purchased from Fisher Chemical and used as sources of ferrous and ferric ions, respectively. Hydrogen peroxide solution (37.6% w/w) received from Skat-Reactiv company was utilized as a source of hydroxyl radicals.

For the photocatalytic experiments, 4-tert-butylphenol (99%) used as a model pollutant and titanium (IV) oxide (nanopowder, 21 nm primary particle size, ≥99.5%) used as a photocatalyst were supplied by Sigma-Aldrich, ultrapure water was obtained from Direct-Q 3UV equipment. Iron (II) chloride (98%) purchased from Sigma-Aldrich was used for doping TiO_2 photocatalyst.

All chemical reagents were used without further purification. Ultrapure water was used in all experiments to dilute samples for analysis.

3.4 Landfill leachate characterization

The leachate used during the experiments was collected in the February-March period 2018, from the municipal solid waste disposal area of Astana city (Kazakhstan). This landfill can be considered as mature one since it was obtained within 10 years, and its pH was equal to 8.16.

The landfill leachate had the initial carbon concentration equal to 5868 mg L^{-1}, and about 42% of total carbon was inorganic (approximately 2450 mg L^{-1}). Total nitrogen of around 2905 mg L^{-1} was 90% inorganic in the form of ammonium, the rest was organic nitrogen (285 mg L^{-1}). The ammonium content in the leachate was investigated with an ion chromatography (IC, 930 Compact IC Flex supplied by Metrohm). It is well-known that the complexity of landfill leachate renders the task of GC-MS analysis complex. The FT-IR spectra of the raw leachate shown in *Figure 3.1* was recorded using Agilent Cary 600 Series FTIR spectrometer to investigate the functional groups and its possible composition. The spectra was described in *Table 3.1*.

Figure 3.1: The FT-IR spectra of the raw leachate

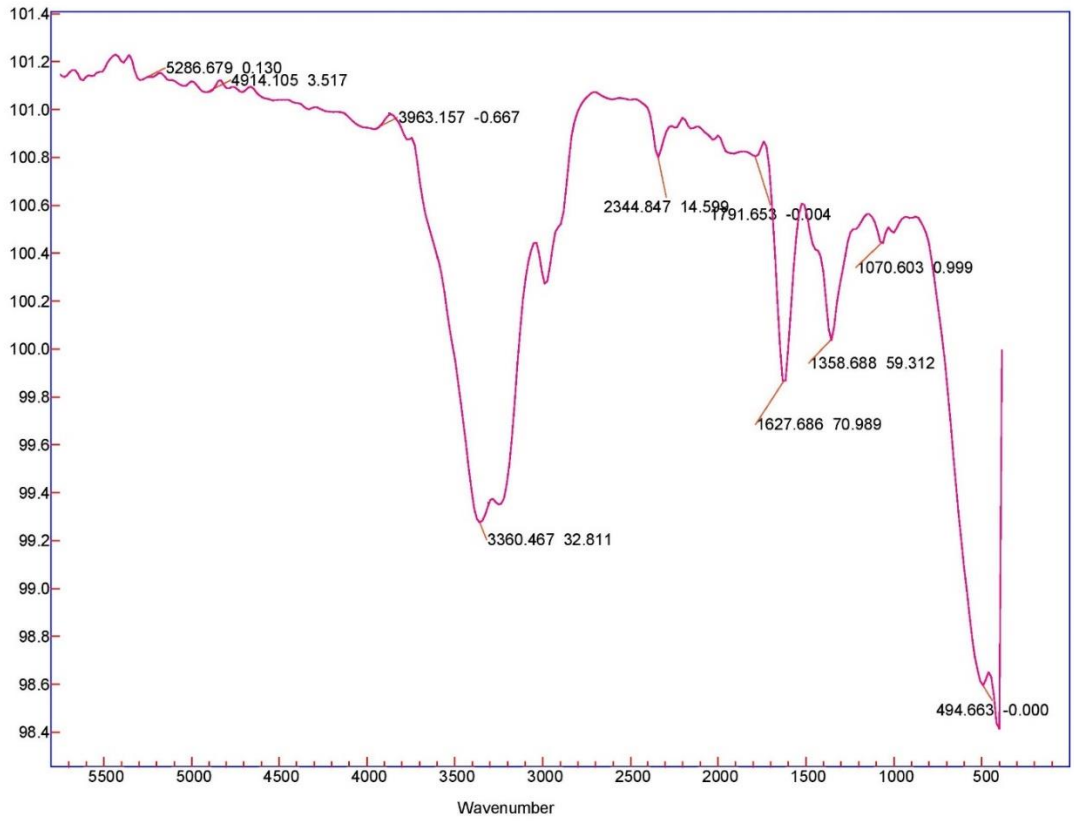

Table 3.1: The description of FT-IR spectra of raw leachate

Wavelength (cm^{-1})	**Vibration**	**Functional group or component**
3963	C-H stretch	Aliphatic methylene
3360	O–H stretch ≡C-H stretch	Bonded and non-bonded hydroxyl groups and water Alkyne group
2900	C-H stretch	Asymmetric and symmetric methyl and methylene groups
2344-2020	C-N	Cyanides (nitriles), cyanates, isocyanates, thiocyanates, and diazo compounds
1791	C=O	Acid (acyl) halide, aryl carbonate, open-chain acid anhydride, five-membered ring anhydride
1628	C=C stretch C=O stretch O-H bend N-H in bend	Alkene and aromatic ring Carboxylate and amide I Absorbed water Amines
1358	C-N stretch N-O stretch	Aromatic secondary and tertiary amine Nitrate
1070	C-O stretch S–O stretch	Alcohol and ether Inorganic sulphates
1055-1020	Si-O-Si, Si-O stretch C-F	Silica and clay minerals Fluoride
508	P-O C-Br	Inorganic phosphate Bromide

Preliminary experiments showed that inorganic carbon inhibited significantly the photo-Fenton process by acting as a scavenger for hydroxyl radicals [93]. Ammonia at concentrations up to about 2000 mg L^{-1} can remain in water over time and be toxic to biological processes for treating the leachate [32]. Therefore, pretreatment process in two steps was applied [94]: firstly, continuous air stripping for 24 hours at pH = 12 to remove ammonia, and then pH adjustment to 5 to remove inorganic carbon. When using air stripping, undesired substances

in the liquid can be removed with a carrier gas, mainly air [95]. The pretreatment of raw leachate led to 25% degradation of organic contaminants, 89% of ammonium removal.

The pretreated leachate was further diluted with tap water in a ratio of 1/2.4 and sent for chemical/photochemical treatment. The initial carbon concentration of pretreated diluted leachate was in the range of 1100-1300 mg L^{-1} (all carbon was organic) and it had also approximately 130-180 mg L^{-1} of total nitrogen and pH 5.1-5.3.

3.5 Preparation of phenolic solution

A stock solution of 4-tert-butylphenol with a concentration of 300 ppm was prepared using heating at 35°C in ultrapure water in a 1000 mL flask. The solution used in this work was prepared by further diluting the stock solution to the desired concentration of 30 ppm of 4-t-BP. The results of high performance liquid chromatography (HPLC) showed 30±1 ppm of 4-t-BP. The organic carbon of 4-tert-butylphenol ($C_{10}H_{14}O$, MW = 150.22 g mol^{-1}, carbon present = 79.88% w/w) in the aqueous solution was 24.5±0.5 mg L^{-1}, which is close to the calculated theoretical value of 23.96 mg L^{-1}. The stock solution was stored in a refrigerator at 5.6°C, and its decomposition was not detected.

3.6 Synthesis of Fe-doped TiO_2 catalysts

Catalysts of TiO_2 doped with iron were synthesized with dopant concentrations of 0.5, 1, 2 and 4 wt.% using the wet impregnation method. 3 g of

TiO_2 (P-25) was suspended in 100 ml of ultrapure water, and then the required amount of $FeCl_2$ (iron precursor) was added. The obtained mixture was constantly stirred for 24 hours and washed three times with distilled water to remove any precursor of physical adsorption before drying in an air oven at 80°C for 12 hours. The dried solids were ground in a mortar and calcined at 500°C for 6 hours in a muffle furnace.

3.7 Reactor configuration

Photochemical/photocatalytic experiments were carried out using the apparatus shown in *Figure 3.2*.

Figure 3.2: The experimental setup for photochemical/photocatalytic experiments

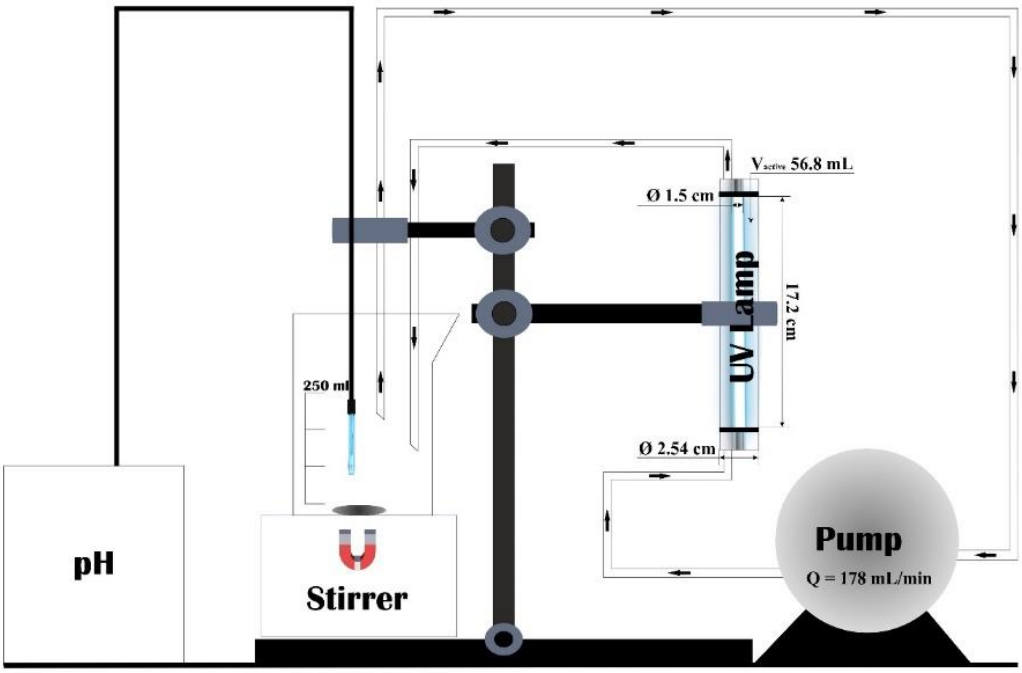

The total volume of the treated solution was 250 mL. An annular photoreactor with 56.8 mL of irradiated volume, operating in a batch recycle mode, was applied for photochemical/photocatalytic treatment. The solution was

continuously pumped at a rate of 178 mL min^{-1} from bottom to top through the photoreactor using a peristaltic pump drive 5006 purchased from Heidolph. The Osram lamp with a power of 6 W, located inside the photoreactor, emitted ultraviolet radiation with a wavelength of 254 nm, and its specifications are given in *Table 3.2.*

Table 3.2: Specifications of Osram Puritec HNS G5 6W lamp

Electrical data	
Nominal wattage	6 W
Nominal voltage	42 V
Construction voltage	42 V
Nominal current	0.16 A
Lamp current	0.16 A
Photometrical data	
Radiated power 200…280 nm (UVC)	1.7 W
Additional product data	
Base (standard designation)	G5
Capabilities	
Burning position	s180

A part of the solution, which was not in the photoreactor, was constantly stirred with a magnetic stirrer (Bibby Scientific, United Kingdom), the level of mixing of which was set at 3. The beginning of the experiment was considered immediately after turning on the UV lamp with the pump. Mettler Toledo LE409 electrode was immersed in the solution for pH measurement, which was carried out throughout the duration of each experiment.

3.8 Experimental procedure and characterization methods

All experiments were performed with 250 mL of the total solution. The initial concentration of compounds plays a significant role in the efficiency of the decomposition process. Therefore, the effects of inorganic carbon, initial concentrations of ferrous (200-600 ppm) and ferric (300-700 ppm) ions and hydrogen peroxide amount in the range of 0-9990 mg L^{-1}, the effect of pH on total carbon and colour removal of landfill leachate were studied to identify the most favourable operating conditions. The parameter considered varied, while the rest remained constant. Each photochemical experiment of landfill leachate lasted 120 minutes, and samples were periodically withdrawn and sent directly to the analysis. A Vitlab 1000 μL automated pipette was used to take samples. The treatment efficiency was assessed through pH measurements, TC/TIC/TN analyses, and color change. The TC/TIC/TN analyses were performed using the Multi N/C 3100 instrument by Analytik Jena AG (Germany), whereas color change was detected using a photoLab® 6000 series UV-Vis spectrophotometer.

In experiments with Fe/TiO_2 catalysts with iron concentrations of 0.5, 1, 2 and 4 wt.%, the catalysts were sonicated in water for 10 minutes just before use, an FB15055 ultrasonic bath from Fisher Scientific was used for this purpose, the technical details of which are given in *Table 3.3*.

Then, the aqueous solution containing 4-tertbutylphenol in concentration of 30 mg L^{-1} was mixed with 0.25 g of photocatalyst under constant magnetic stirring (the total volume of the solution was 250 mL). Before UV irradiation, this solution

was stirred for 1 hour in the dark so that the system reached adsorption equilibrium. Each photocatalytic experiment on the mineralization of 4-tert-butylphenol lasted 60 minutes. 88.31 mg L^{-1} of H_2O_2 was used for experiments with a combination of hydrogen peroxide and catalyst (1 g L^{-1}).

Table 3.3: Technical details of the FB15055 ultrasonic bath

Ultrasound frequency	37 kHz
Power consumption total	550 W
Ultrasonic power RMS	150 W
Ultrasonic maximum peak power (standard sine-wave modulation)	600 W
Heating power	400 W

The photocatalytic activity of the synthesized catalysts was measured via TC and UV-Vis measurements. 4-tert-butylphenol in the solution was identified by HPLC (Agilent 1290 Infinity II system), and the content of acetic and formic acids in the final solution in the experiments with mineralization of 4-tert-butylphenol was detected using IC (930 Compact IC Flex supplied by Metrohm). The iron content in the solution (Fe leaching) after 1 hour in the dark and after the completion of the whole experiment was determined using an atomic absorption spectrometer AAnalyst 400, purchased from Perkin Elmer. The calibration range was from 0.05 to 3 ppm, wavelength was 248 nm.

The structure and morphology of the fresh and used catalysts were determined using powder X-ray diffraction (XRD, SmartLab automated multipurpose X-ray Diffractometer purchased from Rigaku) and scanning electron microscopy (SEM, Auriga Cross Beam 540, Carl Zeiss). The optical

properties of fresh catalysts were measured using a UV-Vis spectroscopy (Evolution 60S UV-Visible spectrophotometer, Thermo Fisher Scientific) in the wavelength range of 200 to 750 nm. For XRD and SEM analyses, the catalysts after the experiments were separated from the solution using a table-type low speed centrifuge (EdLab, Hungary) and dried in an air oven at 105°C for 12 hours.

Prior to TC, UV-Vis, AAS, FT-IR analyses, all samples were filtered using Agilent Captiva premium syringe filters with a 0.45 µm regenerated cellulose (RC) membrane. For HPLC and IC analyses, the catalysts were separated from the solution by filtration through RC membranes with a pore size of 0.2 µm (Agilent Captiva premium syringe filters).

The removal efficiency was calculated according to *Equation 3.1*, where C_t is the concentration after time t and C_0 is the initial concentration:

$$Removal\ efficiency\ (\%) = \left(1 - \frac{C_t}{C_0}\right) \times 100 \qquad (3.1)$$

3.8.1 Multi N/C 3100

Total carbon, total inorganic carbon and total nitrogen in the liquid samples taken during the experiments were measured using the Multi N/C 3100 apparatus from Analytik Jena AG, shown in *Figure 3.3*.

250 µl from the sample is taken for each repetition; there are 2-3 repetitions with one sample. The sample is injected by a syringe pump and transferred to the quartz combustion tube (reactor), which is filled with a platinum catalyst, high-temperature mat and quartz wool. The temperature in the tube rises to 800 °C.

Oxygen is applied as a carrier gas and oxidant agent. *Equations 3.2-3.4* (R is a carbonic substance) represent the pyrolysis and oxidation processes of the sample. Thermocatalytic high-temperature oxidation in the presence of a platinum catalyst occurs in the apparatus, therefore, even very stable complex carbon can be detected.

Figure 3.3: Multi N/C 3100 apparatus

$$R + O_2 \rightarrow CO_2 + H_2O \quad (3.2)$$

$$R - N + O_2 \rightarrow NO + CO_2 + H_2O \quad (3.3)$$

$$R - Cl + O_2 \rightarrow HCl + CO_2 + H_2O \quad (3.4)$$

The heated gas is cooled and dried in a condensation coil, where the condensed water is separated from the testing gas into a TIC condensation vessel. Carbon dioxide is added to the NDIR detector (non-dispersive infrared absorption detector), which measures CO_2 gas using infrared radiation, and the total carbon concentration in the sample is calculated according to the absorbed amount of the light. Total inorganic carbon is measured in a TIC acid reactor. Total nitrogen can

be measured with CLD (chemiluminescent detector) or ChD (electrochemical detector), since nitrogen oxides are formed during combustion.

The equipment performed analysis based on the following calibration ranges:

- TC: 5-50 ppm (linear regression)
- TIC: 5-50 ppm (linear regression)
- TN: 2.5-25 ppm (quadratic regression).

Chapter 4 – Results and Discussion

4.1 Landfill leachate experiments

As mentioned earlier, the landfill leachate used was mature, so the photo-Fenton process is suitable for treatment, because in the case of young leachate, biodegradable organic pollutants are more beneficial to decompose using biological processes [32]. The classical photo-Fenton process was also applied for the treatment of landfill leachates [46–48]. Primo et al. [46] recommended using the photo-Fenton process as the most effective AOP.

The duration of all experiments with leachate was 2 hours, and classic Fenton (Fe(II) and H_2O_2) and Fenton-like (Fe(III) and H_2O_2) processes without UV irradiation have been studied along with photochemical processes.

4.1.1 Effect of inorganic carbon on leachate treatment by the photo-Fenton process

Initially, the effect of inorganic presence on photochemical oxidation was examined, namely without solution acidification. The experiments were conducted with 5 mL (6660 mg L^{-1}) of H_2O_2 and 400 ppm of Fe(II). The total initial carbon of partially pretreated leachate solution without acidification step was 3176 mg L^{-1} with 1541 mg L^{-1} from inorganic carbon (48.5% of total carbon). Inorganic carbon is related to the total by *Equation 4.1*:

$$TC\ [mg\ L^{-1}] = TOC\ [mg\ L^{-1}] + TIC\ [mg\ L^{-1}] \qquad (4.1)$$

As it was mentioned earlier, the initial carbon concentration of the leachate with full pretreatment step was 1342 mg L^{-1} (all carbon was organic) and it had pH 5.34, which was reduced to 4.51 during the experiment. Initial pH of partially pretreated leachate solution without acidification was equal to 10.13, and pH stayed around 10 throughout the experiment.

The obtained results are shown in *Figure 4.1-4.2*. It was clear that presence of inorganic carbon inhibited considerably carbon removal in the photo-Fenton process since only 7.7% TC removal was observed in contrast to 29% achieved along with improved color removal (*Figure A.1, Appendix A*) when full pretreatment was applied.

Figure 4.1: Effect of inorganic carbon on TC removal ($[Fe(II)]_0$ = 400 ppm, $[H_2O_2]_0$ = 6660 mg L^{-1})

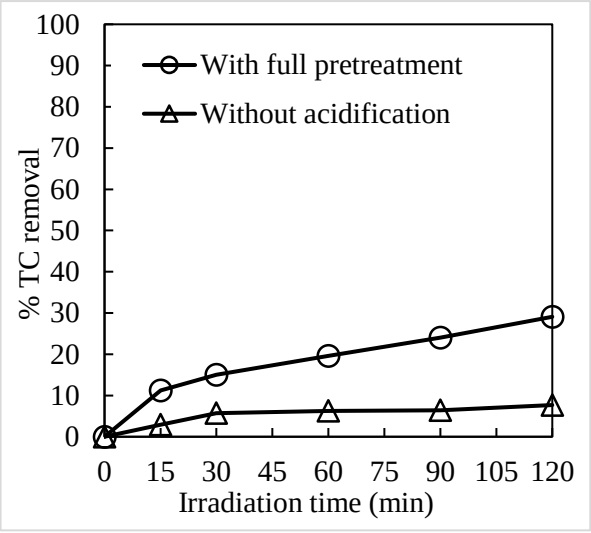

Figure 4.2: Effect of inorganic carbon on pH throughout the experiment ($[Fe(II)]_0$ = 400 ppm, $[H_2O_2]_0$ = 6660 mg L^{-1})

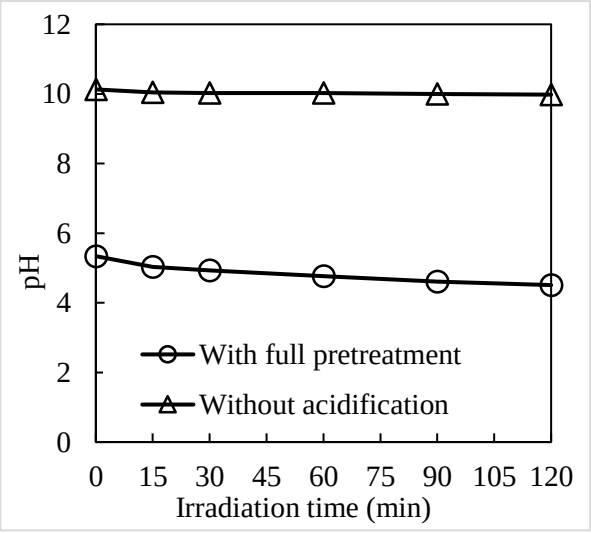

The reason is that inorganic carbon (carbonate CO_3^{2-} and bicarbonate HCO_3^-) can affect the total reaction rate by acting as scavenger for hydroxyl radicals [78,93]. The pH reduction to acidic conditions eliminates this issue, since CO_3^{2-} and HCO_3^- in combination with H^+ form unstable carbonic acid (H_2CO_3),

which is then decomposes to CO_2 and H_2O [78]. Besides the scavenging of radicals, the pH of the solution is too high for the reaction to proceed. Therefore, the second step of the pretreatment process was pH adjustment to 5 in order to remove inorganic carbon.

The TIC conversion of the diluted leachate solution without acidification was zero, as the photo-Fenton process is not intended to remove inorganic carbon from the solution. The TN value (remaining nitrogen after pretreatment) stayed unchanged during both experiments at around 180 mg L^{-1}. Based on the obtained results, for further experiments, pretreated diluted leachate (after full pretreatment process) was used. Since TIC was removed during the pretreatment stage, all carbon was organic.

4.1.2 Effect of Fe(II) concentration on leachate treatment by the photo-Fenton process

The initial concentration of compounds affects the efficiency of the decomposition process. Therefore, first, the initial concentration of ferrous ions was varied to find the most favourable one. The hydrogen peroxide concentration remained constant for these tests at 6660 mg L^{-1} (5 ml). It was observed that the increase of Fe(II) concentration from 200 to 500 ppm increased the TC removal by photochemical oxidation from 8 to 31% (*Figure 4.3-4.4*). After further increasing the concentration of Fe(II) to 600 ppm, the achieved percentage of TC removal decreased slightly to 30.5%. The difference in TC removal between 400 and 500 ppm of Fe(II) is only 2%, and considering that it is more cost-effective

to use a smaller amount of reagent, it was decided to use 400 ppm of Fe(II) for further photo-Fenton experiments. In addition, less iron sludge will need to be treated [54].

According to Deng et al. [32], the removal of organic pollutants by Fenton process increases with increasing iron concentration, but further removal may become insignificant when the iron concentration is high. In addition, there is a limit on the concentration of iron due to scavenging effect of excess iron on •OH (*Equation 4.2*).

$$OH^{\bullet} + Fe^{2+} \rightarrow Fe^{3+} + OH^{-} \qquad (4.2)$$

Figure 4.3: Effect of Fe(II) concentration on TC removal ($[H_2O_2]_0$ = 6660 mg L^{-1})

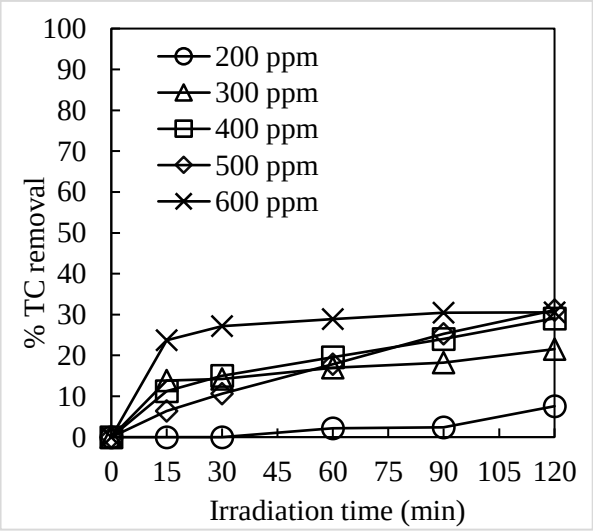

Figure 4.4: Effect of Fe(II) concentration on the final TC removal achieved ($[H_2O_2]_0$ = 6660 mg L^{-1})

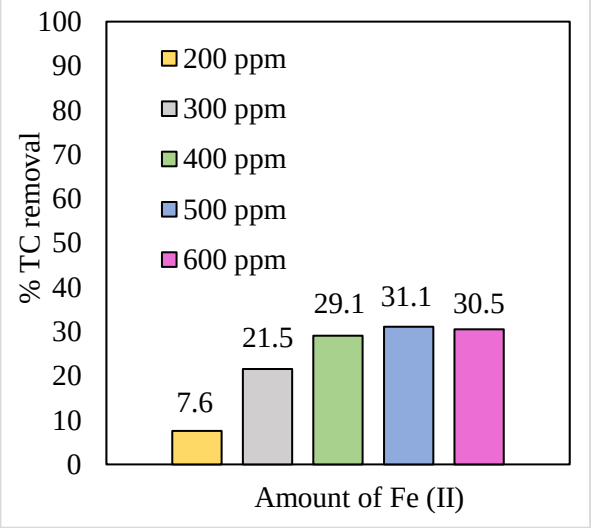

The initial pH for tests with varying Fe(II) concentrations ranged from 5.21 to 5.44 and dropped to about 4.56 during the experiments, possibly due to the formation of organic acids during the process [96]. A color change after the

photochemical treatment was also observed, the UV-Vis spectra of the color change is shown in *Figure A.2* (*Appendix A*).

4.1.3 Effect of Fe(III) concentration on leachate treatment by the photo-Fenton-like process

As a next step, the effect of concentration of ferric ions on the removal of organic contaminants during the photo-Fenton-like process was studied. All experiments were carried out using the same initial concentration of hydrogen peroxide, equal to 6660 mg L^{-1} and different initial dosages of Fe(III), which ranged from 300 to 700 ppm.

Adding Fe(III) instead of Fe(II) in the process was beneficial in terms of removing TC, especially during the first 15 min (*Figure 4.5*). The final conversions in this series of experiments are shown in *Figure 4.6*.

Figure 4.5: Effect of Fe(III) concentration on TC removal ($[H_2O_2]_0$ = 6660 mg L^{-1})

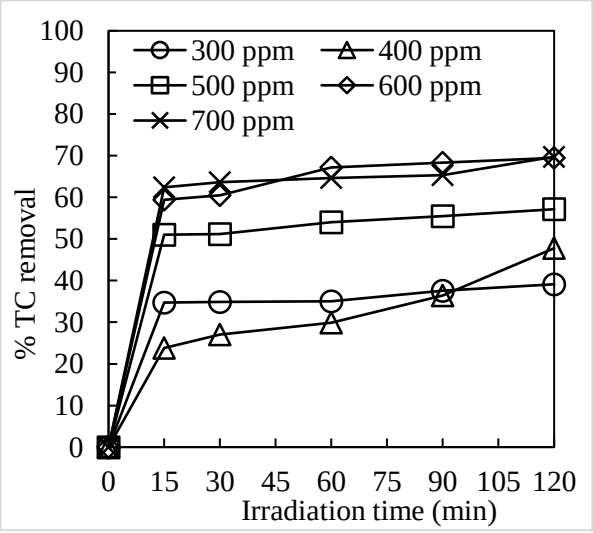

Figure 4.6: Effect of Fe(III) concentration on the final TC removal achieved ($[H_2O_2]_0$ = 6660 mg L^{-1})

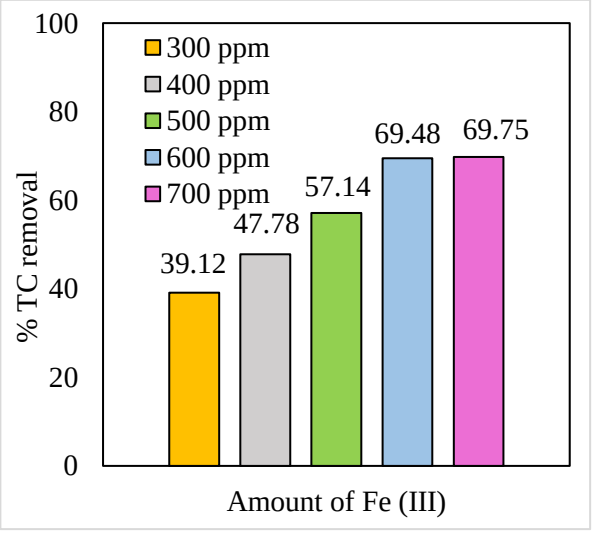

After increasing the concentration of Fe(III) from 300 to 600 ppm, the removal of TC by the photo-Fenton method gradually increased from 39% to

69.5%. However, a further increase to 700 ppm did not improve the TC removal and remained at 70%. Thus, it was not necessary to investigate higher concentrations of ferric ions. 600 ppm of Fe(III) was used for further photo-Fenton-like experiments.

Fe(III) showed the same tendency as Fe(II), namely, increasing the concentration only to a certain amount increased the degree of treatment [32].

Comparing the results with the photo-Fenton process, it is clear that the removal efficiency of TC and colour (*Figure A.3, Appendix A*) in photo-Fenton-like method is higher, although according to Deng et al. [32], it should be exactly the opposite. Both ferrous and ferric ions are in the chain of Fenton reactions (*Equations 2.8-2.14*). Deng et al. [32] states that Fenton-like process has a low rate of formation of hydroxyl radicals, whereas.at the beginning of the Fenton oxidation, very rapid formation of hydroxyl radicals can occur due to a higher rate constant in the Fenton reaction than in the Fenton-like reaction.

The results obtained during the experiments can be explained by chemical complexity of leachate, especially since the used landfill leachate was mature. According to Gogate and Pandit [54], the roles, the mechanisms of action, and the equilibrium concentration of ferrous and ferric ions are complex and unclear in details. Several studies have been conducted to compare both processes, and the results obtained are controversial. Rivas et al. [97] found that similar removal efficiencies of organic matter were obtained with Fenton and Fenton-like

processes; however, Kim et al. [98] reported that the Fenton reaction had higher removal than Fenton-like reaction.

4.1.4 Effect of H_2O_2 dosage on leachate treatment by photo-Fenton and photo-Fenton-like processes

The effect of hydrogen peroxide dosage was studied by maintaining a constant initial iron concentration. Experiments were performed for 0, 1332, 3330, 6660, and 9990 mg L^{-1} of H_2O_2, which corresponds to 0, 1, 2.5, 5, and 7.5 ml, respectively. 400 ppm of Fe(II) were used for photo-Fenton process, 600 ppm of Fe(III) for photo-Fenton-like process. The results obtained are shown in *Figures 4.7-4.10*.

The most favourable concentration of H_2O_2 for carbon removal was 6660 mg L^{-1} leading to 29% TC removal with 400 ppm of Fe(II) and 69.5% TC removal with 600 ppm of Fe(III).

Figure 4.7: Effect of H_2O_2 dosage on TC removal ($[Fe(II)]_0$ = 400 ppm)

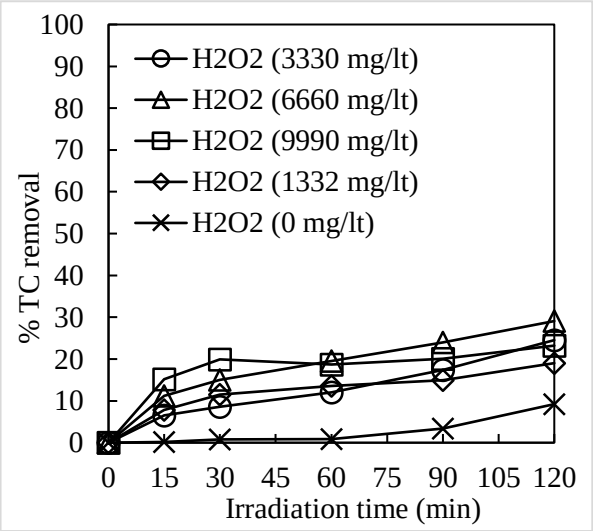

Figure 4.8: Effect of H_2O_2 dosage on the final TC removal achieved ($[Fe(II)]_0$ = 400 ppm)

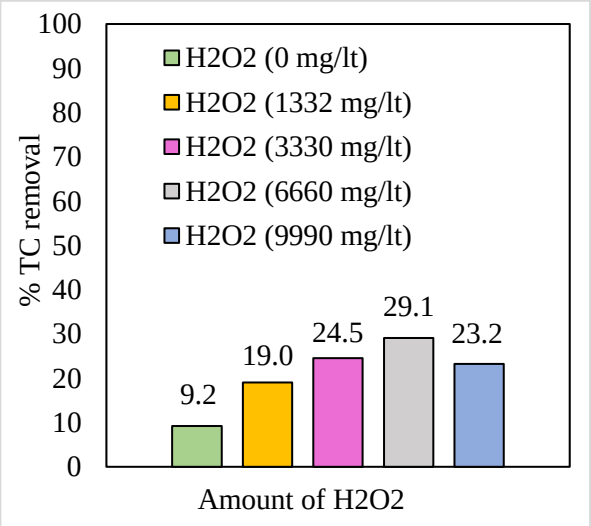

As in the literature [32], it was noted that a higher initial concentration of hydrogen peroxide leads to a higher removal of TC. A further increase in the dosage of hydrogen peroxide to 9990 mg L^{-1} in photo-Fenton-like process led to almost the same TC conversion as for 6660 mg L^{-1} of H_2O_2, 74.4% and 69.5%, respectively. Thus, it was more practical to use 6660 mg L^{-1} of H_2O_2 for the next experiments. In the photo-Fenton process, an increase in the H_2O_2 dosage from 6660 to 9990 mg L^{-1} resulted in a decrease in the removal of TC from 29% to 23%.

Figure 4.9: Effect of H_2O_2 dosage on TC removal ($[Fe(III)]_0$ = 600 ppm)

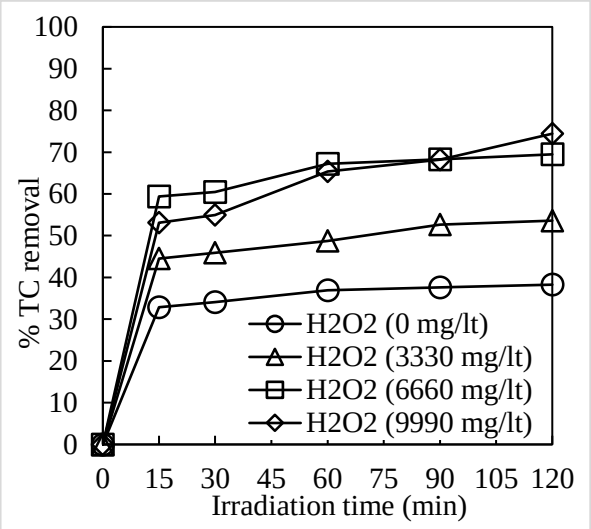

Figure 4.10: Effect of H_2O_2 dosage on pH throughout the experiment ($[Fe(III)]_0$ = 600 ppm)

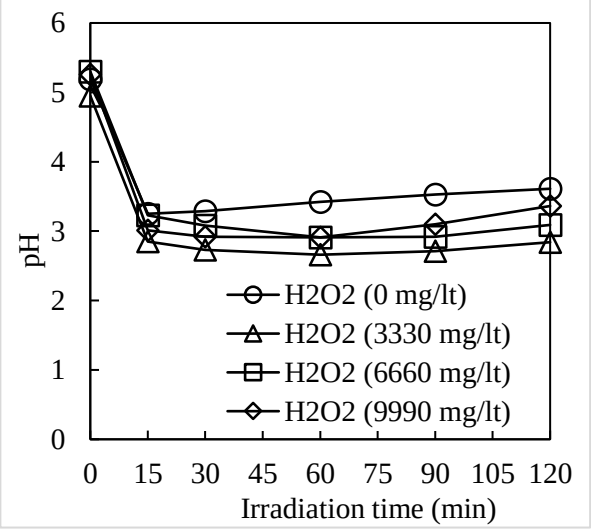

An excess amount of hydrogen peroxide scavenges hydroxyl radicals [32]. An overdose of H_2O_2 will lead to a reaction with •OH radical and the formation of the perhydroxyl radical HO_2•, which is the undesired product [26]. The scavenging effect is presented in *Equation 4.3*.

$$OH^{\bullet} + H_2O_2 \rightarrow HO_2^{\bullet} + H_2O \qquad (4.3)$$

The pH during photo-Fenton processes dropped from about 5.27 to 4.58 for all cases, except for the experiment without hydrogen peroxide, when the pH fluctuated only slightly from the initial value. During photo-Fenton-like processes (*Figure 4.10*), the initial pH value was around 5.18, and it fell as the process progressed due to the conversion of organic carbon into organic acids, and then the pH value rose again, as the organic acids began to decompose slowly to CO_2, leaving the solution [96]. Regarding TN, both processes had no impact on it. The colour change was observed during this batch of photochemical experiments and is shown in *Figures A.4-A.5* (*Appendix A*).

4.1.5 Effect of pH adjustment on leachate treatment by photo-Fenton and photo-Fenton-like processes

Finally, the photo-Fenton process was enhanced by changing the initial pH value of the solution, since pH has a huge impact on the remediation process [28].

The pH effect on the photochemical degradation of organic pollutants was investigated using 6660 mg L^{-1} of H_2O_2 and 400 ppm of Fe(II). The TC removal and pH results are shown in *Figures 4.11-4.12*.

Without any pH adjustment the initial pH of the pretreated diluted leachate was 5.34. First the pH value lowered to 4.02 at 0 minute by addition of 0.15 mL of HCl (>37% (w/w)), which increased TC removal slightly and was 33% compared to 29% without pH adjustment. Further, the effect of changing the pH value throughout the process was studied. For this purpose, the same amount of hydrochloric acid was added to the solution as in the previous case (0.15 mL), but

this was done at 30, 60 and 90 minutes by adding 0.05 ml each time. 31% of TC conversion was obtained, which is less than 33%, achieved by pH adjustment at 0 minute. This proves the assumption that a change of the pH value at the beginning is better than a consistent change.

Figure 4.11: Effect of pH adjustment on TC removal ($[Fe(II)]_0$ = 400 ppm, $[H_2O_2]_0$ = 6660 mg L^{-1})

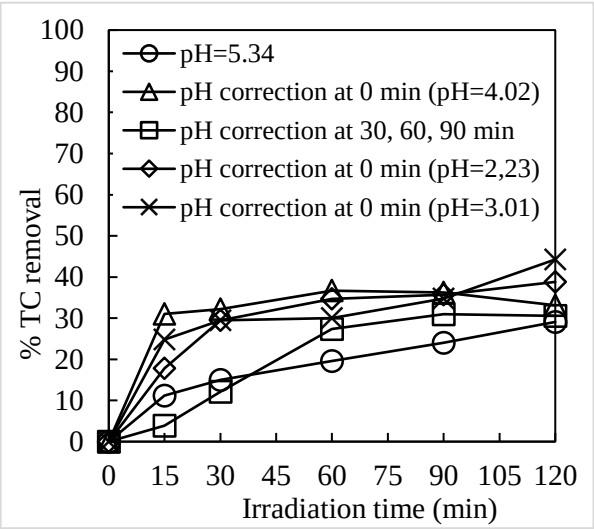

Figure 4.12: Effect of pH adjustment in terms of pH ($[Fe(II)]_0$ = 400 ppm, $[H_2O_2]_0$ = 6660 mg L^{-1})

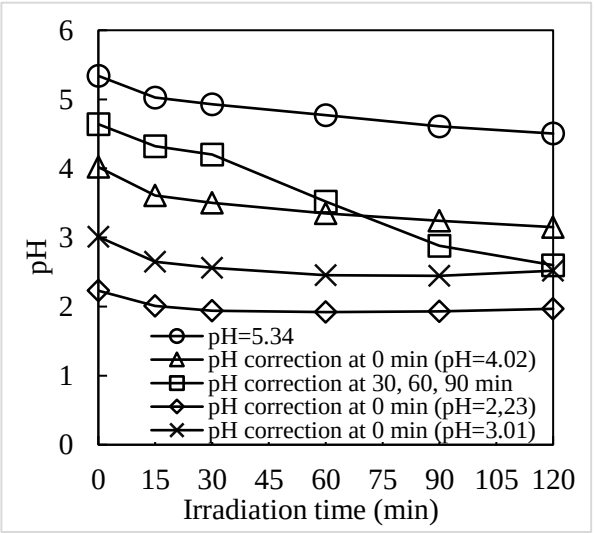

Therefore, the initial pH value was varied from 2.23 to 5.34 to find the most favourable case. The TC conversions at pH 2.23 and 4.02 were equal to 39% and 33%, respectively. The highest colour and TC removal (44%) corresponded to pH 3.01, while the lowest to pH 5.34 (29%). Remaining nitrogen after the pretreatment step (approximately 165 mg L^{-1}) was not affected in all cases. The colour change during these series of experiments is shown in *Figure A.6* (*Appendix A*).

The results obtained (highest TC removal at pH 3) match with the findings of other scientists [31,36,99,100]. The most favorable pH values for Fenton reactions are 2.80-3.20 [36]. Pignatello et al. [31] and Coelho et al. [100]

conducted experiments on Fenton process varying the pH from 2 to 6 in order to study the pH effect on the degradation rate. The highest efficiency of the processes corresponded to pH 3 [31], and pH 2.8 [100], respectively. The $[Fe(OH)]^{2+}$ ion is of great importance for the photo-Fenton process, and it is formed at pH 2.8–3.5 [31]. The ferrous ions are unstable and can be transformed to ferric ions, forming complexes with hydroxyl, at pH above 4. Additionally, H_2O_2 loses its oxidizing ability under alkaline conditions due to its decomposition to oxygen and water [37]. $[Fe(H_2O)]^{2+}$ forms at lower pH (below 2) and reacts slowly with H_2O_2 [101]. Moreover, at lower pH, the scavenging effect of H^+ on hydroxyl radicals becomes more significant, which slows down the process [102]. The reaction between Fe^{3+} and hydrogen peroxide can be inhibited at extremely low pH [41].

Since the treated leachate with Fe(II) achieved better results by adjusting the initial pH of the solution, the best case obtained for Fe(II) (pH adjustment to 3) was tested for Fe(III). 6660 mg L^{-1} of H_2O_2 and 600 ppm of Fe(III) were used. The TC removal and pH results are shown in *Figures 4.13-4.14*.

With the addition of 0.245 ml of hydrochloric acid at 0 min, the pH dropped to 3.04. After two hours of experiment, the TC showed TC degradation efficiency of 63%. However, the experiment without adjusting the pH reached 69.5% conversion. This corresponds to the results obtained by Kim et al. [98], namely the most favourable value for the Fenton process (pH 3) is not the same for Fenton-like process. The colour change is shown in *Figures A.7* (*Appendix A*).

Figure 4.13: Effect of pH adjustment on TC removal ([Fe(III)]$_0$ = 600 ppm, [H_2O_2]$_0$ = 6660 mg L^{-1})

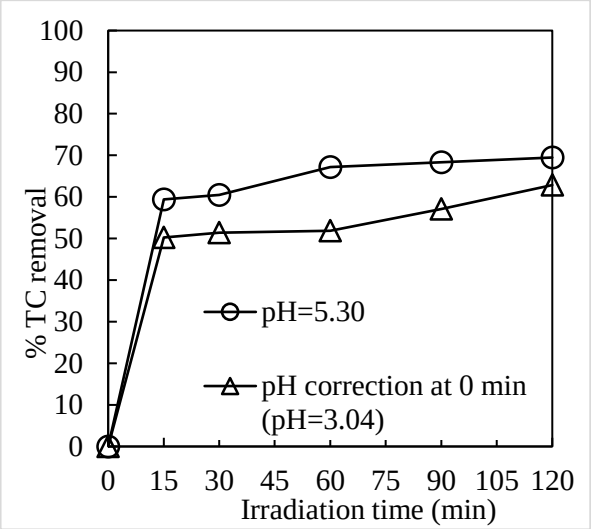

Figure 4.14: Effect of pH adjustment in terms of pH ([Fe(III)]$_0$ = 600 ppm, [H_2O_2]$_0$ = 6660 mg L^{-1})

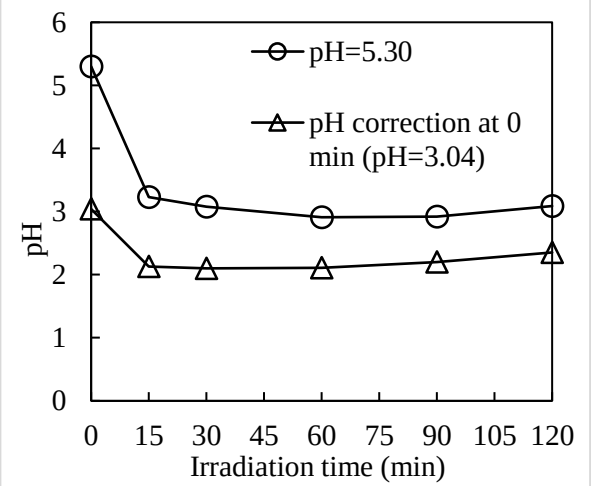

4.1.6 Landfill leachate treatment by Fenton process

The treatment of the pretreated diluted leachate was additionally investigated for the classical Fenton reaction with 6660 mg L^{-1} H_2O_2 for an initial concentration of Fe(II) in the range of 300-500 ppm. As shown in *Figure 4.15*, the results showed the same favourable dosage of Fe(II), as for photo-Fenton process, i.e. 400 ppm, which corresponds to 21% decomposition of organic pollutants. Using classical Fenton process instead of photo-Fenton process led to a lower TC removal: from 29% to 21%. The application of UV light to the oxidation process has been reported to enhance the removal of pollutants [31]. A further increase to 500 ppm resulted in 9% of TC removal, as there is a limit on the concentration of iron due to scavenging effect of excess iron on •OH [32].

In addition, the effect of initial pH value was studied, and the best case obtained for photo-Fenton process was tested (pH adjustment to around 3). 400 ppm of Fe(II) was used, and TC conversion was 41% after 2 hours. That is, the

pH correction increased TC removal, as in the photo-Fenton process, specifically, degradation of organic pollutants increased from 21% (without pH adjustment) to 41% (with pH adjustment to 2.94).

The pH value in this series of experiments basically remained constant, as it is shown in *Figure 4.16*. Improvement in the final color of the solution was observed and is presented in *Figure A.8* (*Appendix A*).

Figure 4.15: TC removal by Fenton process ($[H_2O_2]_0$ = 6660 mg L^{-1})

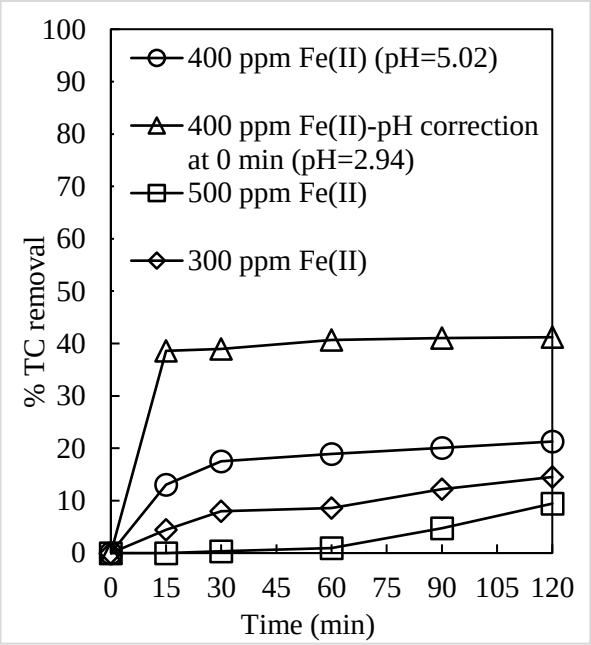

Figure 4.16: pH throughout the experiment in Fenton process ($[H_2O_2]_0$ = 6660 mg L^{-1})

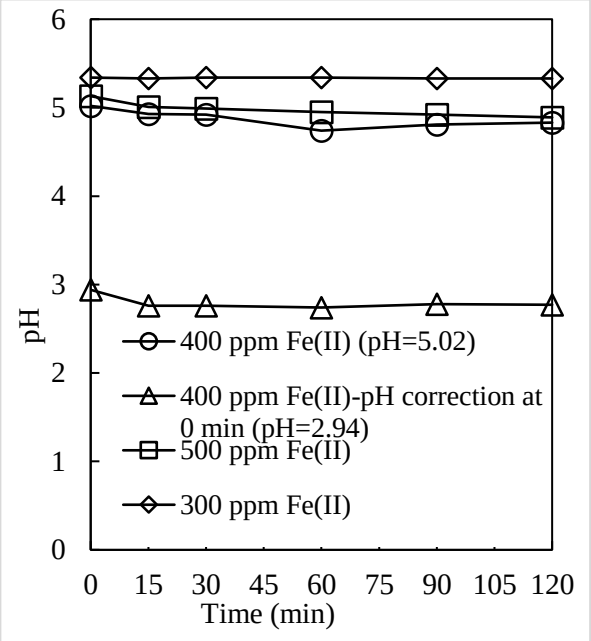

4.1.7 Landfill leachate treatment by Fenton-like process

All experiments were conducted using the same initial H_2O_2 dosage (6660 mg L^{-1}) and different initial Fe(III) amounts (500-800 ppm). An increase in the rate of decomposition is observed with an increase in the initial concentration of Fe(III) from 500 ppm to 800 ppm, which results in 58% and 70% removal of TC,

respectively. However, the difference in TC removal between 700 and 800 ppm of Fe(III) was only 2%, therefore, a higher concentration was not tested.

The effect of initial pH value was also studied, and 600 ppm of Fe(III) and 6660 mg L^{-1} were used. The initial pH without any pH adjustment was 5.11. As with photo-Fenton, changing the initial pH value did not improve the treatment. The initial pH was adjusted to 2.96, 4.06 and 6.62, which resulted in 55, 59 and 63% TC conversions, respectively, compared with 63.24% for the process without pH adjustment (pH 5.11). pH value was increased to 6.62 by addition of NaOH. Summary of these experiments is shown in *Figure 4.17* and *Figure A.9* (colour change).

Figure 4.17: TC removal by Fenton-like process ($[H_2O_2]_0$ = 6660 mg L^{-1})

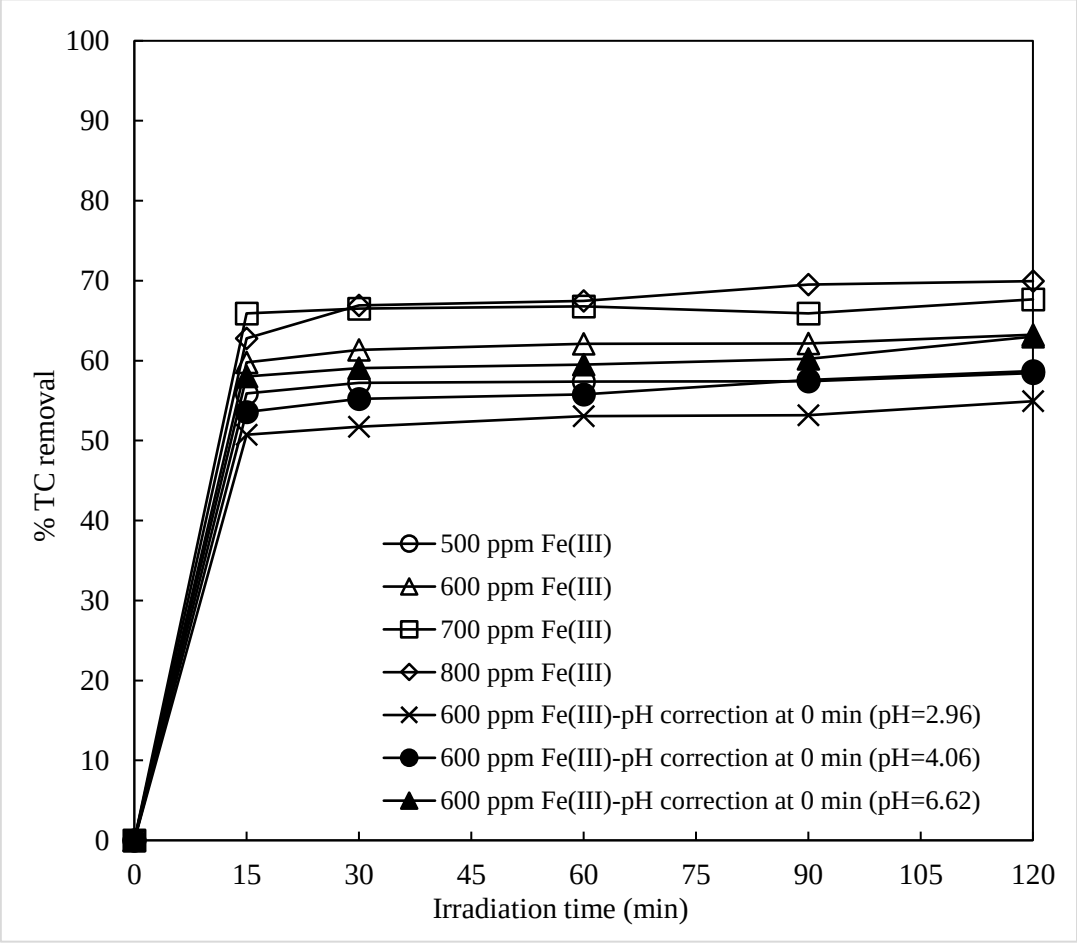

4.1.8 Effect of the process used: Fenton, UV-H_2O_2, photo-Fenton and photo-Fenton-like

This section is devoted to the comparison of the processes used to summarize all findings, specifically, the efficiency of photo-Fenton process was compared with several H_2O_2-based AOPs: UV-H_2O_2, classical Fenton, photo-Fenton and photo-Fenton-like systems. 6660 mg L^{-1} of H_2O_2 and 400 ppm of iron were used. The results are shown in *Figures 4.18-4.19*.

Figure 4.18: Effect of the process used on TC removal ($[Fe]_0$ = 400 ppm, $[H_2O_2]_0$ = 6660 mg L^{-1})

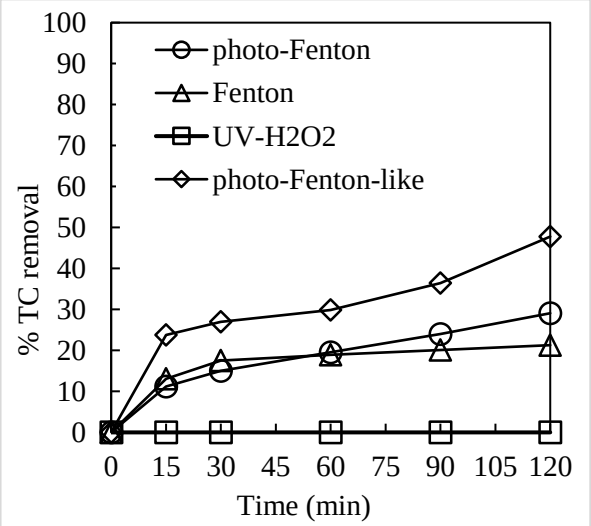

Figure 4.19: Effect of the process used on pH throughout the experiment ($[Fe]_0$ = 400 ppm, $[H_2O_2]_0$ = 6660 mg L^{-1})

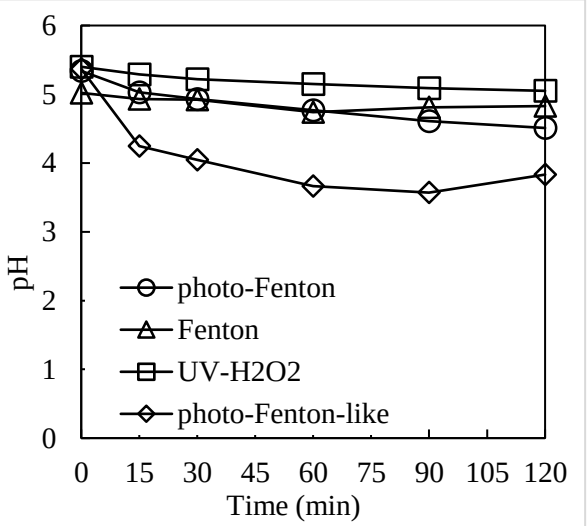

The UV-H_2O_2 treatment did not result in any TC removal, which is in contrast with the results obtained for simple solutions. Using classical Fenton process instead of photo-Fenton process led to a lower TC removal: from 29% to 21%. The application of UV light to the oxidation process has been reported to enhance the removal of pollutants [31]. The photo-Fenton-like process using ferric (Fe^{3+}) ions instead of ferrous (Fe^{2+}) was found to be the most effective approach among the ones applied since the highest TC removal was observed

(48%) along with the highest color removal. The results obtained during the experiments can be explained by chemical complexity of leachate, especially since the used landfill leachate was mature. According to Gogate and Pandit [54], the roles, the mechanisms of action, and the equilibrium concentration of ferrous and ferric ions are complex and unclear in details.

The greatest improvement in color also corresponds to the UV/ Fe^{3+}/H_2O_2 (photo-Fenton-like) process, as it shown in *Figures 4.20.*

Figure 4.20: UV-Vis analysis to observe the effect of the process used on colour change ($[Fe]_0$ = 400 ppm, $[H_2O_2]_0$ = 6660 mg L^{-1})

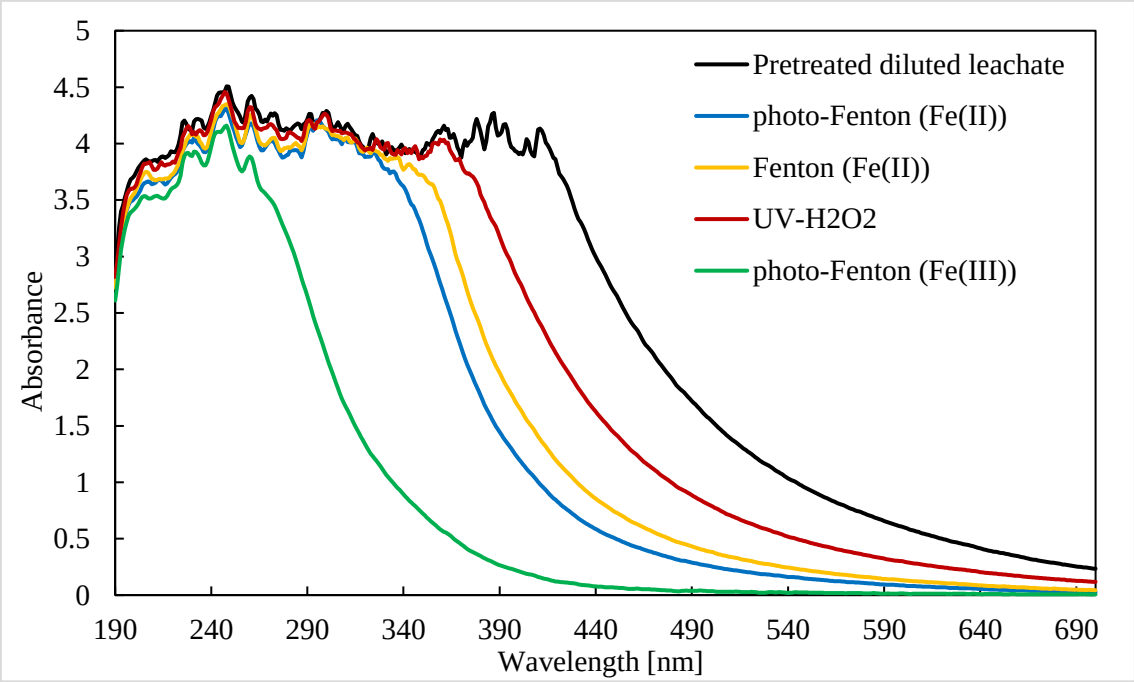

In total, five remediation techniques were examined for the treatment of landfill leachate: UV-H_2O_2, classical Fenton, Fenton-like, photo-Fenton and photo-Fenton-like systems. A pretreatment stage including air stripping and pH adjustment was required for ammonia and inorganic carbon removal before the chemical/photochemical treatment applied. The inorganic carbon removal is

critical for the success of next steps because it can act as hydroxyl radicals scavenger. Specifically, only 7.7% TC removal was observed in the presence of inorganic carbon, while 29% TC (equal to TOC) removal was achieved when the inorganic carbon was removed at the pretreatment step. No further TIC removal was noted for the experiment in the presence of inorganic carbon.

It is also worth noting that the TN value was unchanged throughout all experiments and remained in the range of 130-180 mg L^{-1}, depending on the value achieved after the pretreatment step. Hydroxyl radicals formed during the Fenton process, despite the rather strong oxidizing ability, cannot oxidize ammonia [32].

Foam appeared during pretreatment stage and experiments, as shown in the *Figure 4.21*. Adding antifoaming agents, such as amyl alcohol, is a possible solution to this problem [103].

Figure 4.21: An example of foaming during experiments

Foaming occurs because of carbon dioxide produced from carbonate substances at acidic pH and organic foaming agents in leachate, and results in the need for a much larger reactor volume [32].

In addition, iron sludge accumulates and must be removed at the end of the treatment with iron. The reason of iron sludge formation is conversion of Fe^{3+} to ferric-hydroxo complexes [32]. Nafion membranes, easily separated from the treated solutions, can be used to prevent iron sludge [31]. The sludge disposal should be included in the valuation of this process. All analyses were performed with filtered solutions.

As it was mentioned earlier, the colour improvement of leachate was noticed. The results of UV-Vis spectra for colour change are given in *Appendix A*. In addition, *Figure 4.22* presents the above observations for several experiments with photo-Fenton process.

Figure 4.22: The colour change for treatment of pretreated diluted leachate ($[H_2O_2]_0$ = 6660 mg L^{-1}): (a) pretreated diluted leachate, (b) UV-H_2O_2 process with 400 ppm of Fe(II), (c-g) photo-Fenton process in the range of 200-600 ppm of Fe(II), (h) photo-Fenton-like process with 400 ppm of Fe(III)

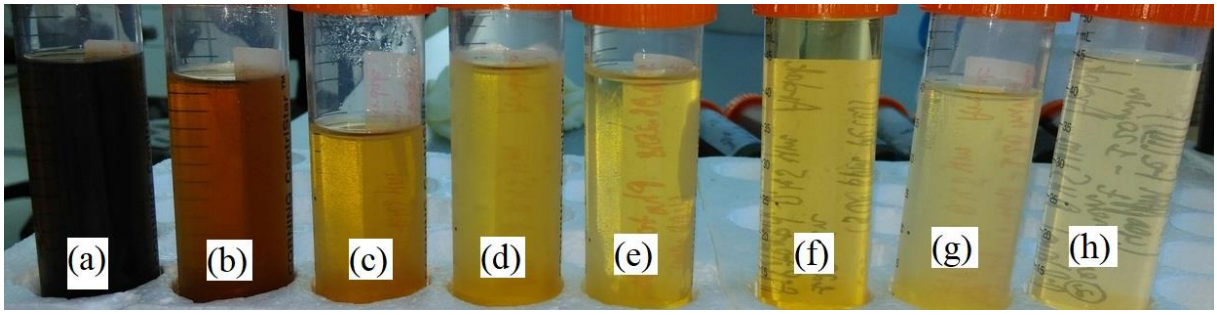

Young leachate contain large quantities of biodegradable organic compounds [74]. As leachate matures, refractory (non-biodegradable) substances, like humic and fulvic acids, dominate the organic fraction of the leachate [76]. The presence of humic acids leads to the dark colour of the leachate [104], and their molecular weight increases as leachate matures [105]. Large organic

compounds are converted into smaller molecules during the treatment process, which leads to colour improvement. Kim and Hugh [106] also observed an improvement in the color of the mature leachate through the Fenton process, resulting in a 92% decolorization efficiency.

4.2 Photocatalytic performance of Fe-doped TiO_2 for the degradation of 4-tert-butylphenol

The photocatalytic activities of the synthesized Fe-doped TiO_2 catalysts with different iron contents (Fe/Ti weight ratio percentage = 0.5%, 1%, 2% and 4%) was examined, 4-tert-butylphenol was used as a model pollutant. TiO_2 catalyst (P-25) was taken as a base catalyst for comparison. Each separate experiment was repeated two times and the average was taken using the standard error of the mean.

The catalysts were sonicated in water for 10 minutes just before use. Then, the aqueous solution containing 4-tertbutylphenol in concentration of 30 mg L^{-1} was mixed with 0.25 g of photocatalyst under constant magnetic stirring (the total volume of the solution was 250 mL). Before UV irradiation, this solution was stirred for 1 hour in the dark so that the system reached adsorption equilibrium. Each photocatalytic experiment on the mineralization of 4-tert-butylphenol lasted 60 minutes. 88.31 mg L^{-1} of H_2O_2 was used for experiments with a combination of hydrogen peroxide and catalyst (1 g L^{-1}).

4.2.1 Catalyst characterization

The structure and morphology of the fresh and used catalysts were determined using powder XRD and SEM. XRD patterns for P-25 and all Fe-doped TiO_2 are shown in *Figure 4.23*.

XRD pattern was recorded with Cu Kα radiation in the 2-theta angular range of 10 to 80°. The diffraction peaks at 2θ = 25.3°, 37.8°, 48.0°, 54.0°, and 55.1° are attributed to the anatase phase of TiO_2 (ICDD No. 86-1048, 86-1157). The diffraction peak at 2θ = 27.4° is attributed to the rutile phase of TiO_2 [107]. The XRD patterns are typical for TiO_2 phase, however, no crystalline iron-related phase was observed, even at the highest iron concentration. The same results were obtained in other studies [66,108]. This result can be explained by the fact that crystalline forms of Fe did not form on the material or that particles of amorphous iron oxides were very dispersed on the surface of TiO_2 particles [109]. The peak associated with iron cannot be observed in the XRD spectra when a low concentration of iron is in Fe-doped TiO_2 [108] or when a solid solution of iron-titanium is formed, which means that all iron ions are incorporated into the TiO_2 structures and replace titanium ion or is at interstitial site due to similar ionic radii (Ti (0.68 Å) and Fe (0.64 Å)) [66,108].

Figure 4.23: X-ray diffraction patterns for: (a) TiO_2, (b) Fe/TiO_2 (0.5%), (c) Fe/TiO_2 (1%), (d) Fe/TiO_2 (2%), (e) Fe/TiO_2 (4%)

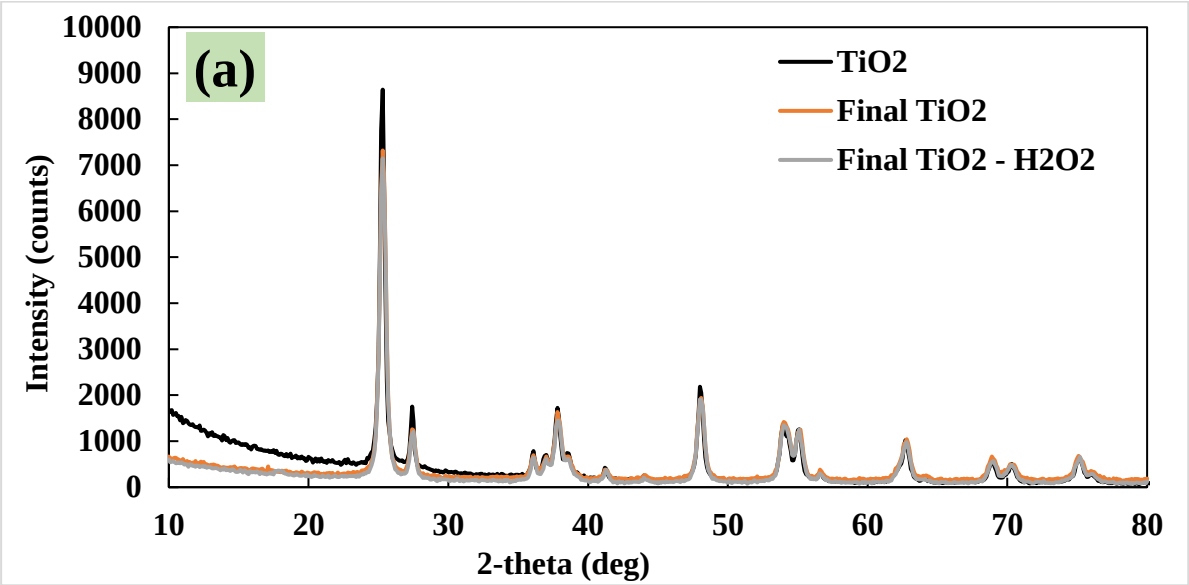

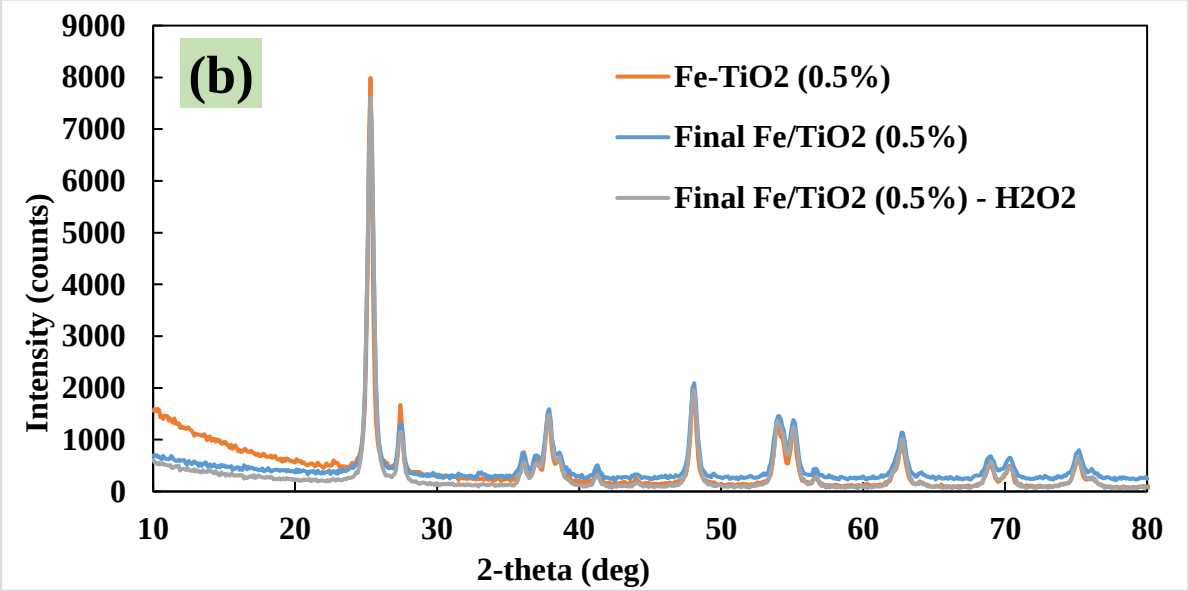

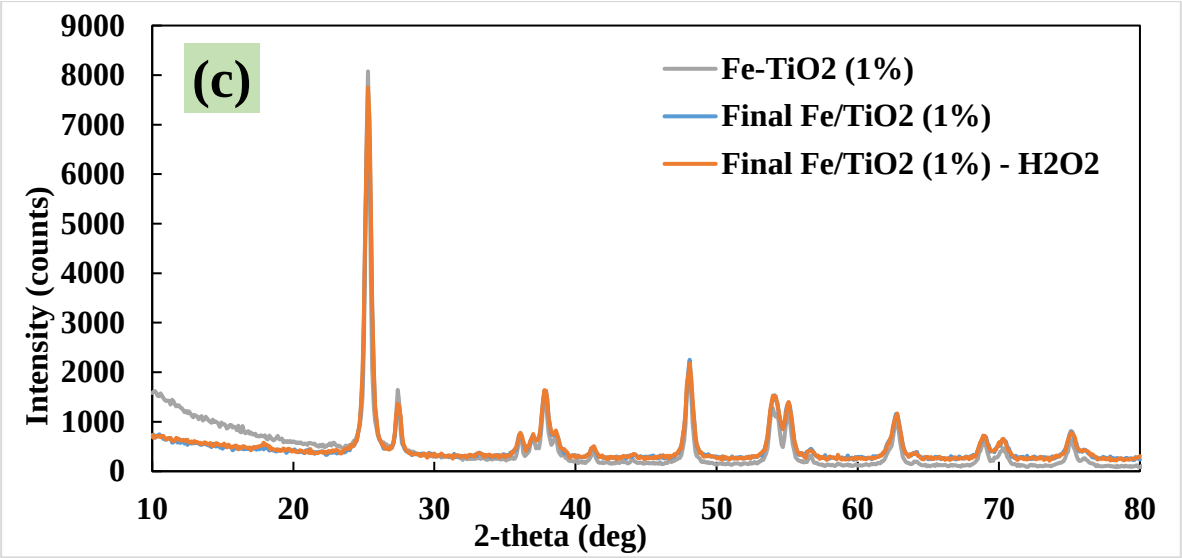
(c)
Fe-TiO2 (1%)
Final Fe/TiO2 (1%)
Final Fe/TiO2 (1%) - H2O2
Intensity (counts)
2-theta (deg)

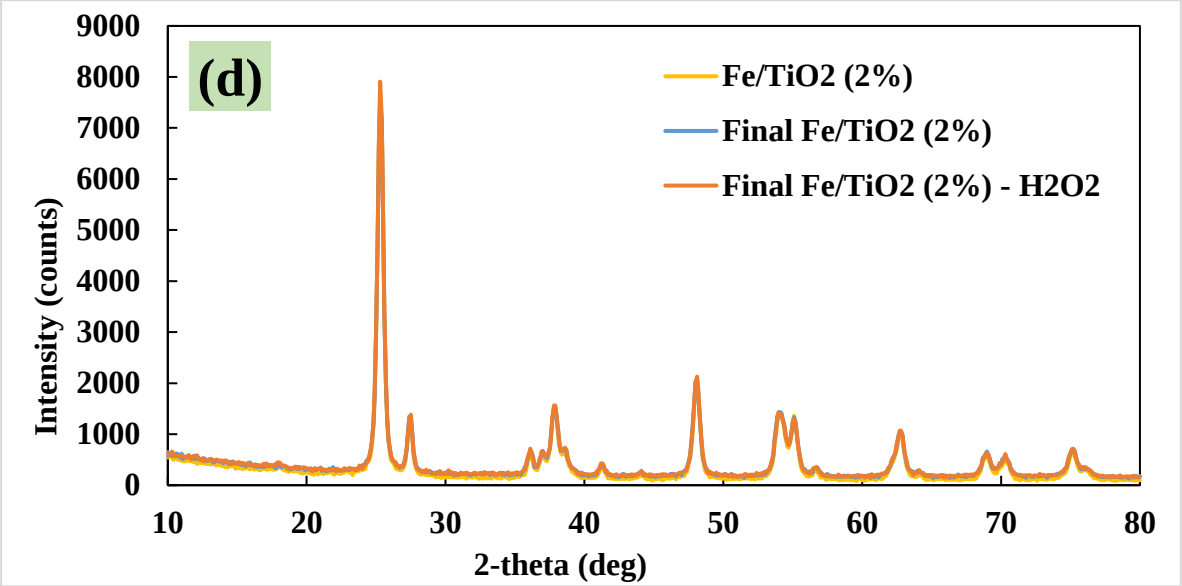
(d)
Fe/TiO2 (2%)
Final Fe/TiO2 (2%)
Final Fe/TiO2 (2%) - H2O2
Intensity (counts)
2-theta (deg)

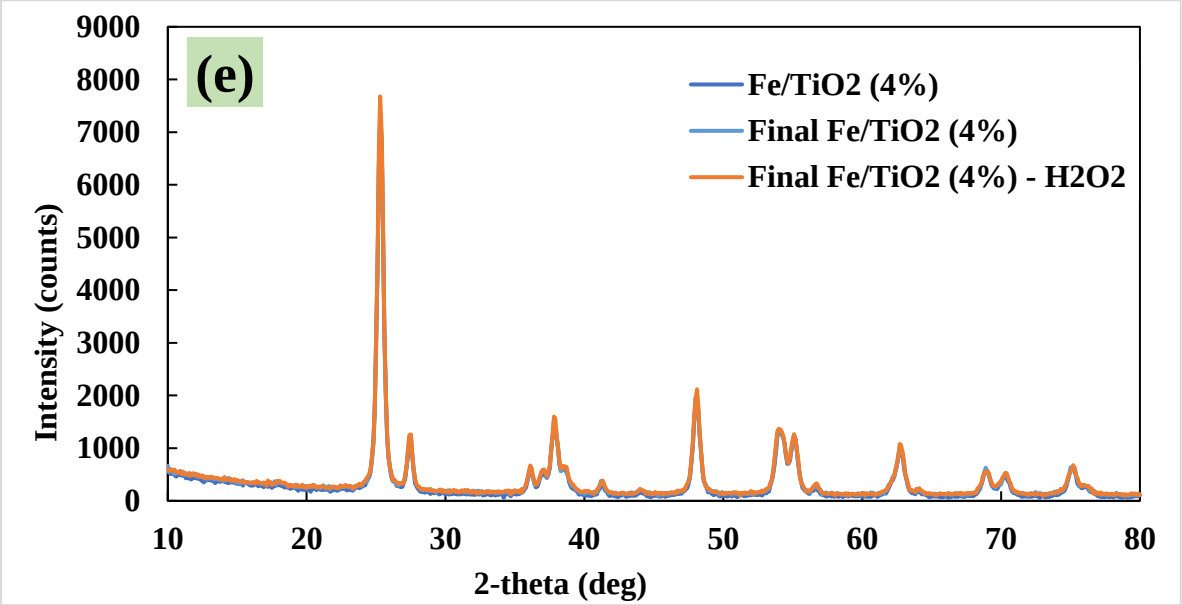
(e)
Fe/TiO2 (4%)
Final Fe/TiO2 (4%)
Final Fe/TiO2 (4%) - H2O2
Intensity (counts)
2-theta (deg)

EDS mapping of SEM analysis for all fresh and used catalysts are presented in *Appendix B*, and it showed spectra that provide information on the elements present and their quantities. A well-distributed iron phase on the surface of TiO_2 was observed for all Fe-doped TiO_2 catalysts.

In addition, X-ray diffraction and SEM analyses showed that the structures of synthesized Fe-doped TiO_2 catalysts remained intact after the photocatalytic reaction. Thus, it can be concluded that Fe-doped TiO_2 catalysts synthesized using the wet impregnation method are resistant to photocatalytic decomposition of organic pollutants, which is very important for their application.

The optical properties of fresh catalysts were measured using a UV-Vis spectroscopy in the wavelength range of 200 to 750 nm (*Figure 4.24*). The prepared Fe/TiO_2 catalysts had relatively the same absorption as base TiO_2, and only 4% Fe/TiO_2 showed a significantly higher absorption in the range of 200-365 nm.

Figure 4.24: The UV-Vis spectra of TiO_2 and Fe-TiO_2 with different iron doping concentrations

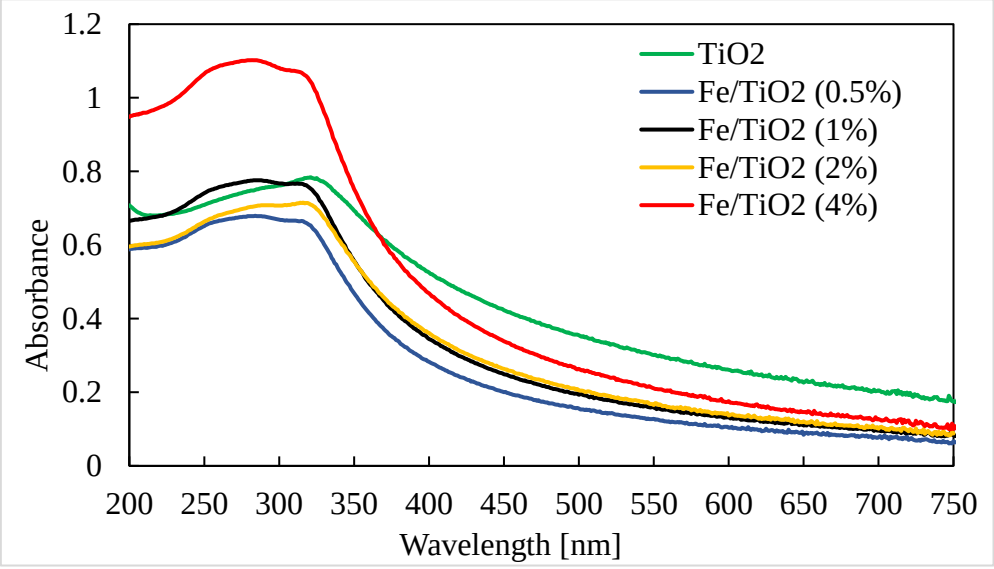

The shift of the absorption edge in 4% Fe/TiO_2 is explained by the transition of charge transfer between the d-electrons of the iron ion and the conduction or valence band of TiO_2 [110].

4.2.2 UV/Catalyst process

The overall reaction of photocatalytic degradation of 4-tert-butylphenol can be presented by *Equation 4.4*.

$$10\ C_{10}H_{14}O + 95\ O_2 \rightarrow 100\ CO_2 + 7H_2O \qquad (4.4)$$

Photocatalytic degradation of 4-tert-butylphenol by Fe-doped TiO_2 was measured by TC (*Figure 4.25*), HPLC (*Figure 4.26*) and UV-Vis analyses (*Figure 4.27*). For 0 minutes, the lamp turn-on time was taken.

Figure 4.25: TC removal of 4-t-BP by UV/TiO₂ and UV/Fe-TiO₂

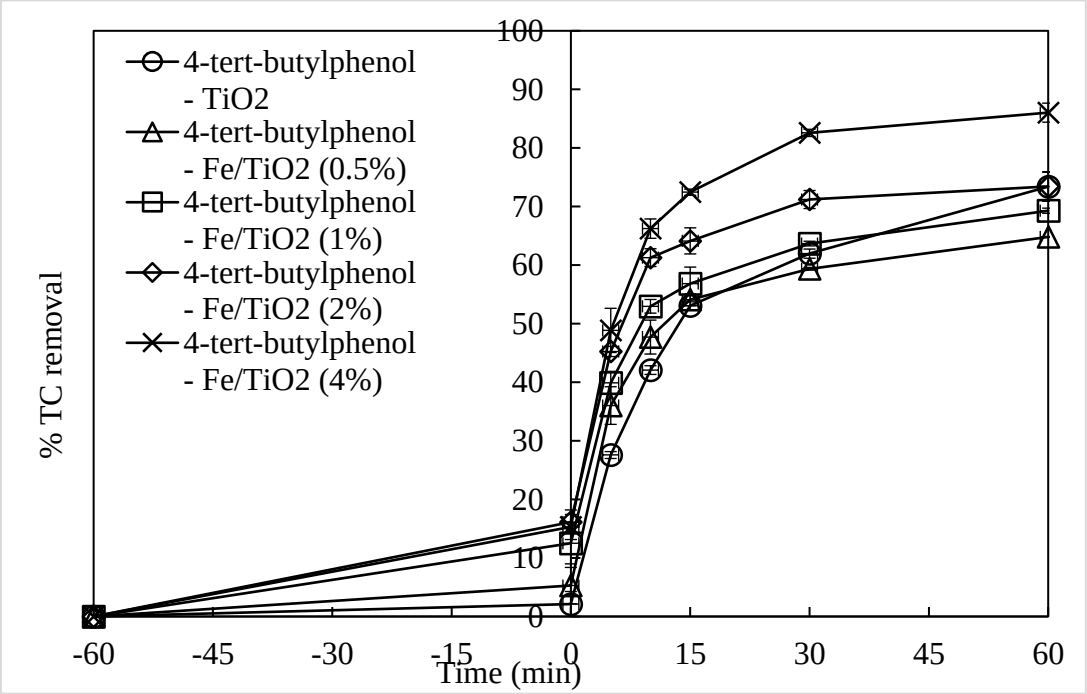

It can be observed that TC value decreased with time. After 60 min UV irradiation, 73% of the TC was eliminated by UV/TiO_2 process. The TC removal

increased with increasing iron doping concentration from 0.5% to 4%, resulting in 65% and 86%, respectively.

Using 2% Fe/TiO_2 led to the same TC removal as for TiO_2 (P-25), whereas 4% Fe/TiO_2 had a higher removal efficiency than TiO_2. UV-Vis spectra of 4% Fe/TiO_2 showed the highest absorption (*Figure 4.24*). Vargas et al. [64] also reported that synthesized Fe-doped TiO_2 had removal efficiencies similar to the commercial photocatalyst Degussa P25.

According to Zhu et al. [65], 0.40% Fe-TiO_2 showed a higher photoactivity than undoped TiO_2 and P25 under UV irradiation, whereas 0.15% Fe-TiO_2 was more effective than TiO_2 and P25 when irradiated with visible light. Much more oxygen vacancies in the crystal lattice and on TiO_2 surface were introduced by doping with Fe^{3+}, and they stimulated H_2O adsorption, the formation of surface hydroxyl groups and photocatalytic activity [65].

Hydroxyl radical are generated during the photocatalytic processes due to absorption of light by photocatalyst (*Equation 2.17-2.19*) [53]. Oxidative degradation of organic compounds can occur through their reactions with hydroxyl and peroxide radicals, valence band holes, and reductive splitting through their reactions with electrons [26].

4-tert-butylphenol was effectively mineralized by all studied catalysts (*Figure 4.26*).

Figure 4.26: HPLC results for 4-t-BP conversion by UV/TiO_2 and UV/Fe-TiO_2

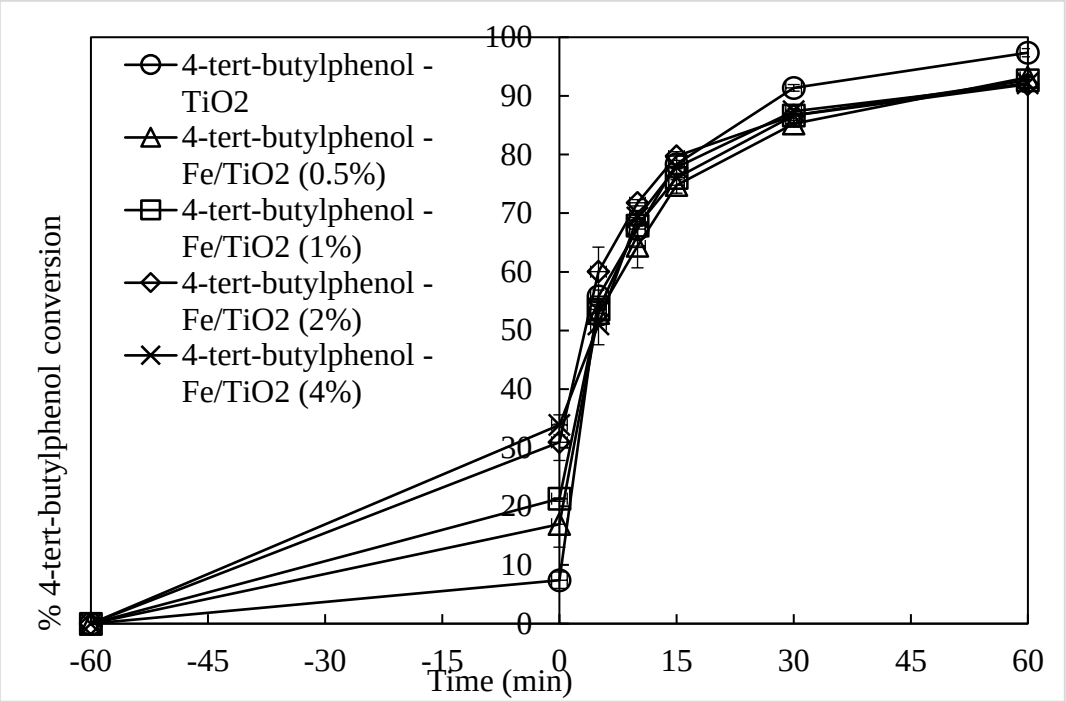

Maximum conversion of model pollutant was observed during UV/TiO_2 process, reaching 97%. Fe-doped TiO_2 had 92-93% conversion of 4-tert-butylphenol. The obtained high values for HPLC analysis, in contrast to the lower TC removal, are due to the formation of 4-t-BP intermediates, which were not completely decomposed to carbon dioxide and water. Thus, even if 4-t-BP is no longer in the solution, but its by-products are present, thereby being displayed in the TC. As it was mentioned in Section 2.5, the path of photodegradation of 4-t-BP in aqueous solution is not completely clear [91]. Various researchers have discovered the following by-products during 4-t-BP photodegradation: 2,4-di-tert-butylphenol [92], 4-tert-butylphenol dimer [91,92], 4-tert-butylcatechol [86,91], isobutyl acetate [88], butyl acetate [88], ethylbenzene [88], 3,3-dimethyl-2-butanone [86], pyruvic acid [86], 6-tert-butyl-3-methylanisole [91], benzene-

1,4-diol [91], and 2-nonen-1-ol, 2-decen-1-ol, 2-dodecenal from the breakdown of the benzene ring [91].

In the solution, there is a competition between pollutants and formed intermediate compounds for oxidizing agents, which reduces the rate of decomposition of 4-t-BP and the TC removal; similar results were observed in other studies [111].

Slow TC removal and 4-t-BP conversion after 15 minutes can be explained by the fact that the active sites of catalysts were occupied by organics [112].

Figure 4.27 shows the UV-Vis absorption data of the 4-t-BP in aqueous solution after the remediation process. These results are consistent with the results obtained with the HPLC analysis.

Figure 4.27: UV-Vis absorption spectra of 4-t-BP in aqueous solution after UV/ TiO_2 and UV/Fe-TiO_2 processes

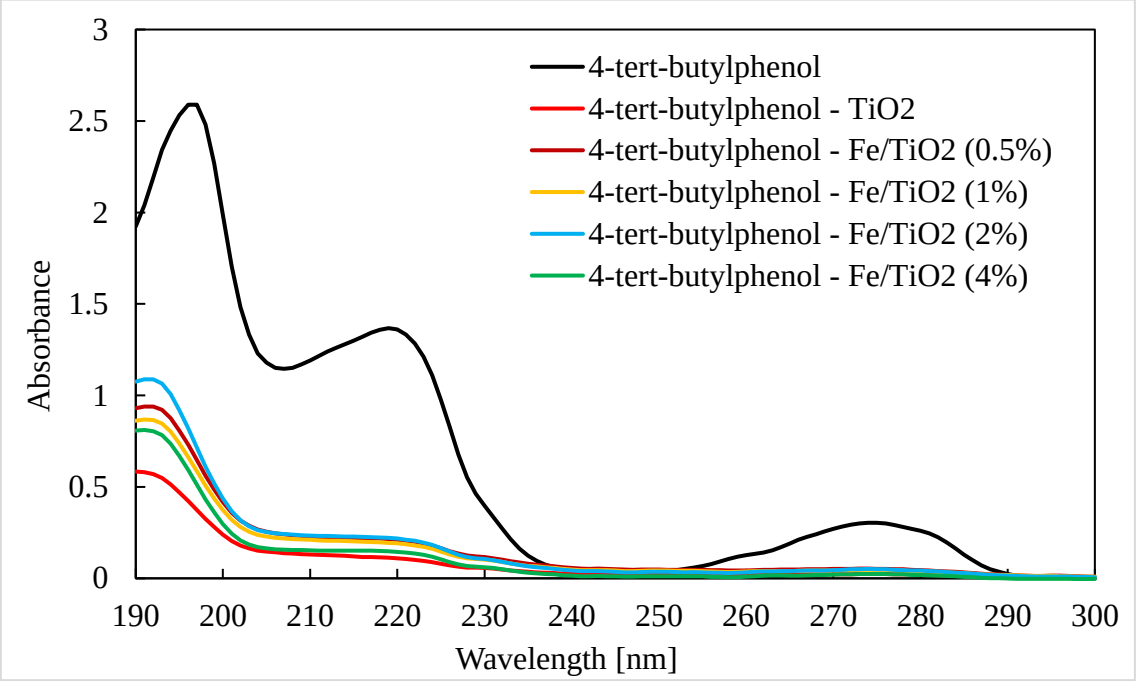

The initial pH of the solution was around 6.3, and the change in pH throughout the experiments was also measured and shown in *Figure 4.28.*

The pH of the solution affects the rate of photocatalytic oxidation. The reaction rate increases at lower pH for weakly acidic contaminants [57], and at higher pH for contaminants that hydrolyze in alkaline medium [58]. At the same time, Wei and Wan [59] noticed that a pH of less than 2 does not favour photocatalytic oxidation of phenol. The rate of phenol decomposition increases with increasing pH and reaches its maximum at pH ~ 6.5. The rate of phenol oxidation decreases quickly with a further increase in the pH value, and then increases again when the pH value is above 11.

Figure 4.28: pH value throughout UV/ TiO_2 and UV/Fe-TiO_2 processes

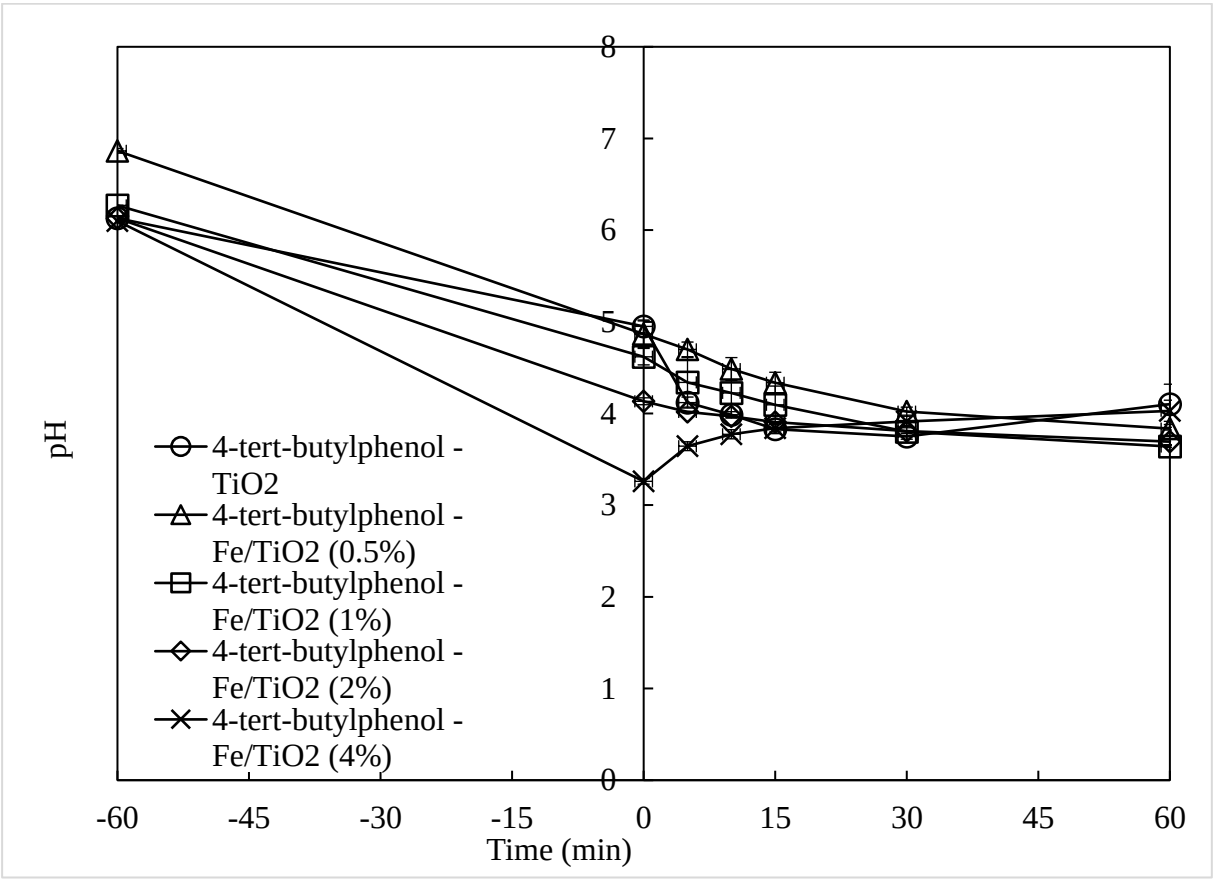

4.2.3 UV/H_2O_2 and UV/H_2O_2/Catalyst processes

The combination of catalysts, hydrogen peroxide and UV irradiation was also investigated on degradation of 4-tert-butylphenol. The results (*Figures 4.29-32)* showed that such combination does not improve the performance of the process.

Initially, a photochemical process with UV/H_2O_2 was tested, and 31% TC removal and 100% 4-t-BP decomposition (after 30 minutes) were obtained. Then, H_2O_2/TiO_2 was examined in the dark. After two hours of treatment in the dark, the results showed 0% TC removal and 4-t-BP conversion, as the source of UV light is needed for TiO_2 [53]. It can be noted that regardless of the Fe doping concentration, all Fe/TiO_2 catalysts showed TC removal in the range of 58-61%. The best TC removal was achieved using TiO_2 and was 74%.

Figure 4.29: TC removal of 4-t-BP by UV/H_2O_2, UV/H_2O_2/TiO_2 and UV/H_2O_2/Fe-TiO_2

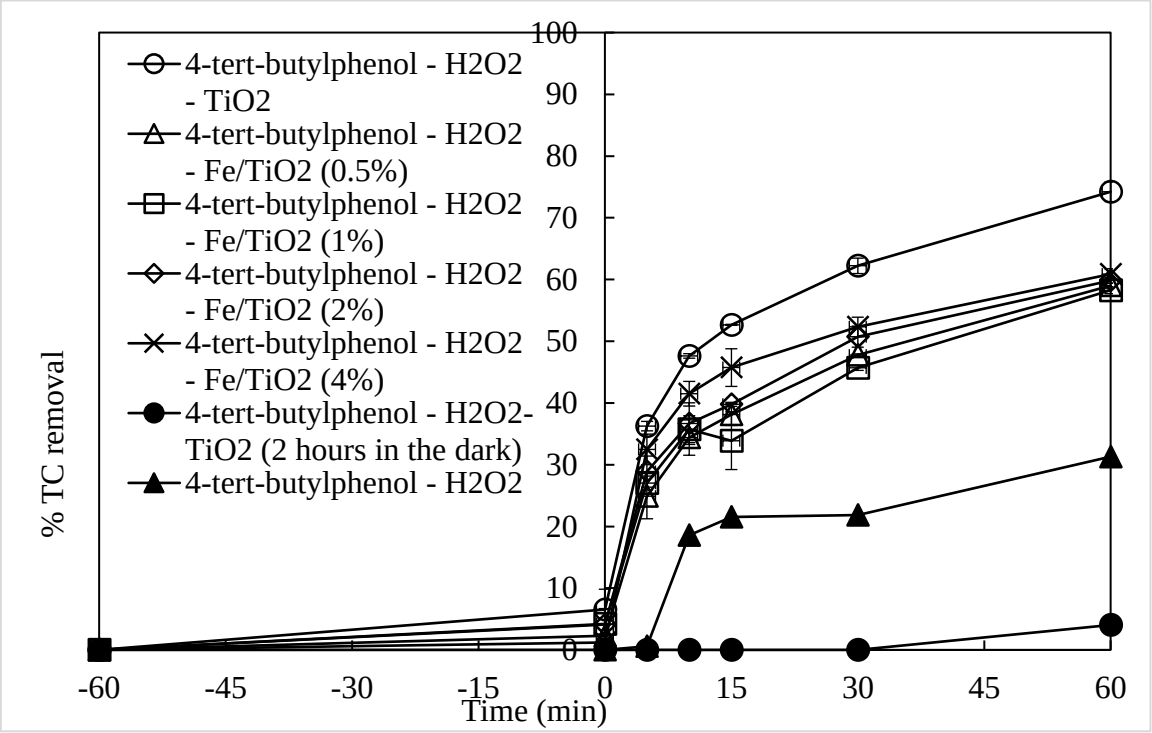

The HPLC results showed that an increase in iron doping concentration led to a decrease in 4-t-BP conversion by UV/H_2O_2/Fe-TiO_2 processes, namely, it decreased from 95%, which corresponded to 0.5% Fe-TiO_2, to 87%, which corresponded to 4% Fe-TiO_2. During UV/H_2O_2/TiO_2, 98% conversion of 4-tert-butylphenol was achieved. The UV-Vis absorption data of the 4-t-BP in aqueous solution after the UV/H_2O_2/Fe-TiO_2, UV/H_2O_2/TiO_2 and UV/H_2O_2 processes are consistent with the results obtained with the HPLC analysis.

Figure 4.30: HPLC results for 4-t-BP conversion by UV/H_2O_2, UV/H_2O_2/TiO_2 and UV/H_2O_2/Fe-TiO_2

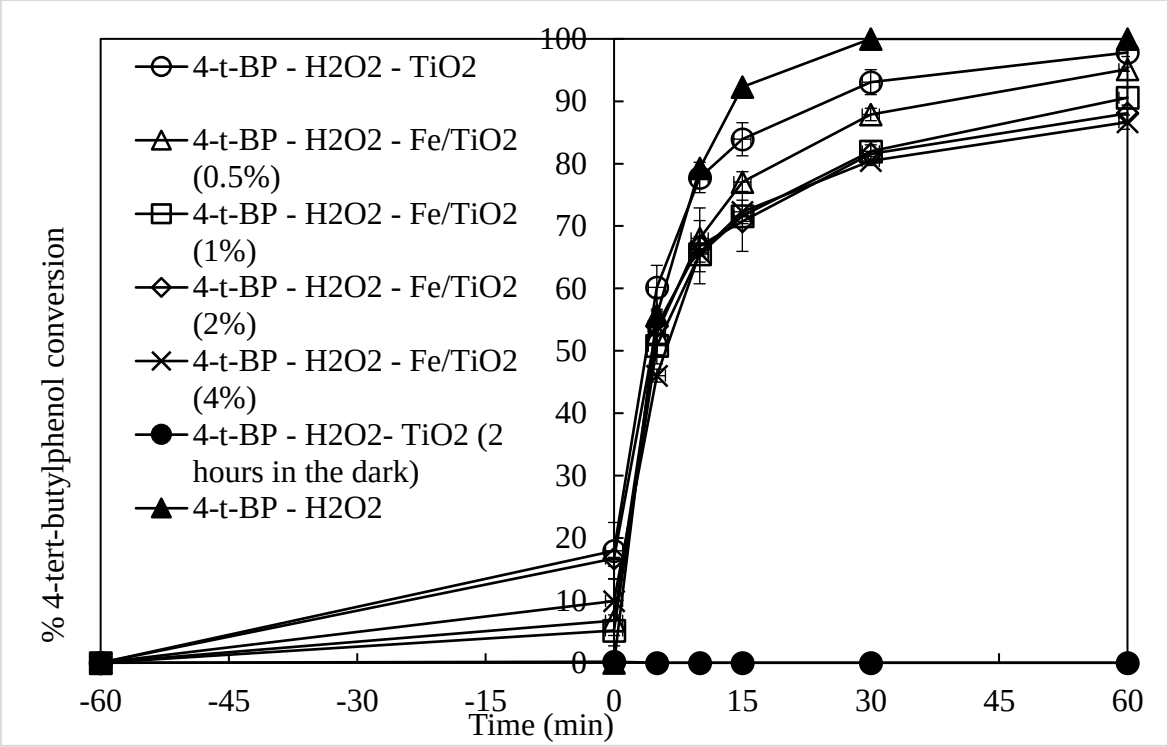

Figure 4.31: UV-Vis absorption spectra of 4-t-BP in aqueous solution after UV/H_2O_2, UV/H_2O_2/TiO_2 and UV/H_2O_2/Fe-TiO_2

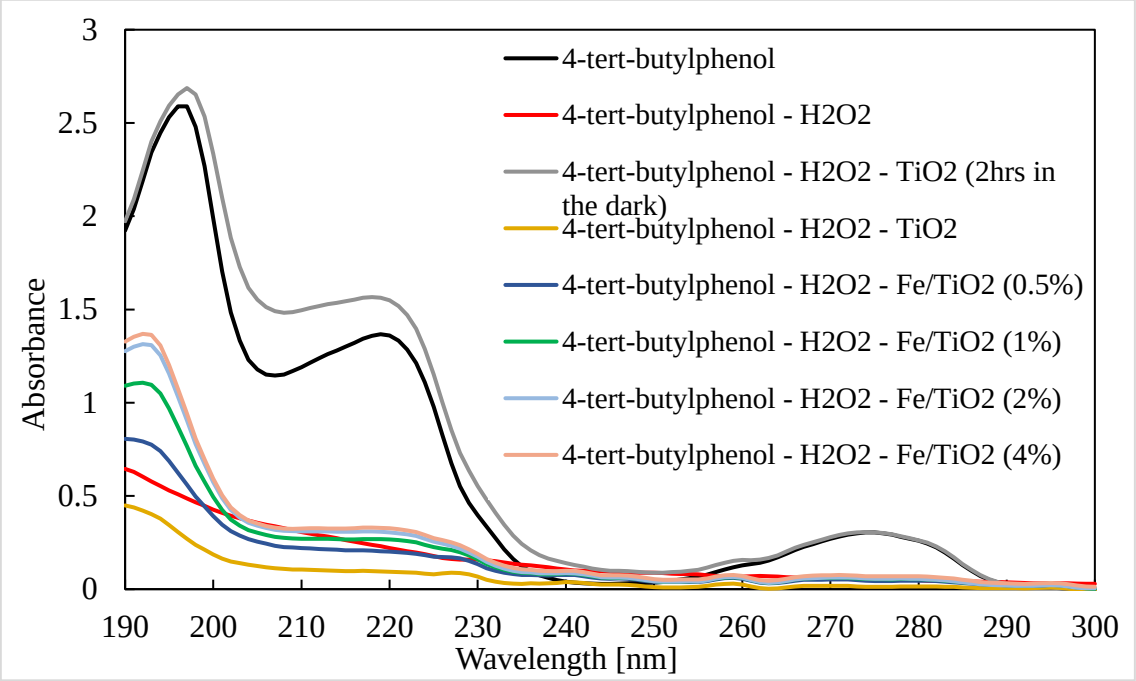

Figure 4.32: pH value throughout UV/H_2O_2, UV/H_2O_2/TiO_2 and UV/H_2O_2/Fe-TiO_2 processes

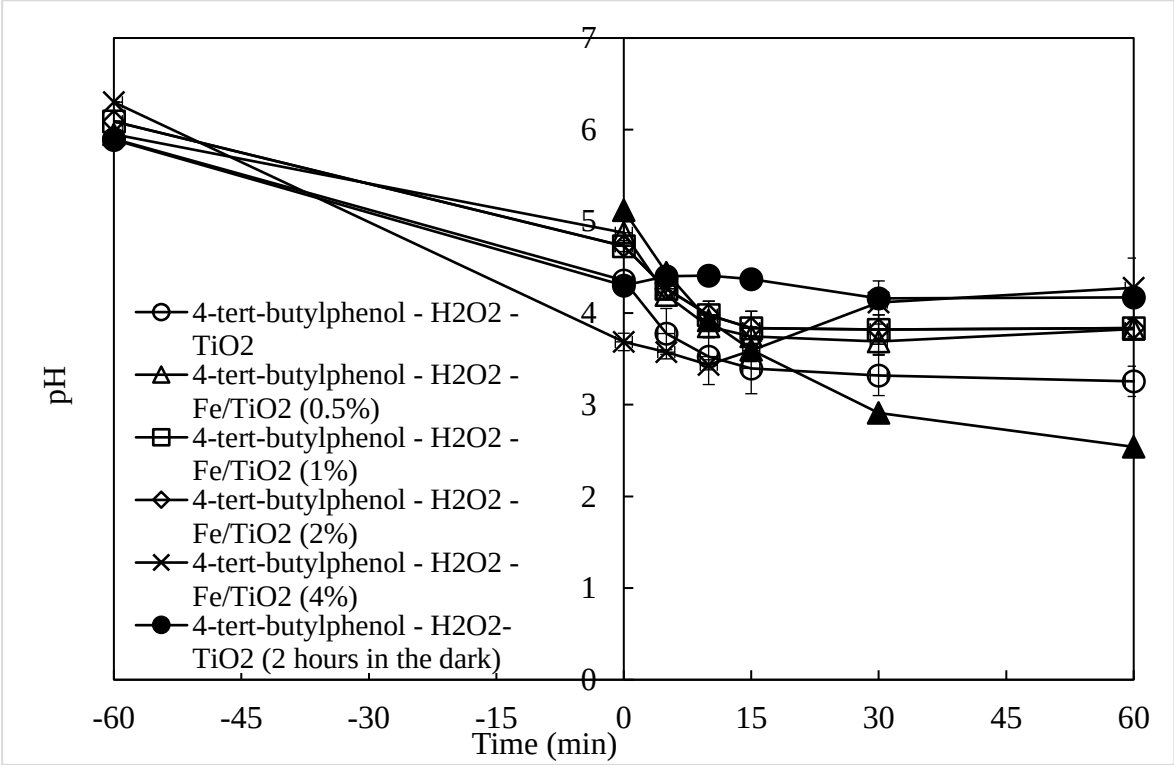

The results of previously published papers on the efficiency of combining hydrogen peroxide with a catalyst under UV irradiation are contradictory. Some

reported that this combination increased the efficiency of the process, since UV light was combined with both the oxidant and the photocatalyst [113], while others claimed that the efficiency of the process was reduced due to competition for ultraviolet irradiation between the oxidant and the photocatalyst [114] or H_2O_2 adsorption on the surface of catalytic particles, which reduces the activity of the catalyst [115]. In addition, the reason that the treatment was not enhanced by the addition of hydrogen peroxide may be that hydrogen peroxide was consumed at the beginning, since its concentration was low, it was used to oxidize iron, and the rest of the organic matter was removed using a catalyst [111].

4.2.4 Summary of the results obtained for experiments with catalysts

The all experimental results for the TC removal of water containing 4-tert-butylphenol as pollutant are presented in *Figure 4.33*. The HPLC results for 4-tert-butylphenol conversion are shown in *Figure 4.34.* The obtained high values for HPLC analysis, in contrast to the lower TC removal, are due to the formation of 4-t-BP intermediates, which were not completely decomposed to carbon dioxide and water. In the solution, there is a competition between pollutants and formed intermediate compounds for oxidizing agents, which reduces the rate of decomposition of 4-t-BP and the TC removal.

Figure 4.33: Summary of TC removal achieved by UV/Catalyst and UV/H_2O_2/Catalyst processes

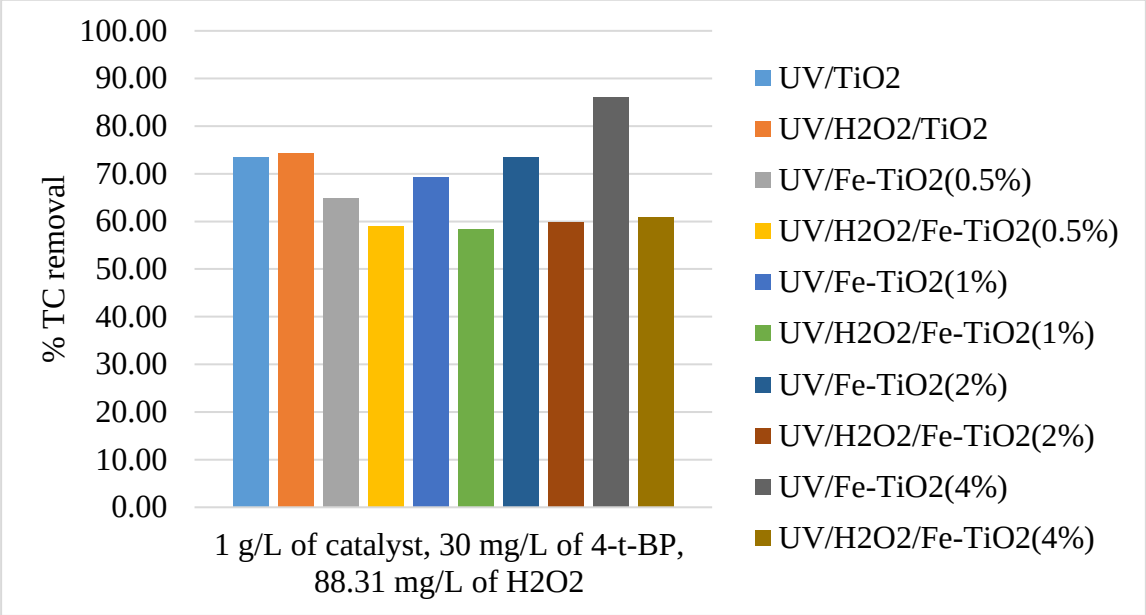

Figure 4.34: Summary of 4-t-BP conversion achieved by UV/Catalyst and UV/H_2O_2/Catalyst processes

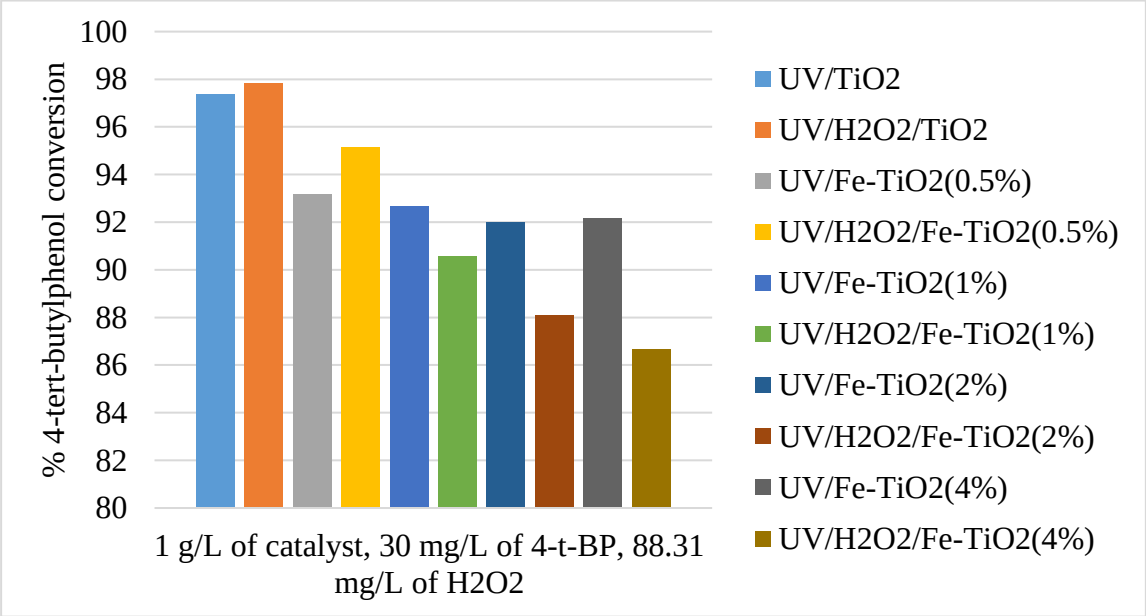

Vargas et al. [64] reported that synthesized Fe-doped TiO_2 had removal efficiencies similar to the commercial photocatalyst Degussa P25, which is consistent with the results obtained.

It should also be noted that 31% TC removal and 100% 4-t-BP decomposition (after 30 minutes) were obtained by UV/H_2O_2 process. After two

hours of treatment in the dark, the results showed 0% TC removal and 4-t-BP conversion by H_2O_2/TiO_2 , as the source of UV light is needed for TiO_2 [53].

The HPLC equipment used to analyze the amount of 4-tert-butylphenol present in the samples could not identify the specific by-products of 4-tert-BP; other apparatus should be used for this purpose, for example GCMS (Gas chromatography mass spectroscopy).

Thus, IC analysis was conducted to check the content of organic acids, such as acetic acid and formic acid, as they may be possible intermediates. The results are summarized in *Table 4.1* and they confirmed the formation of acetic and formic acids during the photocatalytic oxidation of 4-tert-butylphenol. This is the only analysis used to identify intermediate products due to the lack of necessary laboratory equipment.

Table 4.1: Content of acetic and formic acids by IC analysis

Sample		Concentration, mg/L	
		Acetate	**Formate**
4-tert-butylphenol	TiO_2	2.195	0.304
	Fe/TiO_2 (0.5%)	0.904	0.656
	Fe/TiO_2 (1%)	1.009	0.43
	Fe/TiO_2 (2%)	0.238	0.292
	Fe/TiO_2 (4%)	0.021	0.14
	H_2O_2	2.851	1.446
	H_2O_2 - TiO2	2.471	0.361
	H_2O_2 - Fe/TiO_2 (0.5%)	1.785	0.898
	H_2O_2 - Fe/TiO_2 (1%)	1.371	0.833
	H_2O_2 - Fe/TiO_2 (2%)	0.929	0.594
	H_2O_2 - Fe/TiO_2 (4%)	0.622	0.404

In addition, the iron content in the solution (Fe leaching) after 1 hour in the dark (0 min) and after the completion of the whole experiment (60 min) was determined using AAS. The results are summarized in *Table 4.2*. Fe leaching occurred for 4% Fe/TiO_2. It is worth noting that this is the only catalyst, which had the absorption in UV-Vis spectra and TC removal in the case of UV/Catalyst process higher than TiO_2.

Table 4.2: Fe leaching by AAS analysis

Sample	Average concentration, mg/l
Fe/TiO_2 (4%) 0 min	0.01
Fe/TiO_2 (4%) 60 min	0.14
Fe/TiO_2 (2%) 60 min	0.01
Fe/TiO_2 (1%) 60 min	0.00
Fe/TiO_2 (0.5%) 60 min	0.01
H_2O_2 - Fe/TiO_2 (4%) 0 min	0.40
H_2O_2 - Fe/TiO_2 (2%) 0 min	0.03
H_2O_2 - Fe/TiO_2 (1%) 0 min	0.02
H_2O_2 - Fe/TiO_2 (0.5%) 0 min	0.03
H_2O_2 - Fe/TiO_2 (4%) 60 min	0.23
H_2O_2 - Fe/TiO_2 (2%) 60 min	0.05
H_2O_2 - Fe/TiO_2 (1%) 60 min	0.04
H_2O_2 - Fe/TiO_2 (0.5%) 60 min	0.04

Chapter 5 - Conclusion

In this work, the photo-Fenton, photo-Fenton-like, UV-H_2O_2, classical Fenton and Fenton-like processes were used to treat the leachate generated at the municipal solid waste landfill in Astana (Kazakhstan). This type of wastewater is today left untreated in the landfill. The effectiveness of each process was evaluated by means of carbon and color removal. In addition, the efficiency of the synthesized Fe-doped TiO_2 catalysts with different iron contents (Fe/Ti weight ratio percentage = 0.5%, 1%, 2% and 4%) was examined to remove 4-tert-butylphenol under ultraviolet light. The combination of catalysts, hydrogen peroxide and UV irradiation was also investigated for the decomposition of 4-tert-butylphenol. The main conclusions are the following:

a) A pretreatment stage including air stripping and pH adjustment was required for ammonia and inorganic carbon removal before the chemical/photochemical processes applied. The inorganic carbon removal is critical for the success of next steps because it can act as hydroxyl radicals scavenger. Specifically, only 7.7% TC removal was observed in the presence of inorganic carbon, while 29% TC (equal to TOC) removal was achieved when the inorganic carbon was removed at the pretreatment step.

b) The most favourable concentrations of H_2O_2 and Fe(II) for carbon removal were 6660 mg L^{-1} and 400 ppm, respectively, resulting in 29% TC removal

during photo-Fenton process and 21% during Fenton process, while ammonia was not affected.

c) The photo-Fenton process can be significantly enhanced by replacing ferrous ions with ferric ions. Specifically, using 600 ppm Fe(III) instead of Fe(II) in the presence of 6660 mg L^{-1} of H_2O_2 and UV light increased the color removal as well as the TC removal from 27% to 69.5%. The most favourable concentration of H_2O_2 for carbon removal with Fe(III) was also 6660 mg L^{-1}.

d) The most favorable initial pH value for photo-Fenton and Fenton was found to be around 3.0 as it resulted in 44% of TC removal during photo-Fenton process and 41% during Fenton process. The effect of initial pH value was also studied for photo-Fenton-like and Fenton-like processes, 600 ppm of Fe(III) and 6660 mg L^{-1} were used. For both processes with Fe(III), changing the initial pH value did not improve the treatment.

e) An improvement in the color of the leachate was observed during all processes.

f) The whole process of landfill leachate treatment including pretreatment and the best photochemical process (600 ppm Fe(III) and 6660 mg L^{-1} of H_2O_2) resulted in 93.4% TC removal, 100% TIC removal, 88.7% TOC removal, 96.5% TN removal and 98.2% colour removal (at 450 nm).

g) A well-distributed iron phase on the surface of TiO_2 was observed for all Fe-doped TiO_2 catalysts during EDS mapping. X-ray diffraction and SEM

analyses showed that the structures of synthesized Fe-doped TiO_2 catalysts remained intact after the photocatalytic reaction.

h) Maximum conversion of model pollutant was observed during UV/TiO_2 process, reaching 97%. Fe-doped TiO_2 catalysts had 92-93% conversion of 4-tert-butylphenol. The obtained high values for HPLC analysis, in contrast to the lower TC removal, are due to the formation of 4-t-BP intermediates.

i) Acetic and formic acids were formed during the photocatalytic oxidation of 4-tert-butylphenol.

j) The combination of catalysts, hydrogen peroxide and UV irradiation did not improve the performance of the removal.

k) Fe leaching occurred for 4% Fe/TiO_2. This is the only catalyst, which had the absorption in UV-Vis spectra and TC removal in the case of UV/Catalyst process higher than TiO_2, specifically, 4% Fe/TiO_2 had 86% TC removal in contrast 73% achieved with TiO_2.

Future work will include a study of the effectiveness of the combined photochemical, biological and membrane treatment of the leachate. In particular, the effluent from the photochemical treatment can be directed to biological and/or membrane processing in order to see the additional effect of the biological decomposition of organic compounds. As for the Fe-doped TiO_2 catalysts, the effectiveness of the catalysts can be tested by other model pollutants or a combination of several pollutants. In addition, TiO_2 can be doped with other metals.

Bibliography/References

[1] Woodard F. Fundamentals. Ind. Waste Treat. Handb., Woodard & Curran, Inc.; 2006, p. 29–49. doi:10.1016/B978-075067963-3/50004-7.

[2] Akpor OB, Otohinoyi DA, Olaolu TD, Aderiye BI. Pollutants in wastewater effluents: impacts and remediation processes. Int J Environ Res Earth Sci 2014;3:50–9.

[3] Davies PS. The biological basis of wastewater treatment. Glasgow, Scotland: Strathkelvin Instruments Ltd; 2005.

[4] Akpor O, Muchie M. Environmental and public health implications of wastewater quality. African J Biotechnol 2013;10:2379–87. doi:10.5897/AJB10.1797.

[5] Zhang Z, Hou Z, Yang C, Ma C, Tao F, Xu P. Degradation of n-alkanes and polycyclic aromatic hydrocarbons in petroleum by a newly isolated Pseudomonas aeruginosa DQ8. Bioresour Technol 2011;102:4111–6. doi:10.1016/j.biortech.2010.12.064.

[6] Saeed S, Shaker IM. Assessment of heavy metals pollution in water and sediments and their effect on Oreochromis niloticus in the Northern Delta Lakes, Egypt. 8th Int. Symp. Tilapia Aquac., 2008, p. 475–89. doi:10.1007/s12012-007-0018-0.

[7] Krishnan S, Rawindran H, Sinnathambi CM, Lim JW. Comparison of various advanced oxidation processes used in remediation of industrial wastewater laden with recalcitrant pollutants. IOP Conf Ser Mater Sci Eng 2017;206. doi:10.1088/1757-899X/206/1/012089.

[8] Woodard F. Methods for Treating Wastewaters from Industry. Ind. Waste Treat. Handb. (Second Ed., Woodard & Curran, Inc.; 2006, p. 149–334. doi:10.1016/B978-075067963-3/50009-6.

[9] Sonune A, Ghate R. Developments in wastewater treatment methods. Desalination 2004;167:55–63. doi:10.1016/j.desal.2004.06.113.

[10] Davis ML. Water and wastewater engineering Design Principles and Practice. 2010. doi:10.1016/0016-0032(67)90545-5.

[11] Curley R. New Thinking About Pollution. The Rosen Publishing Group, Inc; 2010.

[12] Wang JL, Xu LJ. Advanced oxidation processes for wastewater treatment: Formation of hydroxyl radical and application. Crit Rev Environ Sci Technol 2012;42:251–325. doi:10.1080/10643389.2010.507698.

[13] Halliwell B. Drug Antioxidant Effects: A Basis for Drug Selection. Drugs 1991;42:569–605. doi:10.2165/00003495-199142040-00003.

[14] Tai C, Gu X, Zou H, Guo Q. A new simple and sensitive fluorometric method for the determination of hydroxyl radical and its application. Talanta 2002;58:661–7. doi:10.1016/S0039-9140(02)00370-3.

[15] Sharma S, Ruparelia J, Patel M. A general review on advanced oxidation processes for waste water treatment. Int Conf Curr Trends Technol 2011:8–10.

[16] Naddeo V, Rizzo L, Belgiorno V. Water, wastewater and soil treatment by advanced oxidation processes. 2011. doi:10.1073/pnas.96.12.6908.

[17] Oppenländer T. Photochemical Purification of Water and Air: Advanced Oxidation Processes (AOPs): Principles, Reaction Mechanisms, Reactor Concepts. 2003. doi:10.1002/9783527610884.

[18] Munter R. Advanced oxidation processes - current status and prospect. Proc Est Acad Sci Chem 2001;50:59–80. doi:10.1002/9780470561331.ch18.

[19] Neyens E, Baeyens J. A review of classic Fenton's peroxidation as an advanced oxidation technique. J Hazard Mater 2003;98:33–50. doi:10.1016/S0304-3894(02)00282-0.

[20] TechCommentary. Advanced Oxidation Processes for treatment of industrial wastewater. An EPRI Community Environmetal Center Publ.; 1996.
[21] Yao H. Application of advanced oxidation processes for treatment of air from livestock buildings and industrial facilities. Tech Rep BCE -TR-8 2013:36.
[22] García S, Hernández F, Aragón A, Rivera JA, Rueda R, Sostenible M. Photochemical Wastewater Treatment for Potential Agricultural Use. Curr World Environ 2014;9:663–9. doi:http://dx.doi.org/10.12944/CWE.9.3.15.
[23] Crissot F. Oxydation catalytique de compos´es organiques aqueux par le peroxyde d'hydrog`ene en phase h´et´erog`ene. University of Poitiers, Poitiers, France, 1996.
[24] Catalkaya EC, Kargi F. Color, TOC and AOX removals from pulp mill effluent by advanced oxidation processes: A comparative study. J Hazard Mater 2007;139:244–53. doi:10.1016/j.jhazmat.2006.06.023.
[25] Buxton G V., Greenstock CL, Helman WP, Ross AB. Critical Review of rate constants for reactions of hydrated electrons, hydrogen atoms and hydroxyl radicals in Aqueous Solution. J Phys Chem Ref Data 1988;17:513–886. doi:10.1063/1.555805.
[26] Stasinakis AS. Use of selected advanced oxidation processes (AOPs) for wastewater treatment - A mini review. Glob Nest J 2008;10:376–85. doi:10.1007/10_2013_251.
[27] Andreozzi R, Caprio V, Insola A, Marotta R. Advanced oxidation processes (AOP) for water purification and recovery. Catal Today 1999;53:51–9. doi:10.1016/S0920-5861(99)00102-9.
[28] Oturan MA, Aaron JJ. Advanced oxidation processes in water/wastewater treatment: Principles and applications. A review. Crit Rev Environ Sci Technol 2014;44:2577–641. doi:10.1080/10643389.2013.829765.
[29] Kusic H, Koprivanac N, Bozic AL. Minimization of organic pollutant content in aqueous solution by means of AOPs: UV- and ozone-based technologies. Chem Eng J 2006;123:127–37. doi:10.1016/j.cej.2006.07.011.
[30] Tarr M a. Chemical Degradation Methods for Wastes and Pollutants. 2003. doi:10.1201/9780203912553.
[31] Pignatello JJ, Oliveros E, MacKay A. Advanced oxidation processes for organic contaminant destruction based on the fenton reaction and related chemistry. Crit Rev Environ Sci Technol 2006;36:1–84. doi:10.1080/10643380500326564.
[32] Deng Y, Englehardt JD. Treatment of landfill leachate by the Fenton process. Water Res 2006;40:3683–94. doi:10.1016/j.watres.2006.08.009.
[33] Haber F. The catalytic decomposition of hydrogen peroxide by iron salts. Proc - R Soc Phys Eng Sci 1934;147:332–51. doi:10.1098/rspa.1934.0221.
[34] Brillas E, Sirés I, Oturan MA. Electro-fenton process and related electrochemical technologies based on fenton's reaction chemistry. Chem Rev 2009;109:6570–631. doi:10.1021/cr900136g.
[35] Safarzadeh-Amiri A, Bolton JR, Cater SR. Ferrioxalate-mediated photodegradation of organic pollutants in contaminated water. Water Res 1997;31:787–98. doi:10.1016/S0043-1354(96)00373-9.
[36] Kuo WG. Decolorizing dye wastewater with Fenton's reagent. Water Res 1992;26:881–6.
[37] Niaounakis M, Halvadakis CP. Chapter 2 Characterization of olive processing waste. Waste Manag. Ser., vol. 5, 2006, p. 23–64. doi:10.1016/S0713-2743(06)80004-8.
[38] Bautista P, Mohedano AF, Casas JA, Zazo JA, Rodriguez JJ. An overview of the application of Fenton oxidation to industrial wastewaters treatment. J Chem Technol Biotechnol 2008;83:1323–38. doi:10.1002/jctb.1988.
[39] Bokare AD, Choi W. Review of iron-free Fenton-like systems for activating H2O2in advanced oxidation processes. J Hazard Mater 2014;275:121–35.

doi:10.1016/j.jhazmat.2014.04.054.
[40] Ikehata K, El-Din MG. Degradation of recalcitrant surfactants in wastewater by ozonation and advanced oxidation processes: A review. Ozone Sci Eng 2004;26:327–43. doi:10.1080/01919510490482160.
[41] Pignatello JJ. Dark and photoassisted iron(3+)-catalyzed degradation of chlorophenoxy herbicides by hydrogen peroxide. Environ Sci Technol 1992;26:944–51.
[42] Malato S, Blanco J, Alarcón DC, Maldonado MI, Fernández-Ibáñez P, Gernjak W. Photocatalytic decontamination and disinfection of water with solar collectors. Catal Today 2007;122:137–49. doi:10.1016/j.cattod.2007.01.034.
[43] Bandala ER, Peláez MA, García-López AJ, Salgado M de J, Moeller G. Photocatalytic decolourisation of synthetic and real textile wastewater containing benzidine-based azo dyes. Chem Eng Process Process Intensif 2008;47:169–76. doi:10.1016/j.cep.2007.02.010.
[44] Sirtori C, Zapata A, Oller I, Gernjak W, Agüera A, Malato S. Solar photo-fenton as finishing step for biological treatment of a pharmaceutical wastewater. Environ Sci Technol 2009;43:1185–91. doi:10.1021/es802550y.
[45] Moraes JEF, Quina FH, Nascimento CAO, Silva DN, Chiavone-Filho O. Treatment of Saline Wastewater Contaminated with Hydrocarbons by the Photo-Fenton Process. Environ Sci Technol 2004;38:1183–7. doi:10.1021/es034217f.
[46] Primo O, Rivero MJ, Ortiz I. Photo-Fenton process as an efficient alternative to the treatment of landfill leachates. J Hazard Mater 2008;153:834–42. doi:10.1016/j.jhazmat.2007.09.053.
[47] Hermosilla D, Cortijo M, Huang CP. Optimizing the treatment of landfill leachate by conventional Fenton and photo-Fenton processes. Sci Total Environ 2009;407:3473–81. doi:10.1016/j.scitotenv.2009.02.009.
[48] Kondo MM, Leite KUCG, Silva MRA, Reis ADP. Fenton and photo-fenton processes coupled to uasb to treat coffee pulping wastewater. Sep Sci Technol 2010;45:1506–11. doi:10.1080/01496395.2010.487451.
[49] Thiruvenkatachari R, Vigneswaran S, Moon IS. A review on UV/TiO2photocatalytic oxidation process. Korean J Chem Eng 2008;25:64–72. doi:10.1007/s11814-008-0011-8.
[50] Bickley RI, Gonzalez-Carreno T, Lees JS, Palmisano L, Tilley RJD. A structural investigation of titanium dioxide photocatalysts. J Solid State Chem 1991;92:178–90. doi:10.1016/0022-4596(91)90255-G.
[51] Xu N, Shi Z, Fan Y, Dong J, Shi J, Hu M. Effects of particle size of TiO2 on photocatalytic degradation of methylene blue in Aqueous Suspensions. Ind Eng Chem Res 1999;38:373–9.
[52] Ahmad R, Ahmad Z, Khan AU, Mastoi NR, Aslam M, Kim J. Photocatalytic systems as an advanced environmental remediation: Recent developments, limitations and new avenues for applications. J Environ Chem Eng 2016;4:4143–64. doi:10.1016/j.jece.2016.09.009.
[53] Crittenden JC, Trussell RR, Hand DW, Howe KJ, Tchobanoglous G. Water Treatment: Principles and Design. 2nd ed. New Jersey: 2005.
[54] Gogate PR, Pandit AB. A review of imperative technologies for wastewater treatment I: Oxidation technologies at ambient conditions. Adv Environ Res 2004;8:501–51. doi:10.1016/S1093-0191(03)00032-7.
[55] Laoufi NA, Tassalit D, Bentahar F. The degradation of phenol in water solution by TiO2 photocatalysis in a helical reactor. Glob Nest J 2008.
[56] Herrmann JM. Heterogeneous photocatalysis: Fundamentals and applications to the removal of various types of aqueous pollutants. Catal Today 1999;53:115–29.

doi:10.1016/S0920-5861(99)00107-8.

[57] Andreozzi R, Caprio V, Insola A, Longo G, Tufano V. Photocatalytic oxidation of 4-nitrophenol in aqueous TiO2 slurries: An experimental validation of literature kinetic models. J Chem Technol Biotechnol 2000;75:131–6. doi:10.1002/(SICI)1097-4660(200002)75:2<131::AID-JCTB191>3.0.CO;2-F.

[58] Choi W, Hoffmann MR. Novel photocatalytic mechanisms for CHCl3, CHBr3, and CCl3CO2degradation and the fate of photogenerated trihalomethyl radicals on TiO2. Environ Sci Technol 1997;31:89–95. doi:10.1021/es960157k.

[59] Wei TY, Wan CC. Heterogeneous Photocatalytic Oxidation of Phenol with Titanium Dioxide Powders. Ind Eng Chem Res 1991;30:1293–300. doi:10.1021/ie00054a033.

[60] Chatterjee D, Dasgupta S. Visible light induced photocatalytic degradation of organic pollutants. J Photochem Photobiol C Photochem Rev 2005;6:186–205. doi:10.1016/j.jphotochemrev.2005.09.001.

[61] Song S, Tu J, Xu L, Xu X, He Z, Qiu J, et al. Preparation of a titanium dioxide photocatalyst codoped with cerium and iodine and its performance in the degradation of oxalic acid. Chemosphere 2008;73:1401–6. doi:10.1016/j.chemosphere.2008.08.032.

[62] Choi W, Termin A, Hoffmann MR. The role of metal ion dopants in quantum-sized TiO2: Correlation between photoreactivity and charge carrier recombination dynamics. J Phys Chem 1994;98:13669–79. doi:10.1021/j100102a038.

[63] Zhu J, Ren J, Huo Y, Bian Z, Li H. Nanocrystalline Fe/TiO2 visible photocatalyst with a mesoporous structure prepared via a nonhydrolytic sol-gel route. J Phys Chem C 2007;111:18965–9. doi:10.1021/jp0751108.

[64] Vargas XM, Juan MM, Restrepo G. Characterization and Photocatalytic Evaluation (UV-Visible) of Fe-doped TiO2 Systems Calcined at Different Temperatures. J Adv Oxid Technol 2015;18:129–38.

[65] Zhu J, Chen F, Zhang J, Chen H, Anpo M. Fe3+-TiO2 photocatalysts prepared by combining sol-gel method with hydrothermal treatment and their characterization. J Photochem Photobiol A Chem 2006;180:196–204. doi:10.1016/j.jphotochem.2005.10.017.

[66] Nasralla N, Yeganeh M, Astuti Y, Piticharoenphun S, Shahtahmasebi N, Kompany A, et al. Structural and spectroscopic study of Fe-doped TiO2 nanoparticles prepared by sol-gel method. Sci Iran 2013;20:1018–22. doi:10.1016/j.scient.2013.05.017.

[67] Sood S, Umar A, Mehta SK, Kansal SK. Highly effective Fe-doped TiO2 nanoparticles photocatalysts for visible-light driven photocatalytic degradation of toxic organic compounds. J Colloid Interface Sci 2015;450:213–23. doi:10.1016/j.jcis.2015.03.018.

[68] Asiltürk M, Sayilkan F, Arpaç E. Effect of Fe3+ion doping to TiO2 on the photocatalytic degradation of Malachite Green dye under UV and vis-irradiation. J Photochem Photobiol A Chem 2009;203:64–71. doi:10.1016/j.jphotochem.2008.12.021.

[69] Renou S, Givaudan JG, Poulain S, Dirassouyan F, Moulin P. Landfill leachate treatment: Review and opportunity. J Hazard Mater 2008;150:468–93. doi:10.1016/j.jhazmat.2007.09.077.

[70] Lin H, Peng W, Zhang M, Chen J, Hong H, Zhang Y. A review on anaerobic membrane bioreactors: Applications, membrane fouling and future perspectives. Desalination 2013;314:169–88. doi:10.1016/j.desal.2013.01.019.

[71] Kurniawan TA, Lo W, Chan G, Sillanp MET. Biological processes for treatment of landfill leachate. J Environ Monit 2010;12:2032–47. doi:10.1039/c0em00076k.

[72] James SC. Metals in municipal landfill leachate and their health effects. Am J Public Health 1977;67:429–32. doi:10.2105/AJPH.67.5.429.

[73] Baig S, Coulomb I, Courant P, Liechti P. Treatment of landfill leachates: Lapeyrouse and Satrod case studies. Ozone Sci Eng 1999;21:1–22.

doi:10.1080/01919519908547255.
[74] Welander U, Henryson T, Welander T. Nitrification of landfill leachate using suspended-carrier biofilm technology. Water Res 1997;31:2351–2355.
[75] Harsem J. Identification of organic compounds in leachate from a waste tip. Water Res 1983;17:699–705.
[76] Chian ESK, DeWalle FB. Sanitary landfill leachates and their treatment. J Environ Eng Div 1976:411–31.
[77] Ehrig H, Stegmann R. Biological process. Landfilling of Waste: Leachate. London, New York: Elsevier Applied Science; 1992.
[78] Deng Y. Advanced Oxidation Processes (AOPs) for reduction of organic pollutants in landfill leachate: a review. Int J Environ Waste Manag 2009;4:366–84. doi:10.1504/IJEWM.2009.027402.
[79] Liu Z, Kanjo Y, Mizutani S. Removal mechanisms for endocrine disrupting compounds (EDCs) in wastewater treatment - physical means, biodegradation, and chemical advanced oxidation: A review. Sci Total Environ 2009;407:731–48. doi:10.1016/j.scitotenv.2008.08.039.
[80] Wu Y, Brigante M, Dong W, De Sainte-Claire P, Mailhot G. Toward a better understanding of Fe(III)-EDDS photochemistry: Theoretical stability calculation and experimental investigation of 4- tert -butylphenol degradation. J Phys Chem A 2014;118:396–403. doi:10.1021/jp409043e.
[81] Barse A V., Chakrabarti T, Ghosh TK, Pal AK, Jadhao SB. One-tenth dose of LC50 of 4-tert-butylphenol causes endocrine disruption and metabolic changes in Cyprinus carpio. Pestic Biochem Physiol 2006;86:172–9. doi:10.1016/j.pestbp.2006.03.006.
[82] Haavisto TE, Adamsson NA, Myllymäki SA, Toppari J, Paranko J. Effects of 4-tert-octylphenol, 4-tert-butylphenol, and diethylstilbestrol on prenatal testosterone surge in the rat. Reprod Toxicol 2003;17:593–605. doi:10.1016/S0890-6238(03)00103-5.
[83] Myllymäki S, Haavisto T, Vainio M, Toppari J, Paranko J. In vitro effects of diethylstilbestrol, genistein, 4-tert-butylphenol, and 4-tert-octylphenol on steroidogenic activity of isolated immature rat ovarian follicles. Toxicol Appl Pharmacol 2005;204:69–80. doi:10.1016/j.taap.2004.08.009.
[84] OECD. Oecd Sids: P-Tert-Butyl Phenol (Cas: 98-54-4) 2000:1–75.
[85] Yadav GD, Doshi NS. Alkylation of phenol with methyl-tert-butyl ether and tert-butanol over solid acids: Efficacies of clay-based catalysts. Appl Catal A Gen 2002;236:129–47. doi:10.1016/S0926-860X(02)00300-9.
[86] Toyama T, Momotani N, Ogata Y, Miyamori Y, Inoue D, Sei K, et al. Isolation and characterization of 4-tert-butylphenol-utilizing sphingobium fuliginis strains from phragmites australis rhizosphere sediment. Appl Environ Microbiol 2010;76:6733–40. doi:10.1128/AEM.00258-10.
[87] Ogata Y, Toyama T, Yu N, Wang X, Sei K, Ike M. Occurrence of 4-tert-butylphenol (4-t-BP) biodegradation in an aquatic sample caused by the presence of Spirodela polyrrhiza and isolation of a 4-t-BP-utilizing bacterium. Biodegradation 2013;24:191–202. doi:10.1007/s10532-012-9570-9.
[88] Xiao X, Xing C, He G, Zuo X, Nan J, Wang L. Solvothermal synthesis of novel hierarchical Bi4O5I2nanoflakes with highly visible light photocatalytic performance for the degradation of 4-tert-butylphenol. Appl Catal B Environ 2014;148–149:154–63. doi:10.1016/j.apcatb.2013.10.055.
[89] Kühn R, Pattard M, Pernak KD, Winter A. Results of the harmful effects of selected water pollutants (anilines, phenols, aliphatic compounds) to Daphnia magna. Water Res 1989;23:495–9. doi:10.1016/0043-1354(89)90141-3.
[90] Sun H, Xu XL, Qu JH, Hong X, Wang YB, Xu LC, et al. 4-Alkylphenols and related

chemicals show similar effect on the function of human and rat estrogen receptor α in reporter gene assay. Chemosphere 2008;71:582–8. doi:10.1016/j.chemosphere.2007.09.031.

[91] Wu Y, Shi J, Chen H, Zhao J, Dong W. Aqueous photodegradation of 4-tert-butylphenol: By-products, degradation pathway and theoretical calculation assessment. Sci Total Environ 2016;566–567:86–92. doi:10.1016/j.scitotenv.2016.05.064.

[92] Wu Y, Zhu X, Chen H, Dong W, Zhao J. Photodegradation of 4-tert-butylphenol in aqueous solution by UV-C, UV/H2O2 and UV/S2O82-system. J Environ Sci Heal - Part A Toxic/Hazardous Subst Environ Eng 2016;51:440–5. doi:10.1080/10934529.2015.1120541.

[93] Gottschalk C, Libra JA, Saupe A. Ozonation of water and waste water: A practical guide to understanding ozone and its application. 2008. doi:10.1002/9783527613342.

[94] Inglezakis VJ, Amzebek A, Kuspangaliyeva B, Sabrassov Y, Balbayeva G, Yerkinova A, et al. Treatment of municipal solid waste landfill leachate by use of combined biological, physical and photochemical processes. Desalin Water Treat 2018;112:218–31. doi:10.5004/dwt.2018.22252.

[95] Huang J, Shang C. Air Stripping. Handb. Environ. Eng. Adv. Physicochem. Treat. Process., vol. 4, 1993, p. 261–94. doi:10.1016/S0166-1116(08)70529-6.

[96] Poulopoulos SG, Nikolaki M, Karampetsos D, Philippopoulos CJ. Photochemical treatment of 2-chlorophenol aqueous solutions using ultraviolet radiation, hydrogen peroxide and photo-Fenton reaction. J Hazard Mater 2008;153:582–7. doi:10.1016/j.jhazmat.2007.09.002.

[97] Rivas FJ, Beltrán F, Gimeno O, Carvalho F. Fenton-like oxidation of landfill leachate. J Environ Sci Heal - Part A Toxic/Hazardous Subst Environ Eng 2003;38:371–9. doi:10.1081/ESE-120016901.

[98] Kim J-S, Kim H-Y, Won C-H, Kim J-G. Treatment of Leachate Produced in Stabilized Landfills by Coagulation and Fenton Oxidation Process. J Chinese Inst Chem Eng 2001;32:425–9.

[99] Arnold SM, Hickey WJ, Harris RF. Degradation of Atrazine by Fenton's Reagent: Condition Optimization and Product Quantification. Environ Sci Technol 1995;29:2083–9. doi:10.1021/es00008a030.

[100] Coelho A, Castro A V., Dezotti M, Sant'Anna GL. Treatment of petroleum refinery sourwater by advanced oxidation processes. J Hazard Mater 2006;137:178–84. doi:10.1016/j.jhazmat.2006.01.051.

[101] Gallard H, de Laat J, Legube B. Effect of pH on the oxidation rate of organic compounds by Fe-II/H2O2, mechanisms and simulation. New J Chem 1998;22:263–8. doi:10.1039/a708335a.

[102] Tang WZ, Huang CP. 2,4-Dichlorophenol Oxidation Kinetics by Fenton's Reagent. Environ Technol (United Kingdom) 1996;17:1371–8. doi:10.1080/09593330.1996.9618465.

[103] Segweni D. Options for treatment of ammonia in landfill leachate. Master thesis. University of Canterbury, New Zealand, 2017.

[104] Adhikari B, Khanal SN. Qualitative Study of Landfill Leachate from Different Ages of Landfill Sites of Various Countries Including Nepal. IOSR J Environ Sci Ver III 2015;9:2319–99. doi:10.9790/2402-09132336.

[105] Kang KH, Shin HS, Park H. Characterization of humic substances present in landfill leachates with different landfill ages and its implications. Water Res 2002;36:4023–32. doi:10.1016/S0043-1354(02)00114-8.

[106] Kim YK, Huh IR. Enhancing biological treatability of landfill leachate by chemical oxidation. Environ Eng Sci 1997;14:73–9. doi:10.1089/ees.1997.14.73.

[107] Singla P, Sharma M, Pandey OP, Singh K. Photocatalytic degradation of azo dyes using Zn-doped and undoped TiO 2 nanoparticles. Appl Phys A Mater Sci Process 2014;116:371–8. doi:10.1007/s00339-013-8135-z.
[108] Nguyen VN, Nguyen NKT, Nguyen PH. Hydrothermal synthesis of Fe-doped TiO2nanostructure photocatalyst. Adv Nat Sci Nanosci Nanotechnol 2011;2. doi:10.1088/2043-6262/2/3/035014.
[109] Zhao B, Mele G, Pio I, Li J, Palmisano L, Vasapollo G. Degradation of 4-nitrophenol (4-NP) using Fe-TiO2 as a heterogeneous photo-Fenton catalyst. J Hazard Mater 2010;176:569–74. doi:10.1016/j.jhazmat.2009.11.066.
[110] Borgarello E, Kiwi J, Pelizzetti E, Visca M, Grätzel M. Sustained Water Cleavage by Visible Light. J Am Chem Soc 1981;103:6324–9. doi:10.1021/ja00411a010.
[111] Lopez-Lopez C, Martín-Pascual J, Martínez-Toledo M V., Muñío MM, Hontoria E, Poyatos JM. Kinetic modelling of TOC removal by H2O2/UV, photo-Fenton and heterogeneous photocatalysis processes to treat dye-containing wastewater. Int J Environ Sci Technol 2015;12:3255–62. doi:10.1007/s13762-015-0755-8.
[112] Matafonova G, Christofi N, Batoev V, Sosnin E. Degradation of chlorophenols in aqueous media using UV XeBr excilamp in a flow-through reactor. Chemosphere 2008;70:1124–7. doi:10.1016/j.chemosphere.2007.08.022.
[113] Dixit A, Mungray AK, Chakraborty M. Photochemical oxidation of phenolic wastewaters and its kinetic study. Desalin Water Treat 2012;40:56–62. doi:10.1080/19443994.2012.671141.
[114] Poulopoulos SG, Philippopoulos CJ. Photo-assisted oxidation of chlorophenols in aqueous solutions using hydrogen peroxide and titanium dioxide. J Environ Sci Heal - Part A Toxic/Hazardous Subst Environ Eng 2004;39:1385–97. doi:10.1081/ESE-120037840.
[115] Tanaka K, Hisanaga T, Harada K. Efficient photocatalytic degradation of chloral hydrate in aqueous semiconductor suspension. J Photochem Photobiol A Chem 1989;48:155–9. doi:10.1016/1010-6030(89)87098-4.

Appendices

Appendix A

All the results of the UV-VIS spectra for color changes during the treatment of landfill leachate are presented in this section.

Figure A.1: UV-VIS analysis to observe the effect of inorganic carbon on colour change ($[Fe(II)]_0$ = 400 ppm, $[H_2O_2]_0$ = 6660 mg L^{-1})

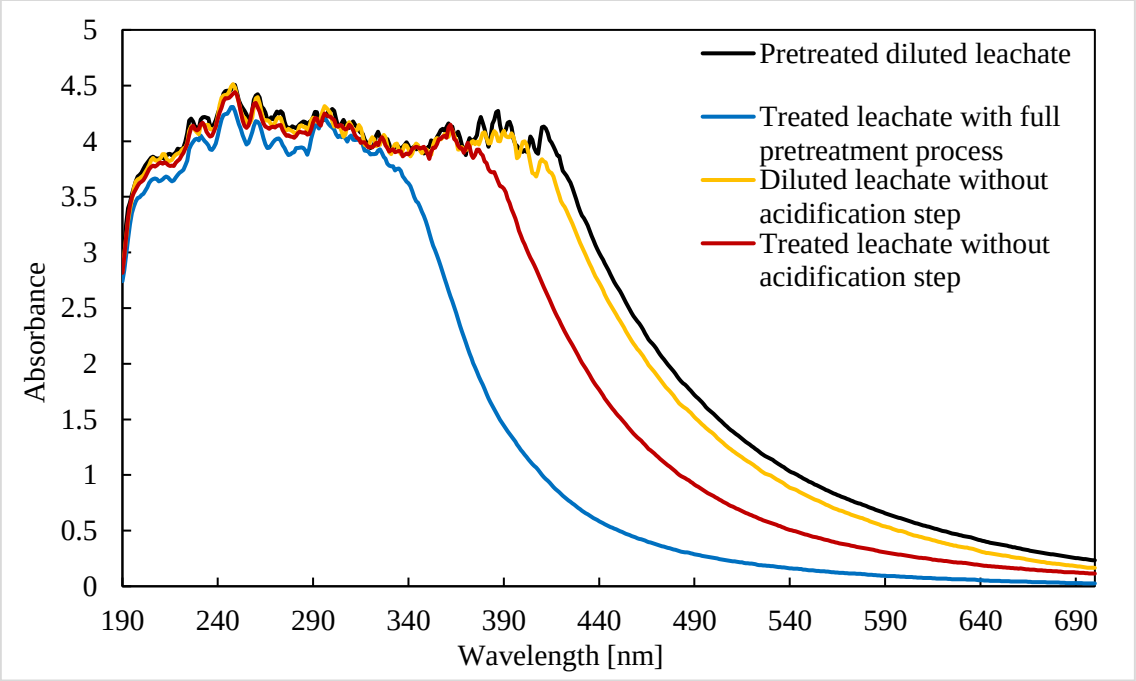

Figure A.2: UV-VIS analysis to observe the effect of Fe(II) concentration on colour change ($[H_2O_2]_0$ = 6660 mg L^{-1})

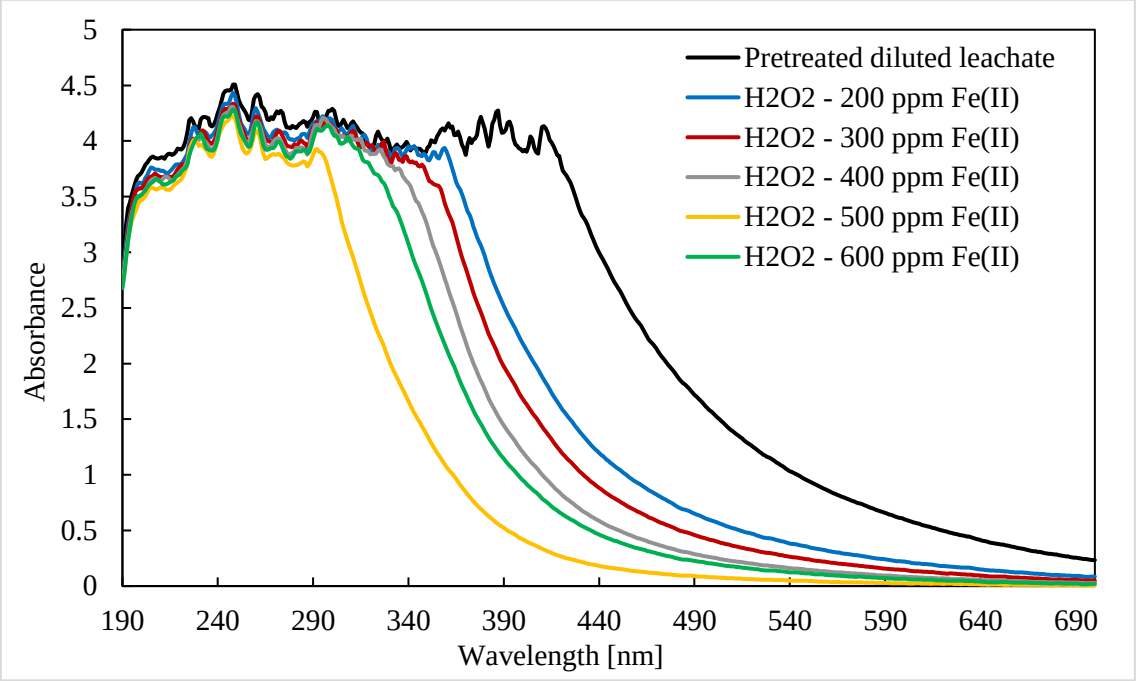

Figure A.3: UV-VIS analysis to observe the effect of Fe(III) concentration on colour change ($[H_2O_2]_0$ = 6660 mg L^{-1})

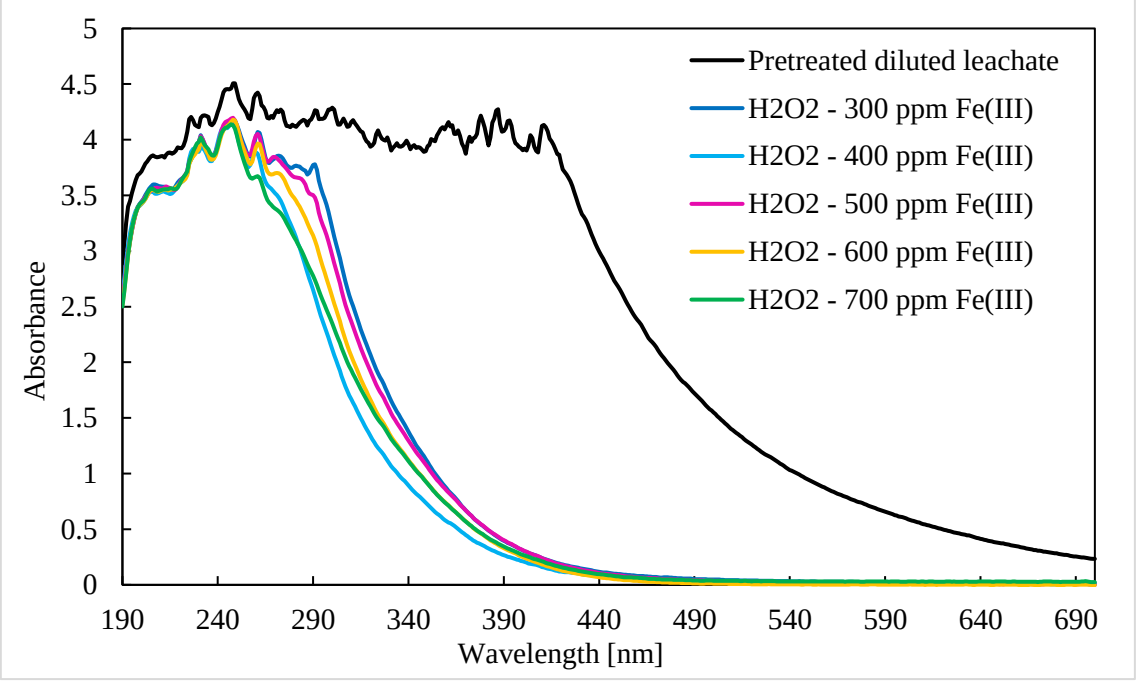

Figure A.4: UV-VIS analysis to observe the effect of H_2O_2 dosage on colour change ($[Fe(II)]_0$ = 400 ppm)

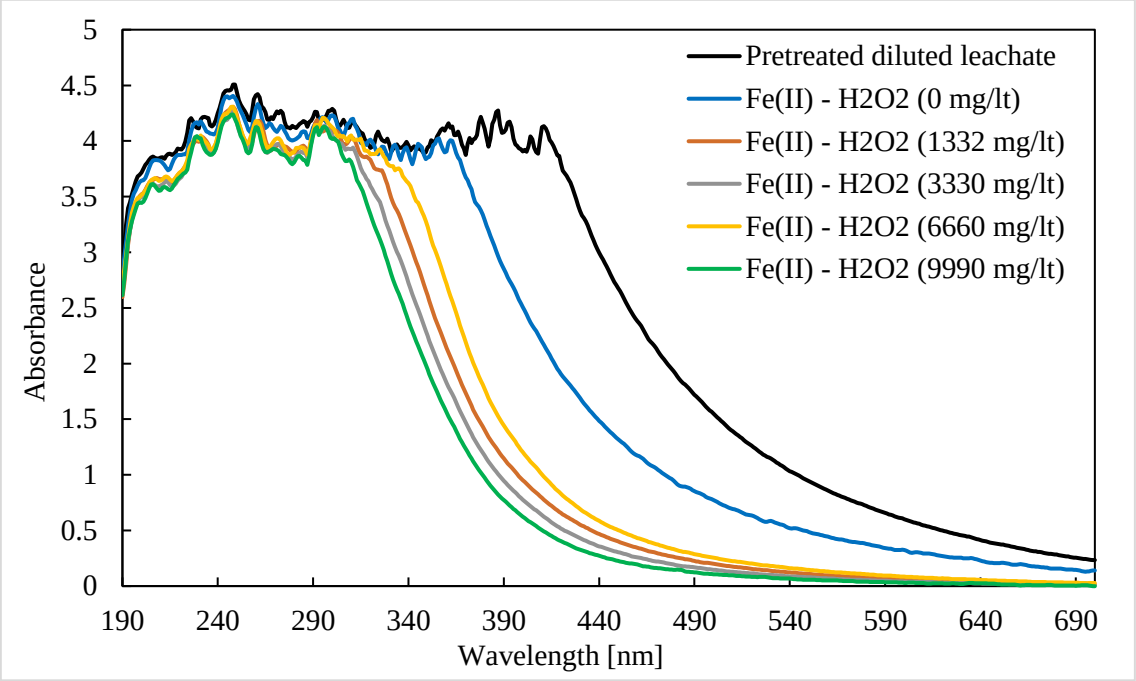

Figure A.5: UV-VIS analysis to observe the effect of H_2O_2 dosage on colour change ($[Fe(III)]_0$ = 600 ppm)

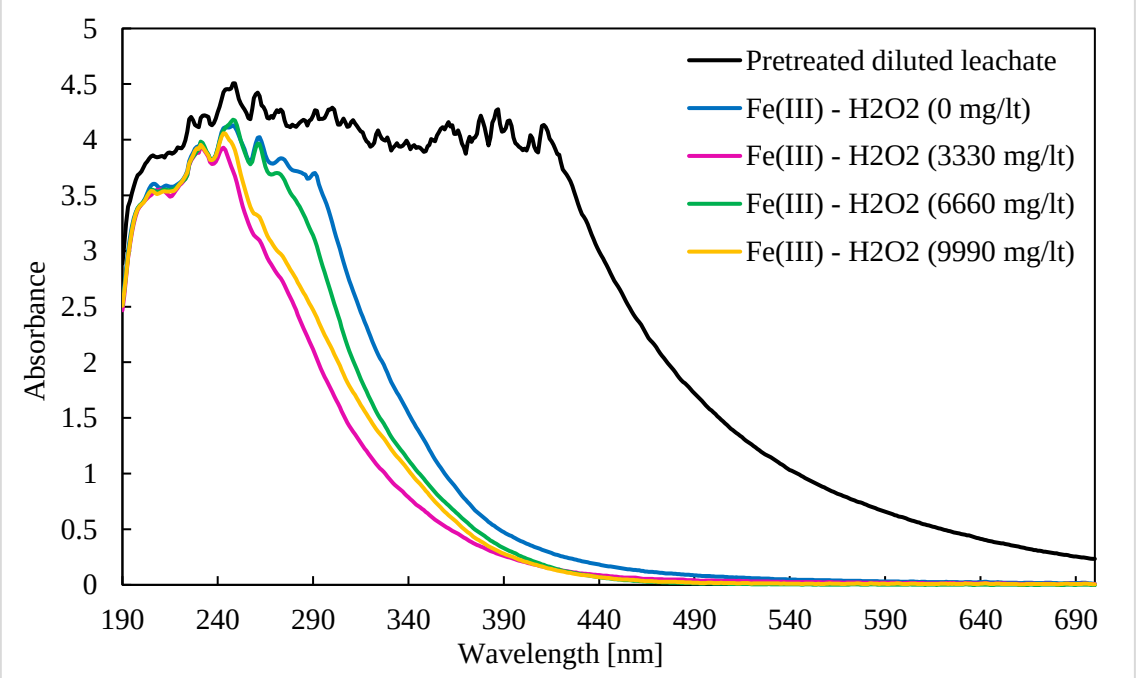

Figure A.6: UV-VIS analysis to observe the effect of pH adjustment on colour change ($[Fe(II)]_0$ = 400 ppm, $[H_2O_2]_0$ = 6660 mg L^{-1})

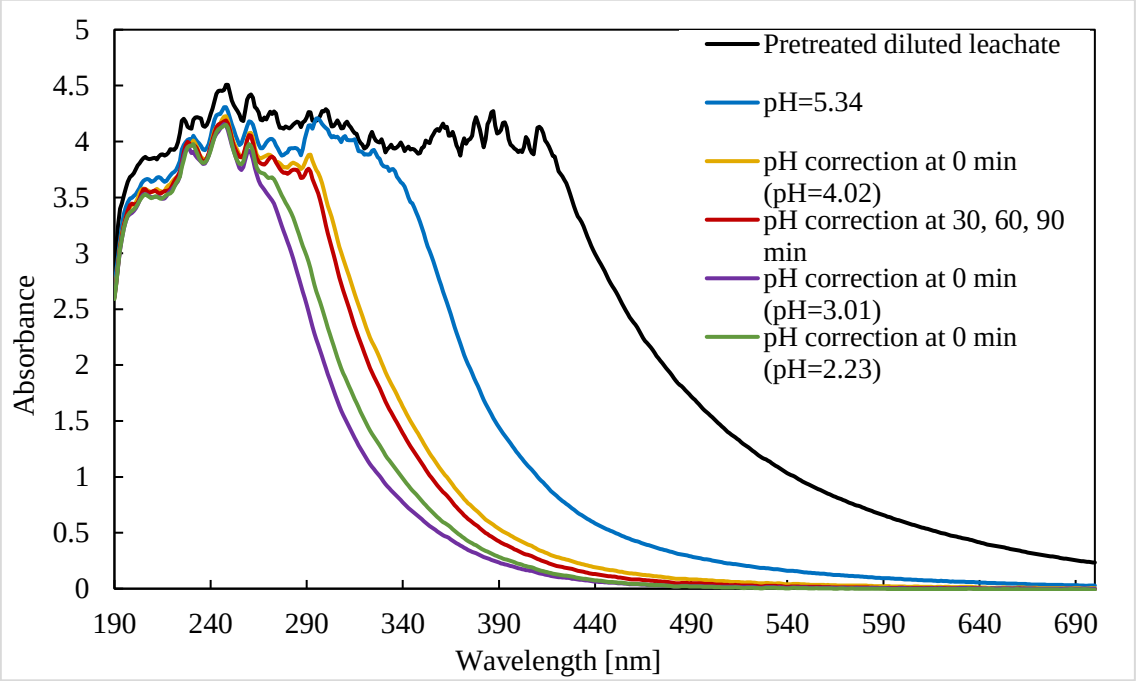

Figure A.7: UV-VIS analysis to observe the effect of pH adjustment on colour change ($[Fe(III)]_0$ = 600 ppm, $[H_2O_2]_0$ = 6660 mg L^{-1})

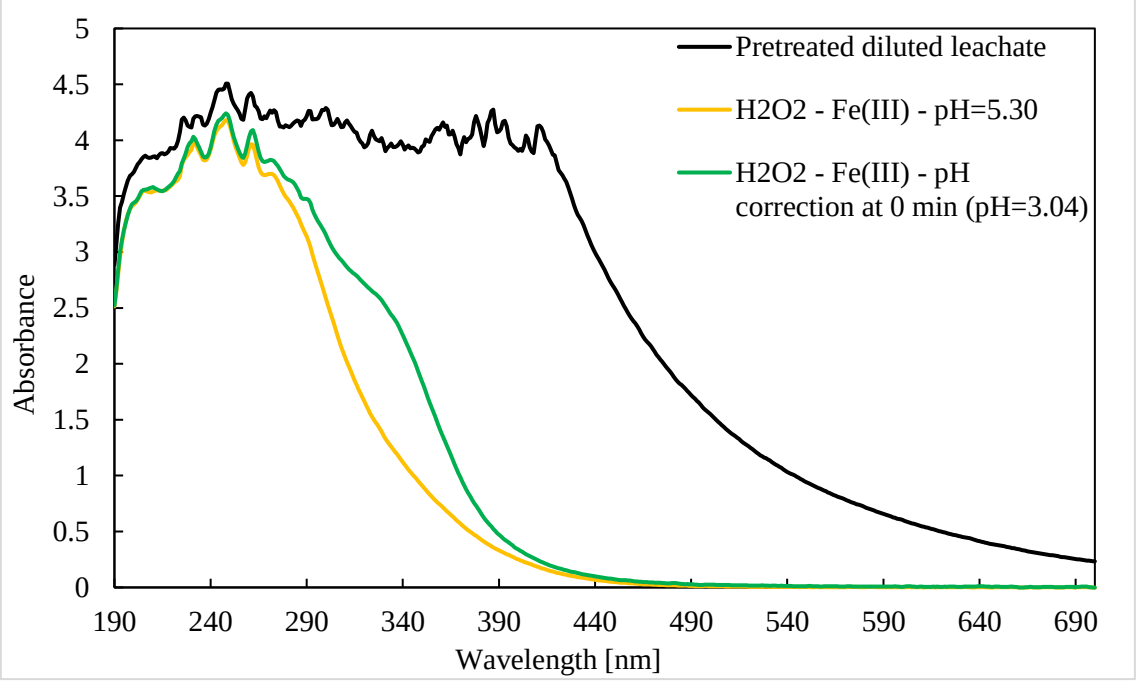

Figure A.8: UV-VIS analysis to observe colour change by Fenton process ($[H_2O_2]_0$ = 6660 mg L^{-1})

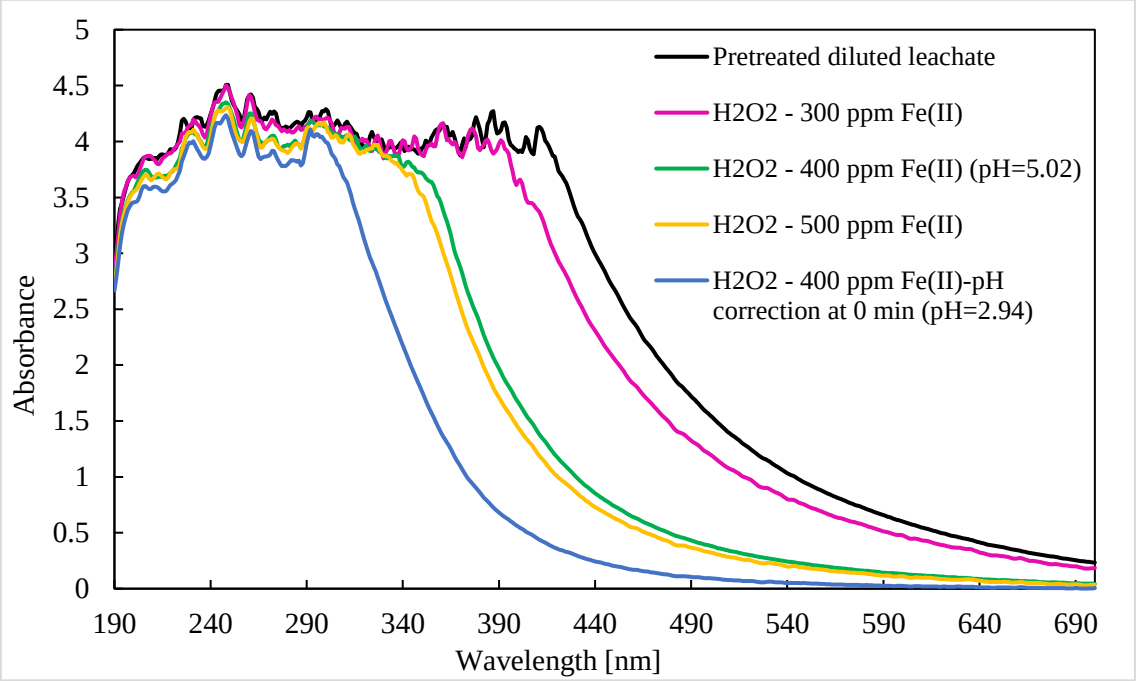

Figure A.9: UV-VIS analysis to observe colour change by Fenton-like process ($[H_2O_2]_0$ = 6660 mg L^{-1})

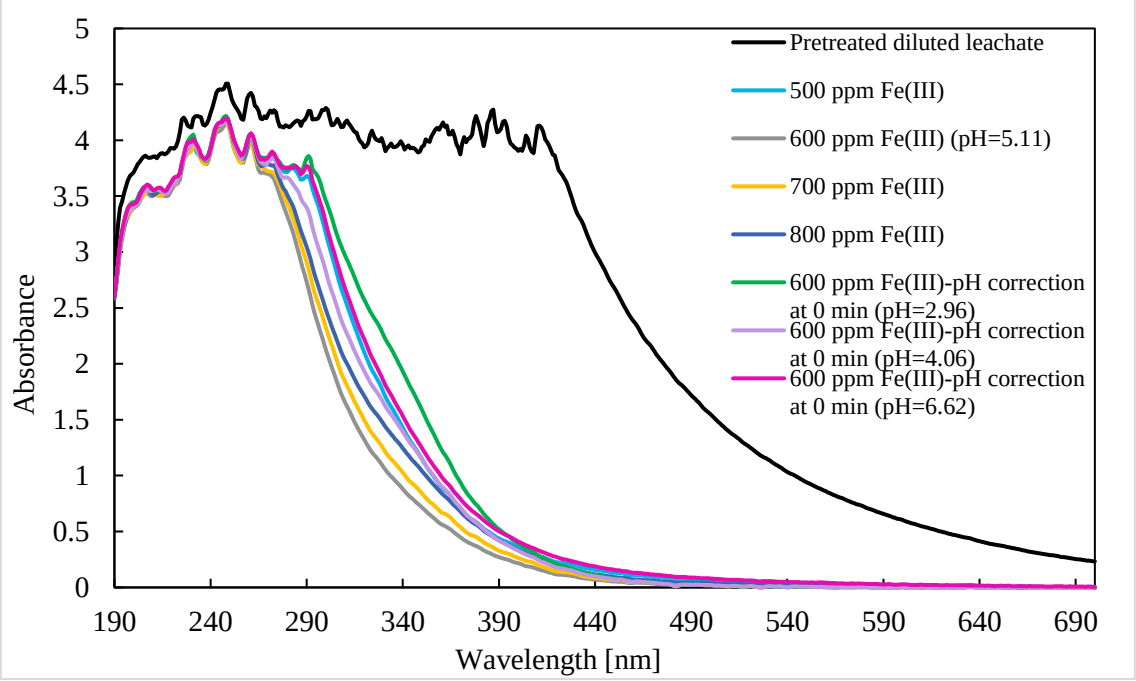

Appendix B

EDS mapping of SEM analysis of fresh and used catalysts are presented in this section.

Figure B.1: EDS mapping of SEM analysis of fresh TiO_2

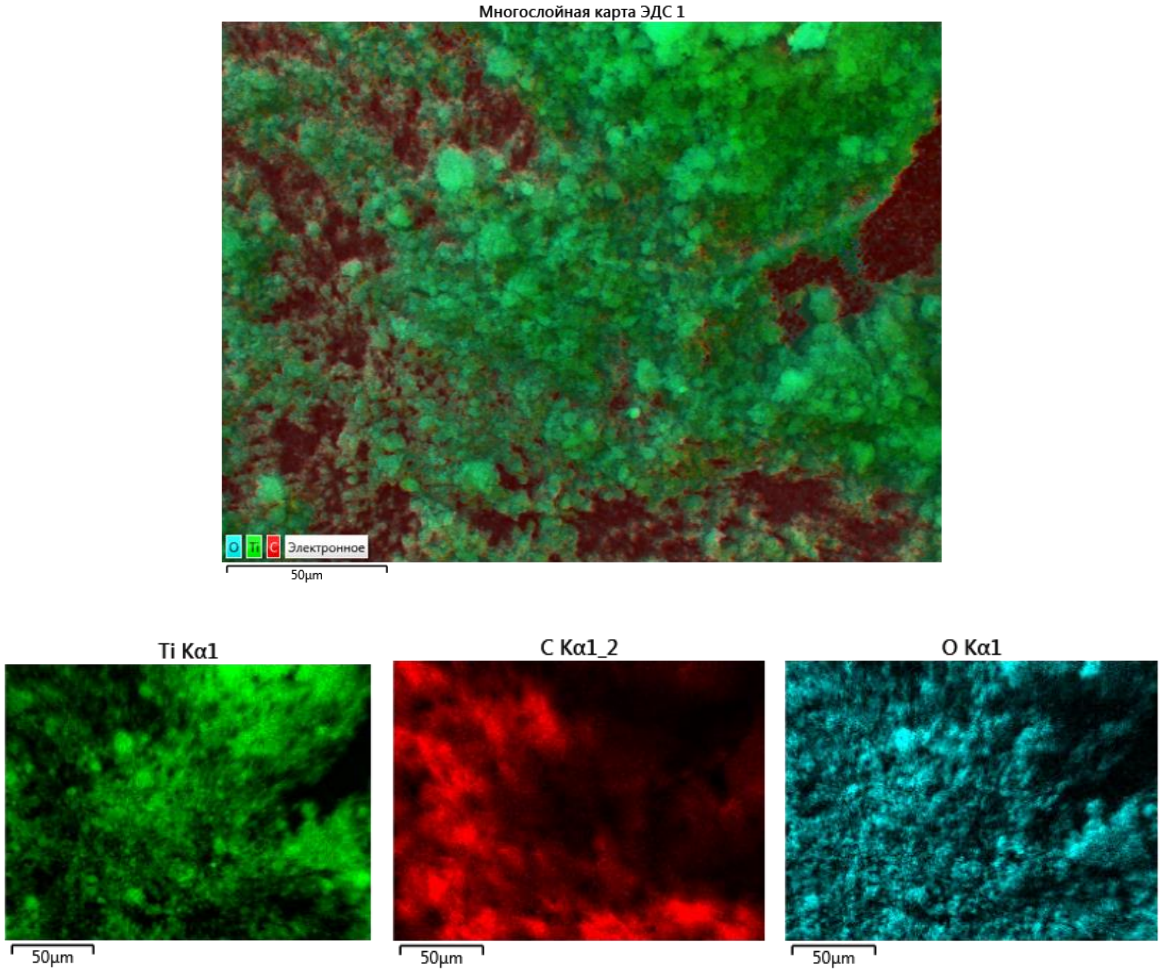

Figure B.2: EDS mapping of SEM analysis of used TiO_2 after UV/TiO_2

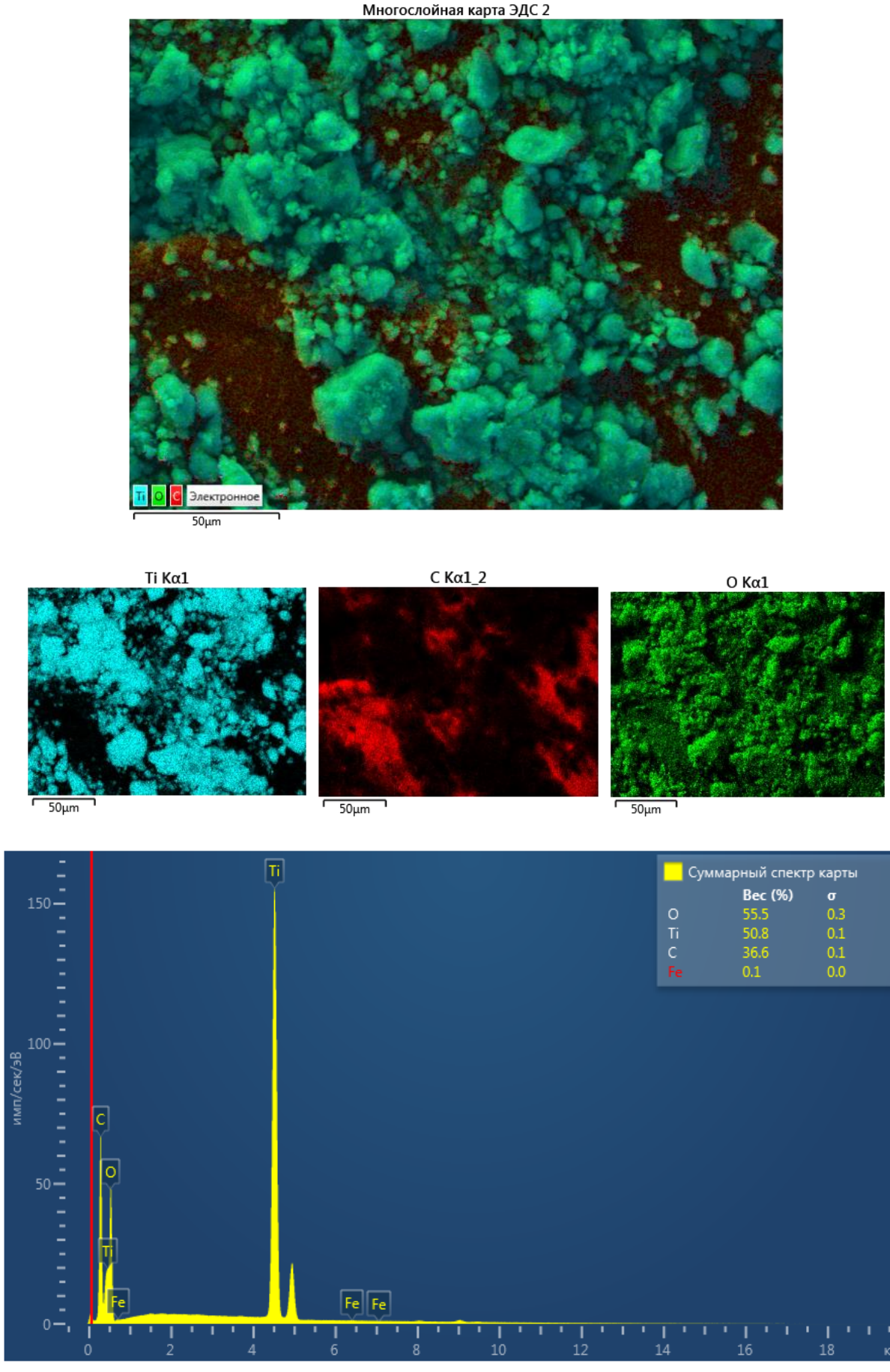

Figure B.3: EDS mapping of SEM analysis of used TiO_2 after UV/H_2O_2/TiO_2

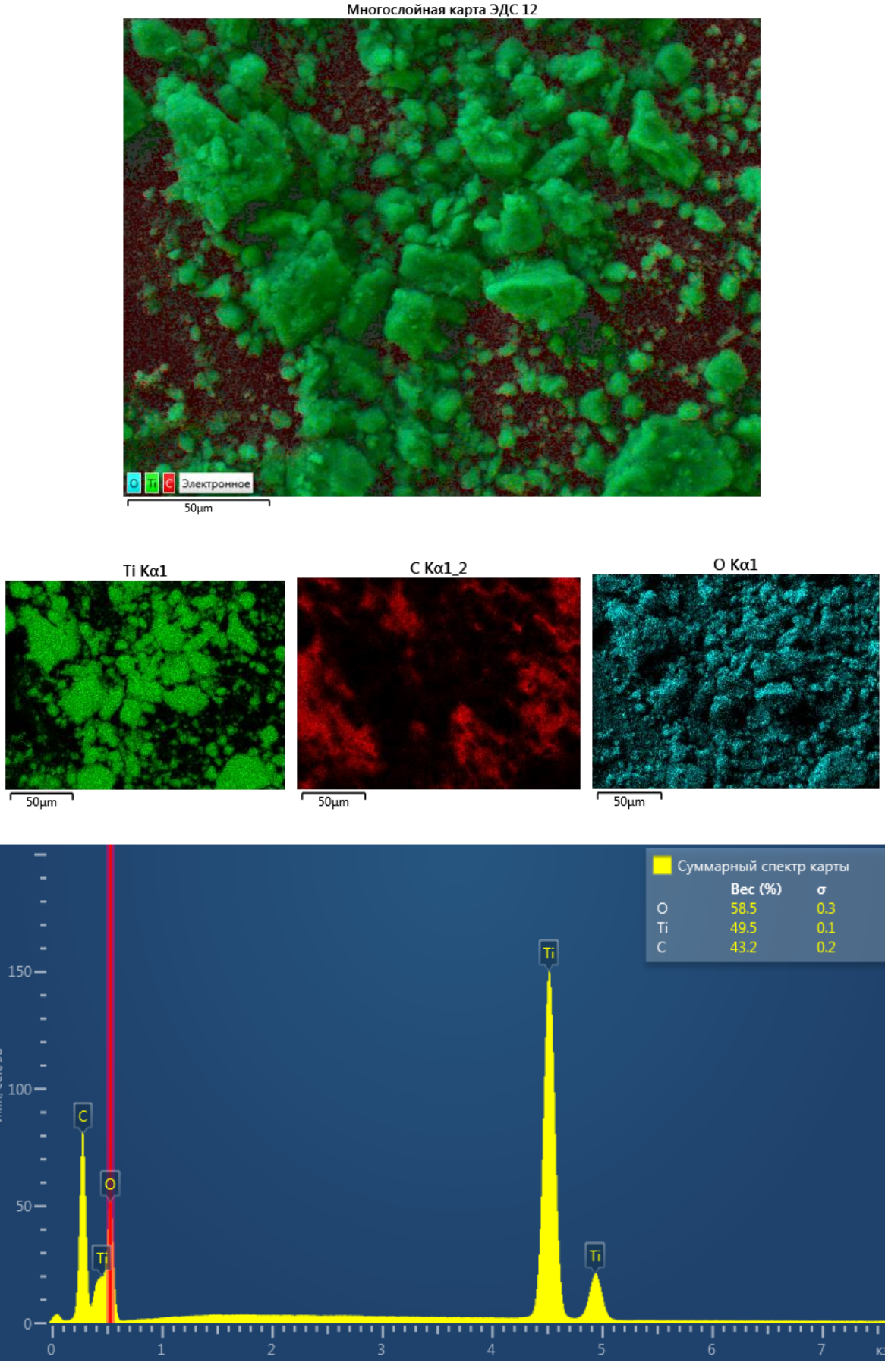

Figure B.4: EDS mapping of SEM analysis of fresh Fe-TiO_2 (0.5%)

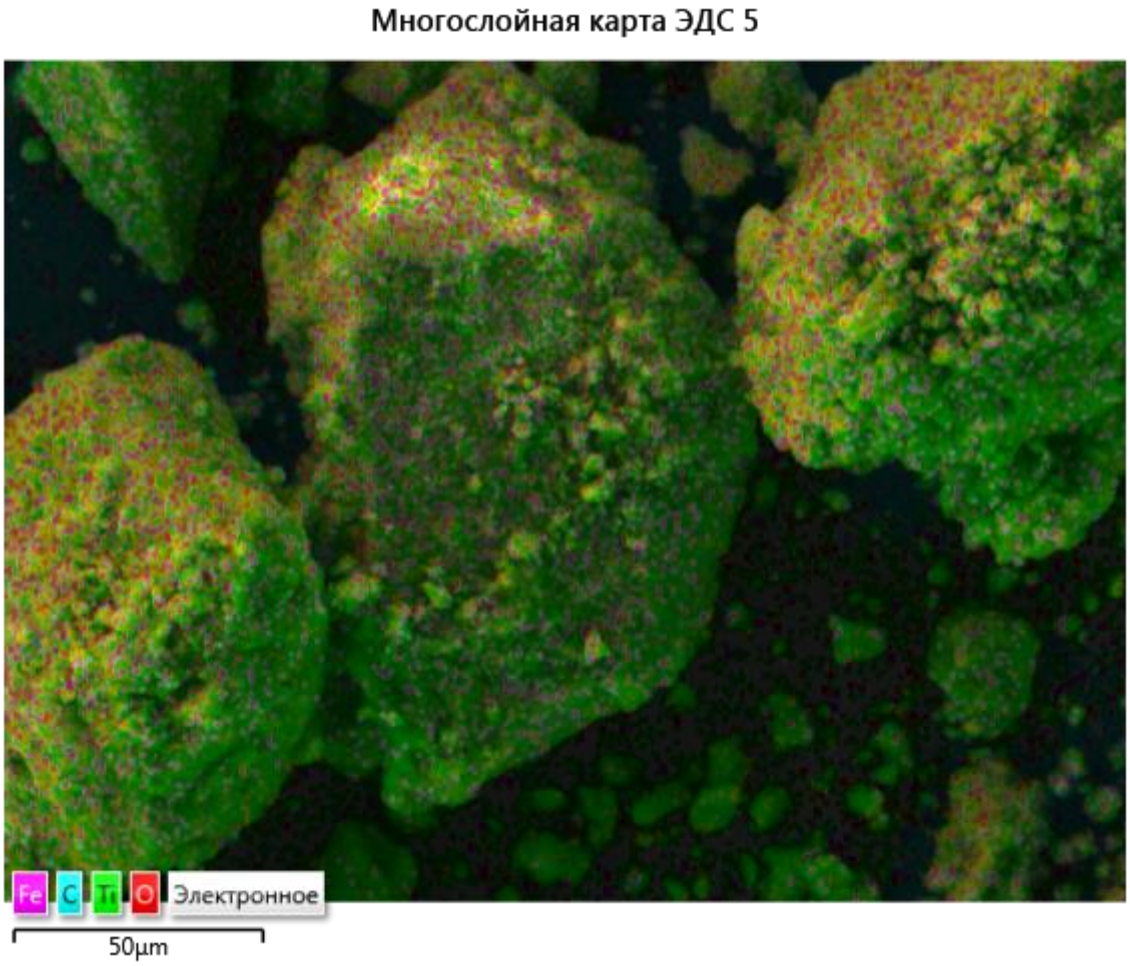

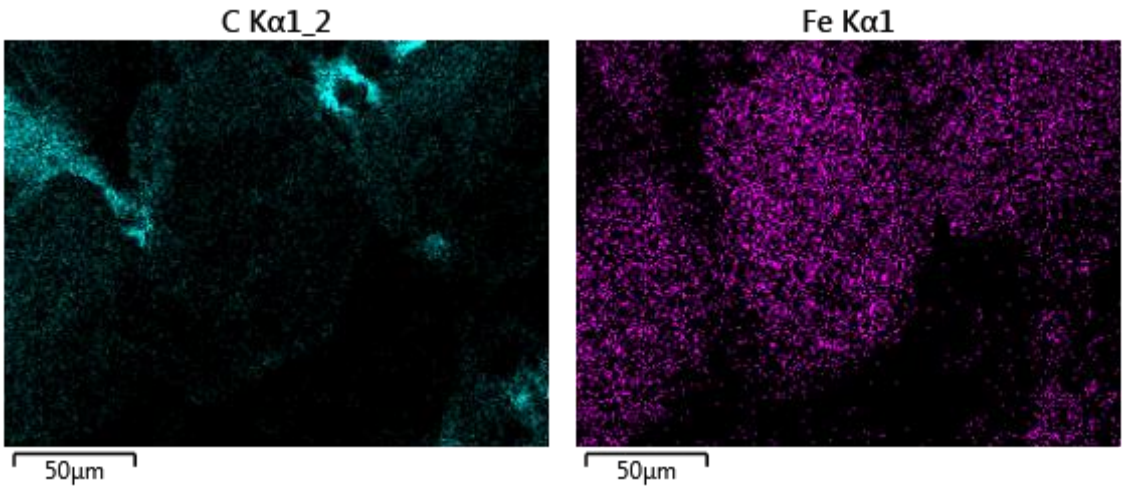
C Kα1_2
Fe Kα1
50µm
50µm

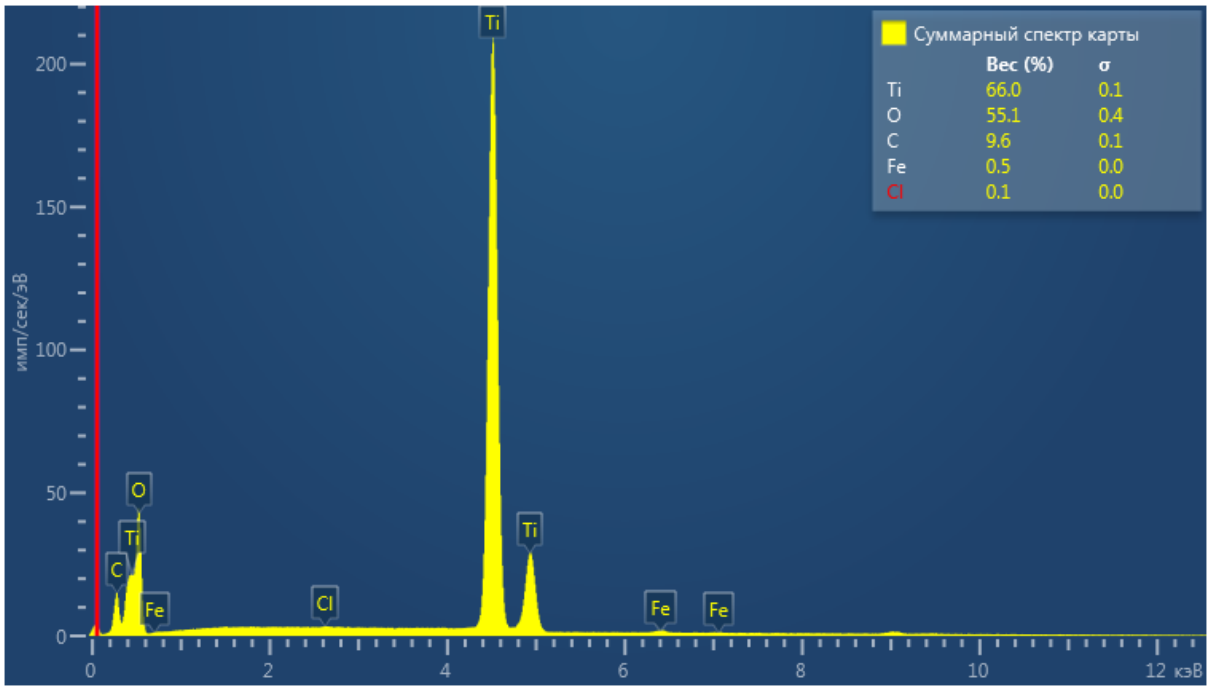
Суммарный спектр карты
Вес (%) σ
Ti 66.0 0.1
O 55.1 0.4
C 9.6 0.1
Fe 0.5 0.0
Cl 0.1 0.0
имп/сек/эВ
200
150
100
50
0
O
Ti
C
Fe
Cl
Ti
Ti
Fe
Fe
0
2
4
6
8
10
12 кэВ

Figure B.5: EDS mapping of SEM analysis of used Fe-TiO_2 (0.5%) after UV/Fe-TiO_2 (0.5%)

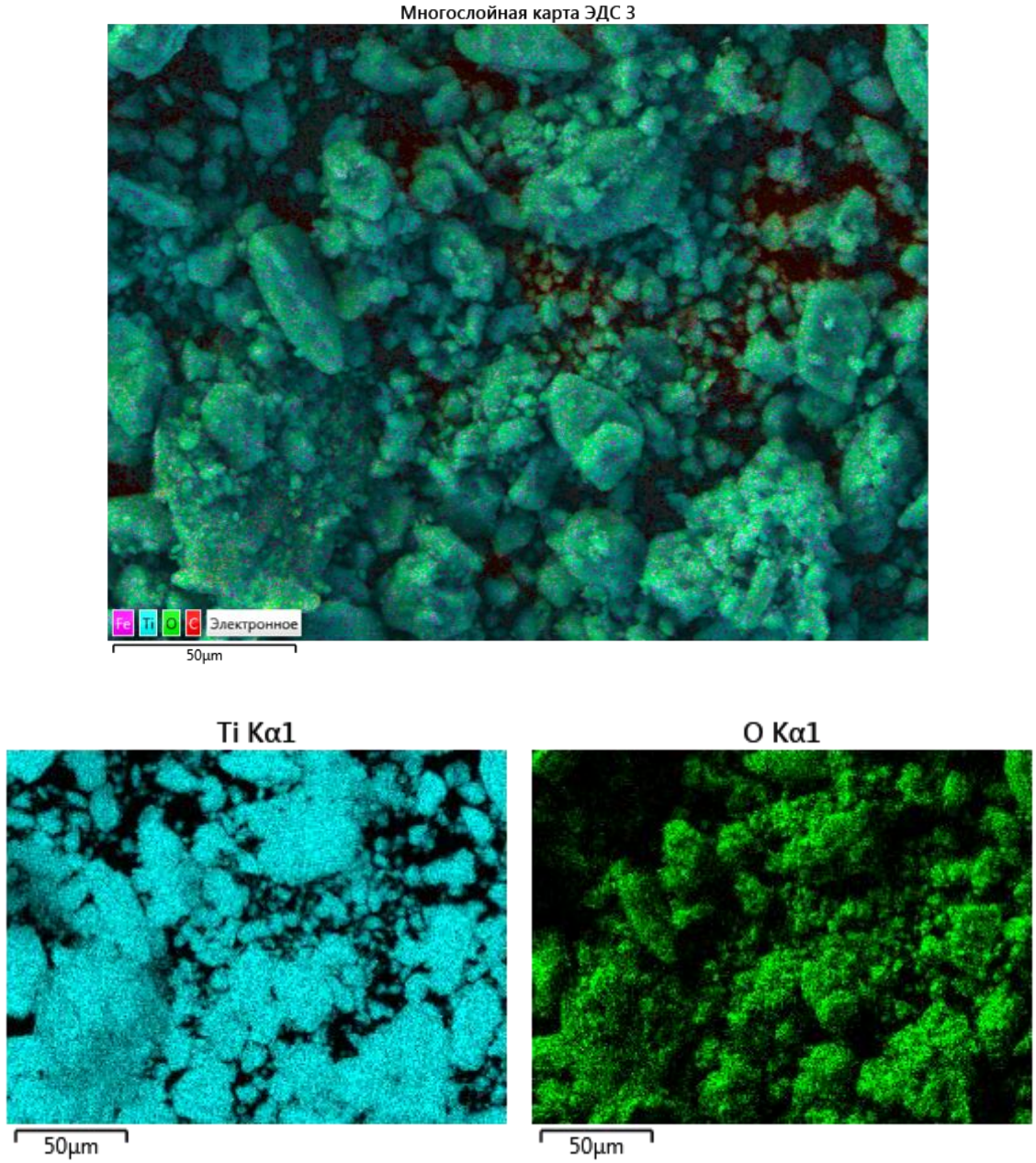

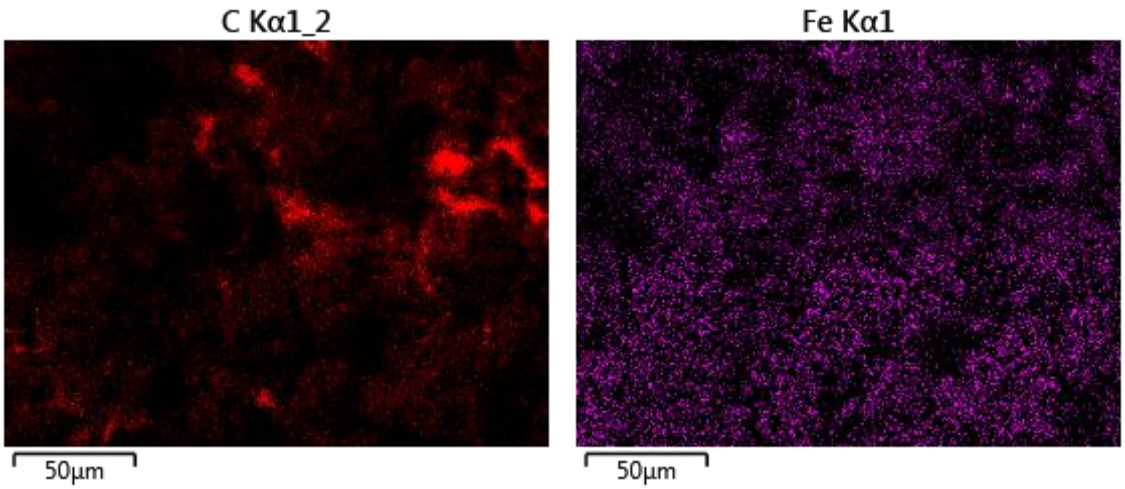
C Kα1_2
Fe Kα1
50µm
50µm

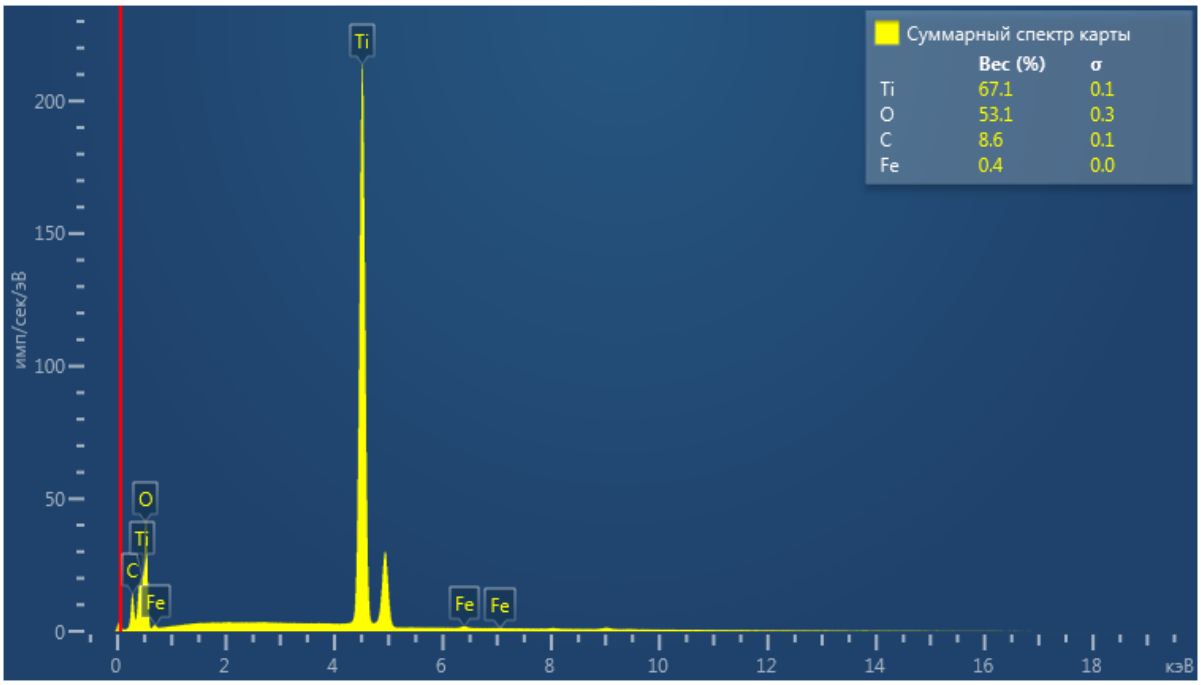
Суммарный спектр карты
Вес (%) σ
Ti 67.1 0.1
O 53.1 0.3
C 8.6 0.1
Fe 0.4 0.0
имп/сек/эВ
кэВ
Ti
O
Ti
C
Fe
Fe
Fe

Figure B.6: EDS mapping of SEM analysis of used Fe-TiO_2 (0.5%) after UV/H_2O_2/Fe-TiO_2 (0.5%)

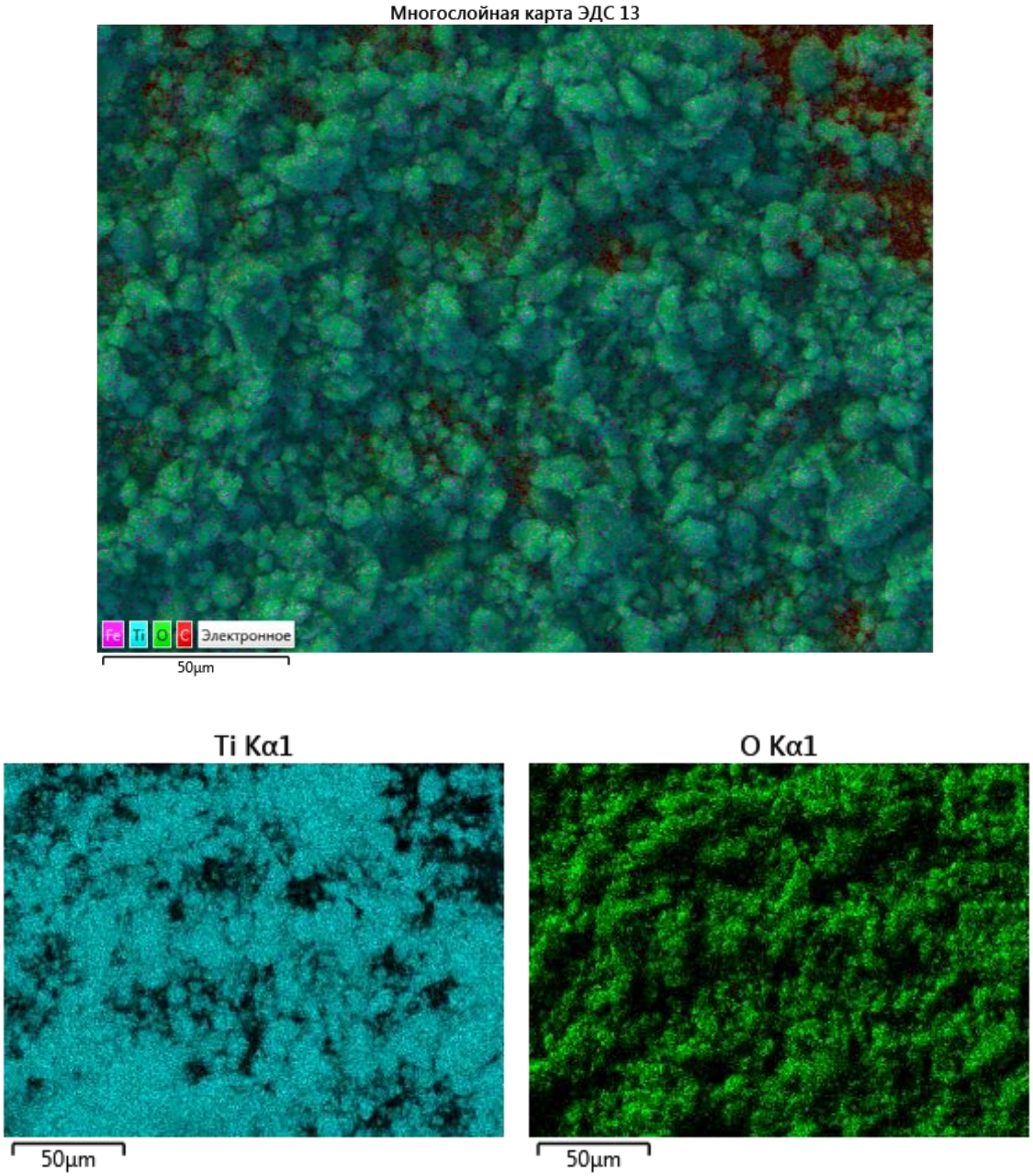

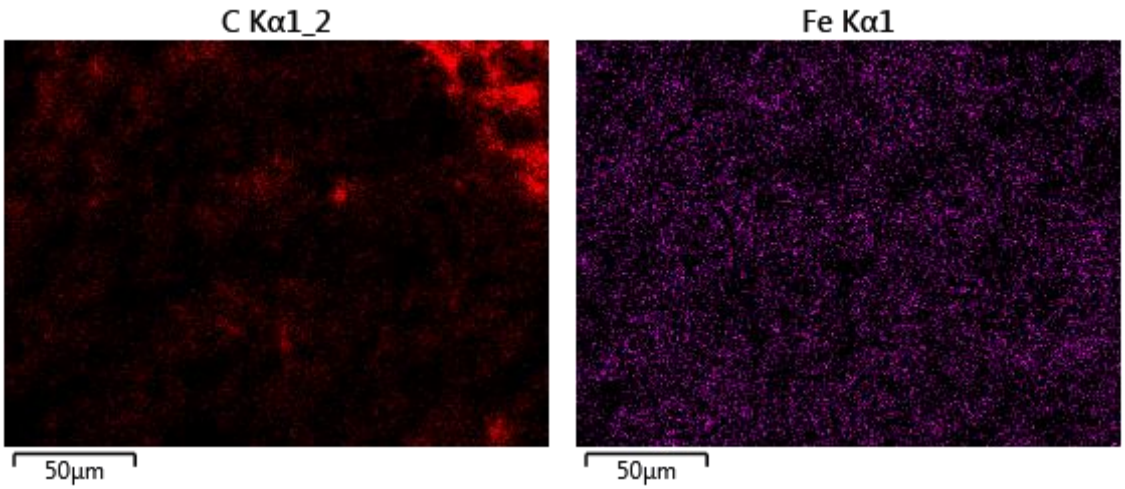
C Kα1_2
Fe Kα1
50µm
50µm

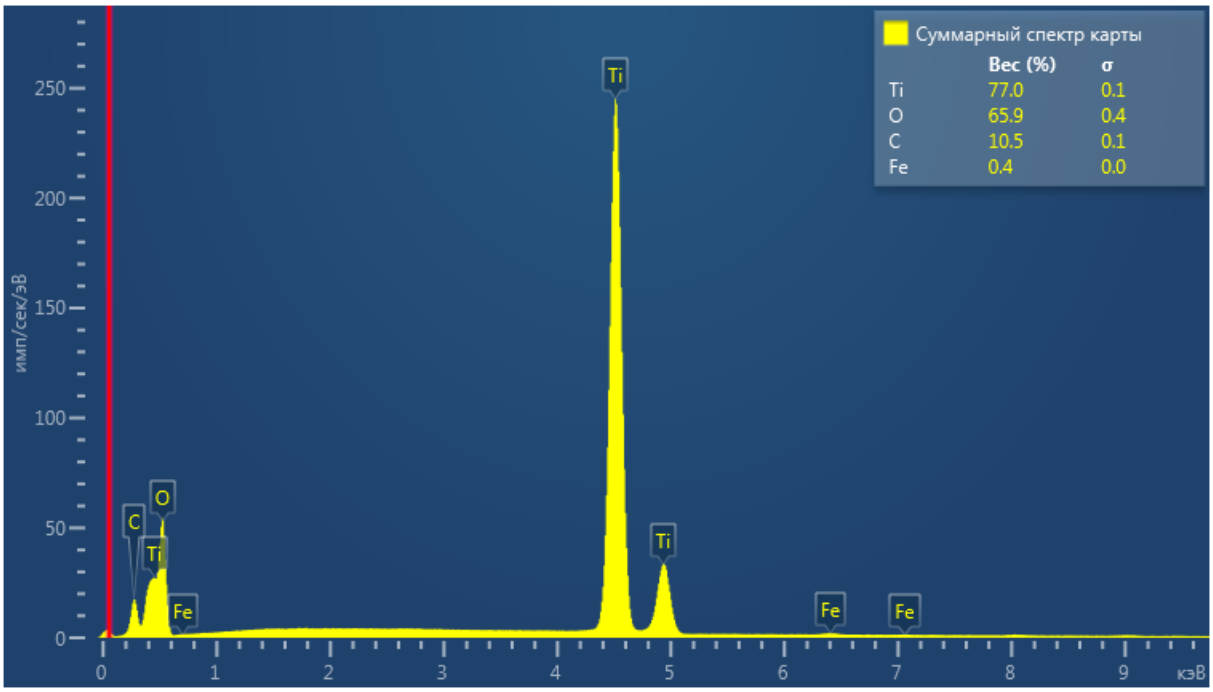
Суммарный спектр карты
Вес (%) σ
Ti 77.0 0.1
O 65.9 0.4
C 10.5 0.1
Fe 0.4 0.0
имп/сек/эВ
кэВ
C
O
Ti
Fe
Ti
Ti
Fe
Fe

Figure B.7: EDS mapping of SEM analysis of fresh Fe-TiO_2 (1%)

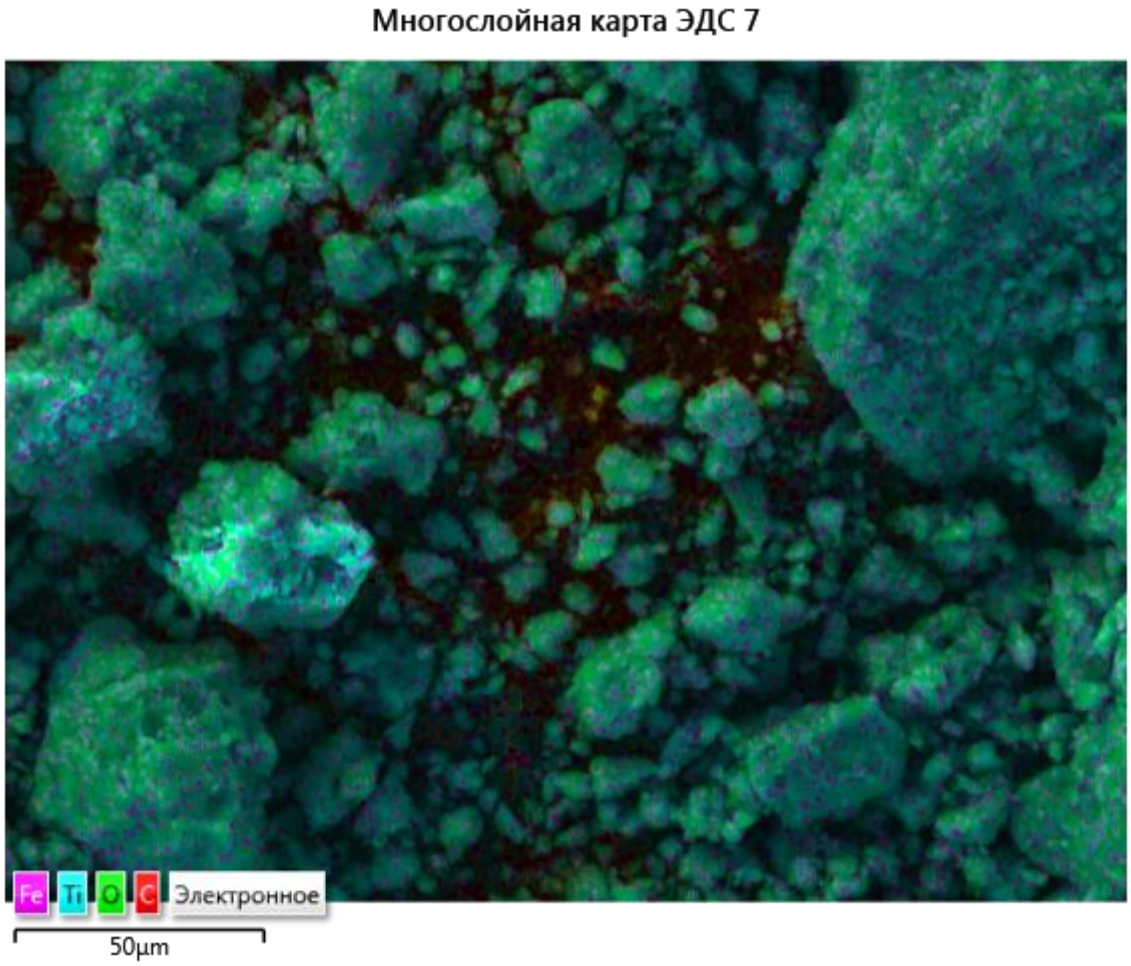

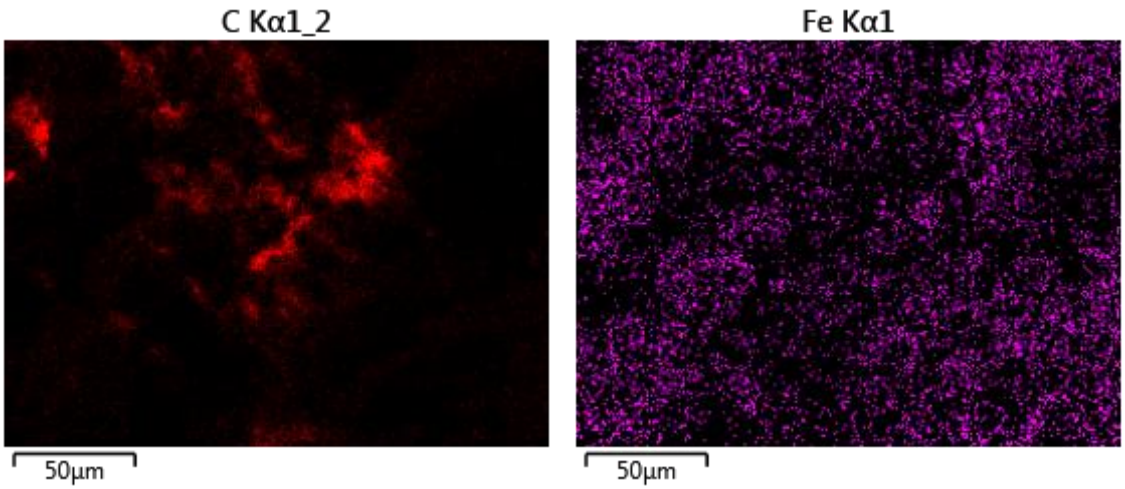
C Kα1_2
Fe Kα1
50µm
50µm

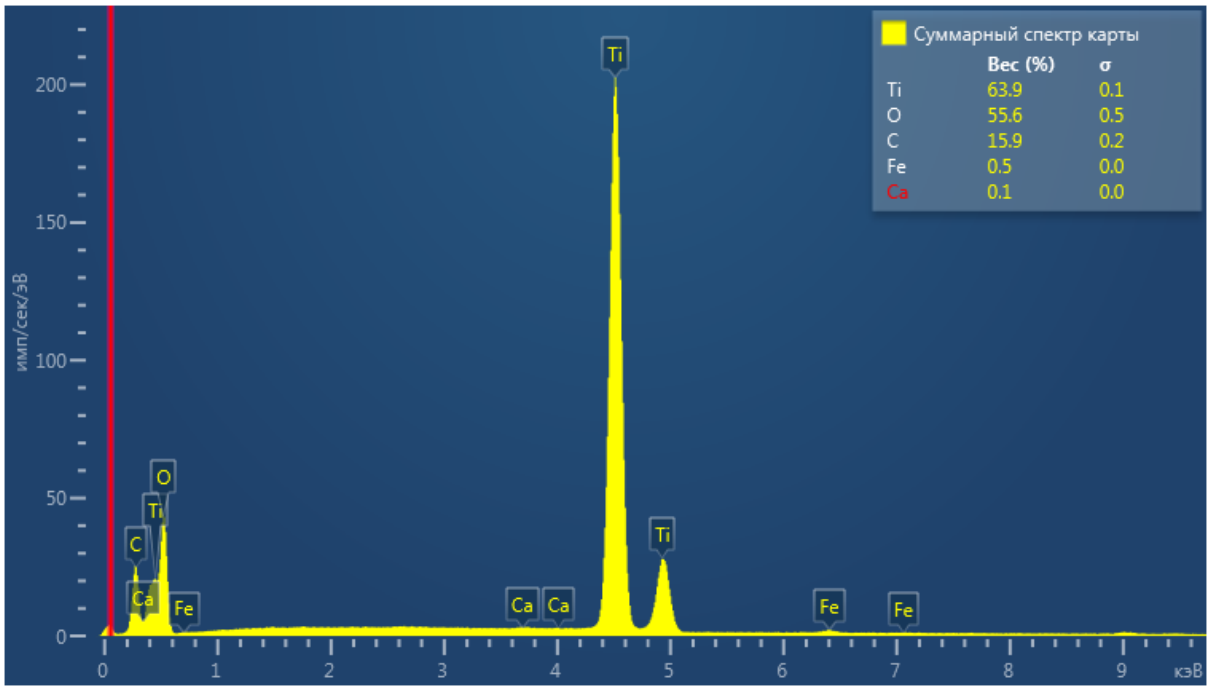
Суммарный спектр карты
Вес (%) σ
Ti 63.9 0.1
O 55.6 0.5
C 15.9 0.2
Fe 0.5 0.0
Ca 0.1 0.0
имп/сек/эВ
кэВ
Ti
O
Ti
C
Ca
Fe
Ca
Ca
Ti
Fe
Fe

Figure B.8: EDS mapping of SEM analysis of used Fe-TiO_2 (1%) after UV/Fe-TiO_2 (1%)

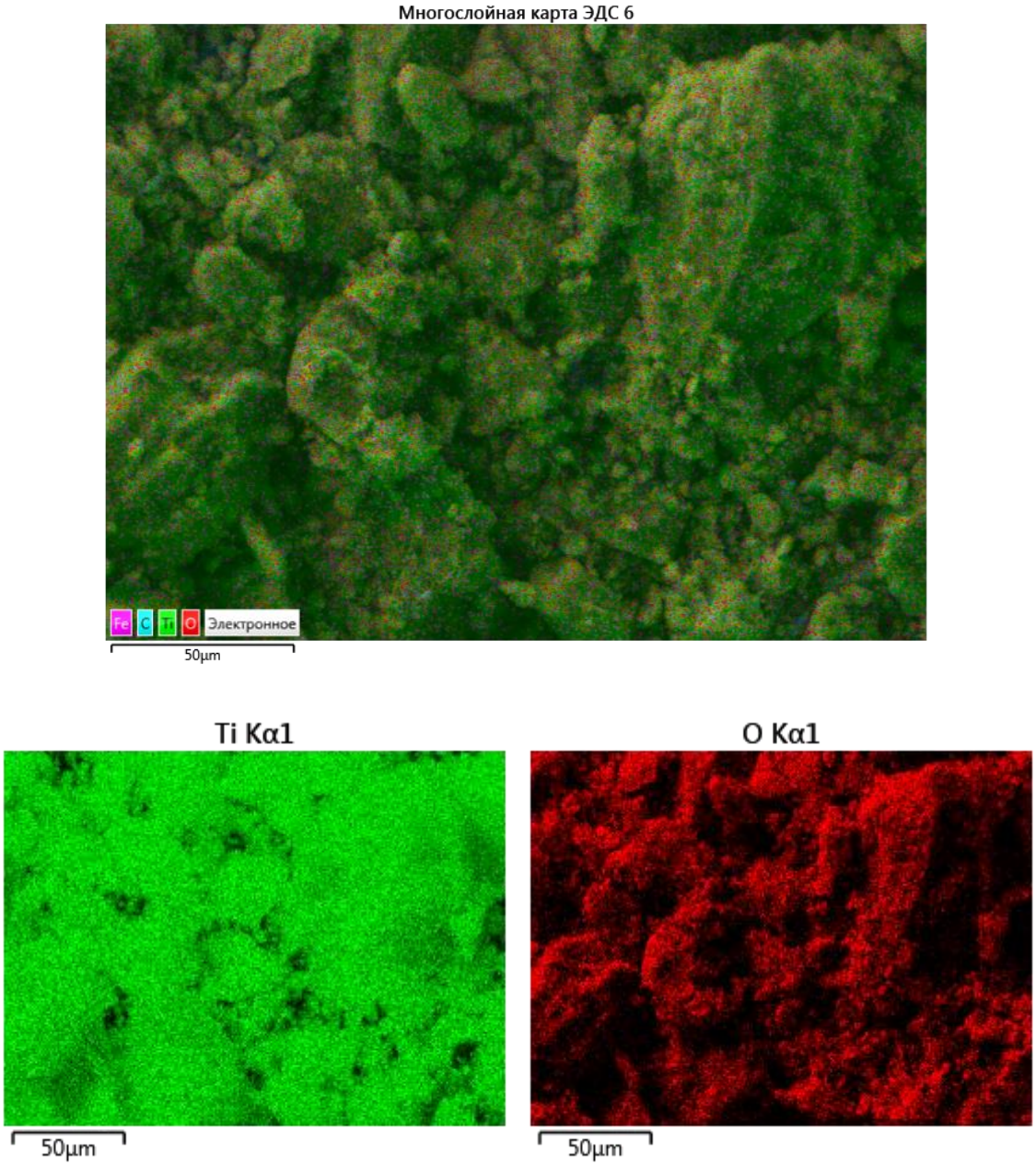

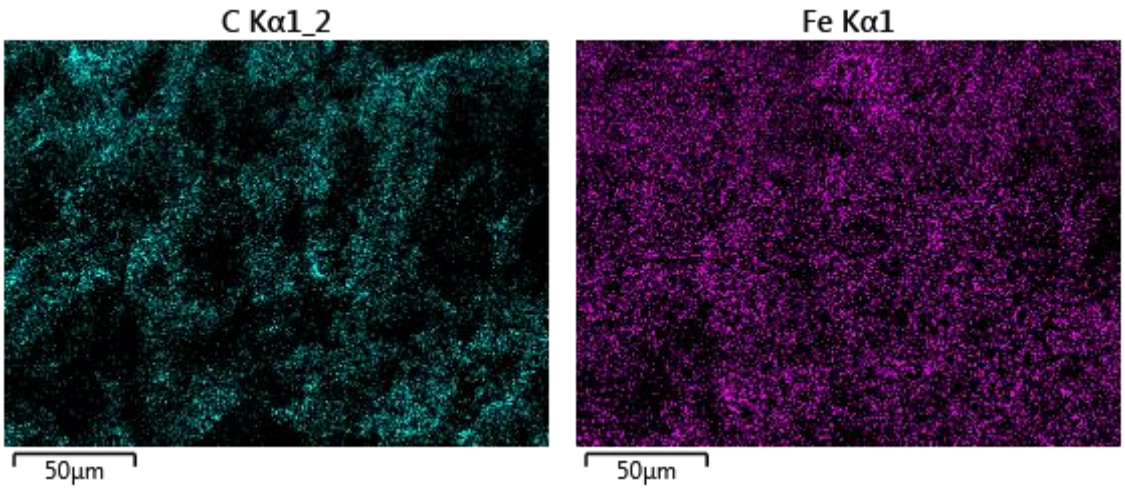
C Kα1_2
Fe Kα1
50µm
50µm

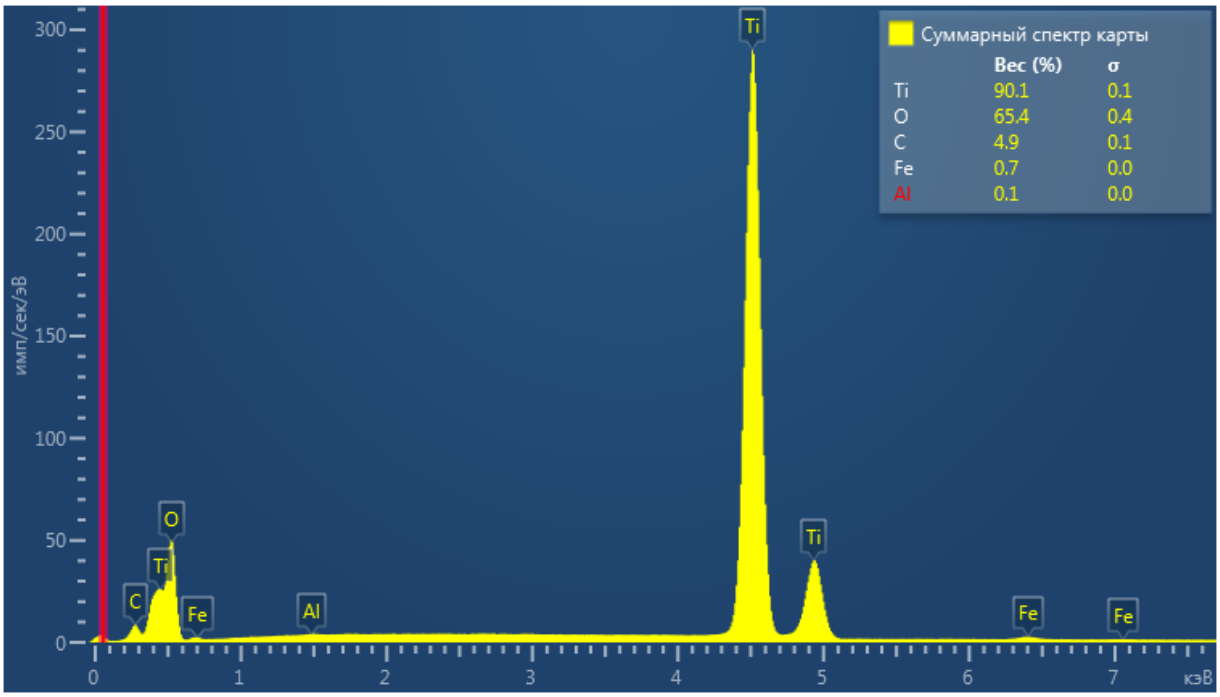
Суммарный спектр карты
Вес (%) σ
Ti 90.1 0.1
O 65.4 0.4
C 4.9 0.1
Fe 0.7 0.0
Al 0.1 0.0
имп/сек/эВ
кэВ
Ti
O
Ti
C
Fe
Al
Ti
Fe
Fe

Figure B.9: EDS mapping of SEM analysis of used Fe-TiO_2 (1%) after UV/H_2O_2/Fe-TiO_2 (1%)

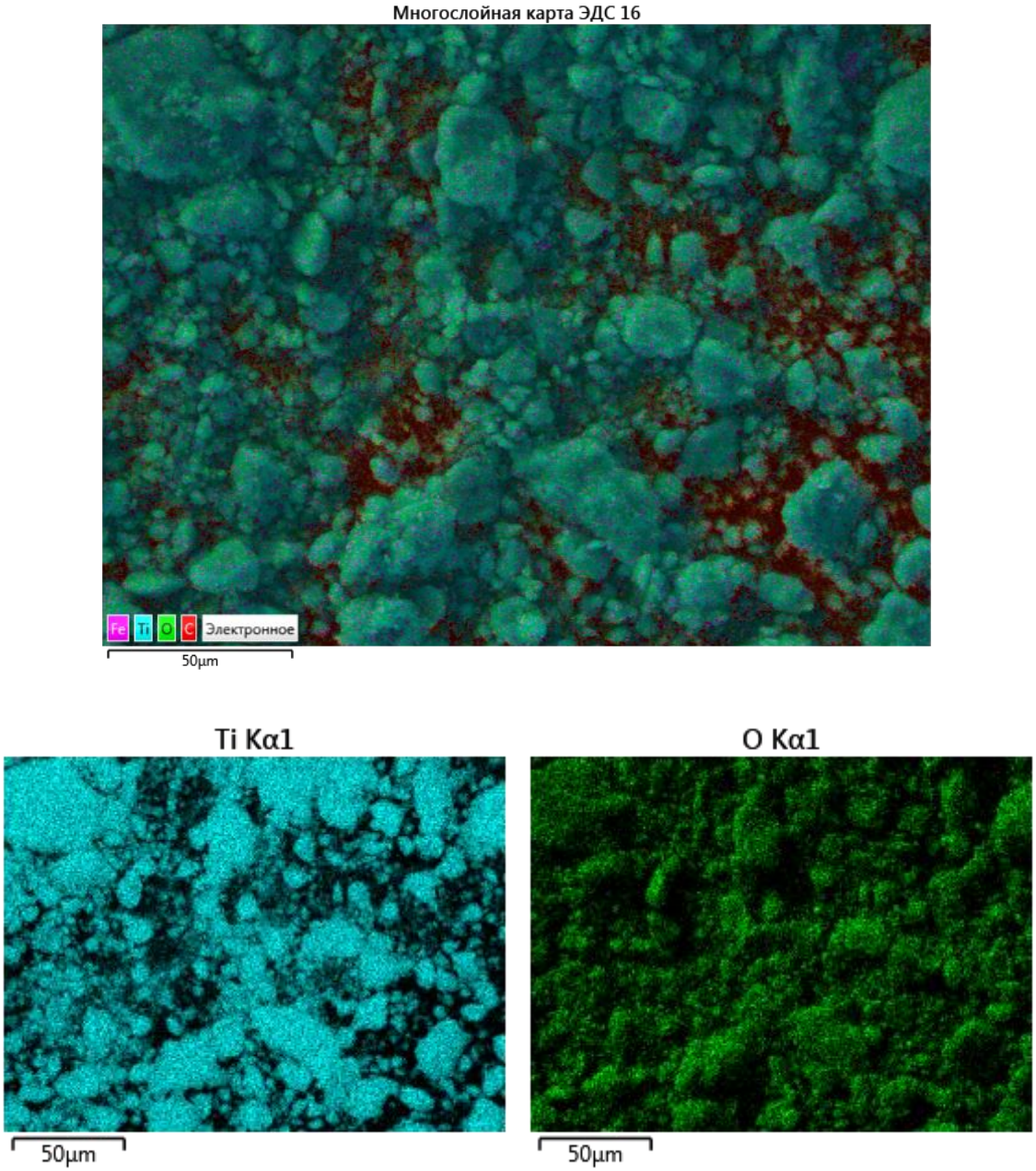

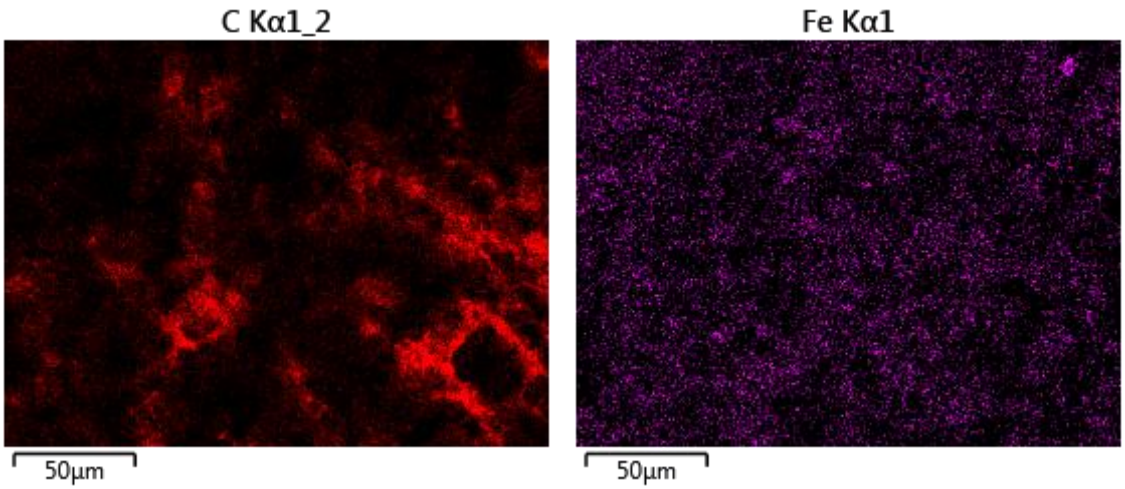
C Kα1_2
Fe Kα1
50µm
50µm

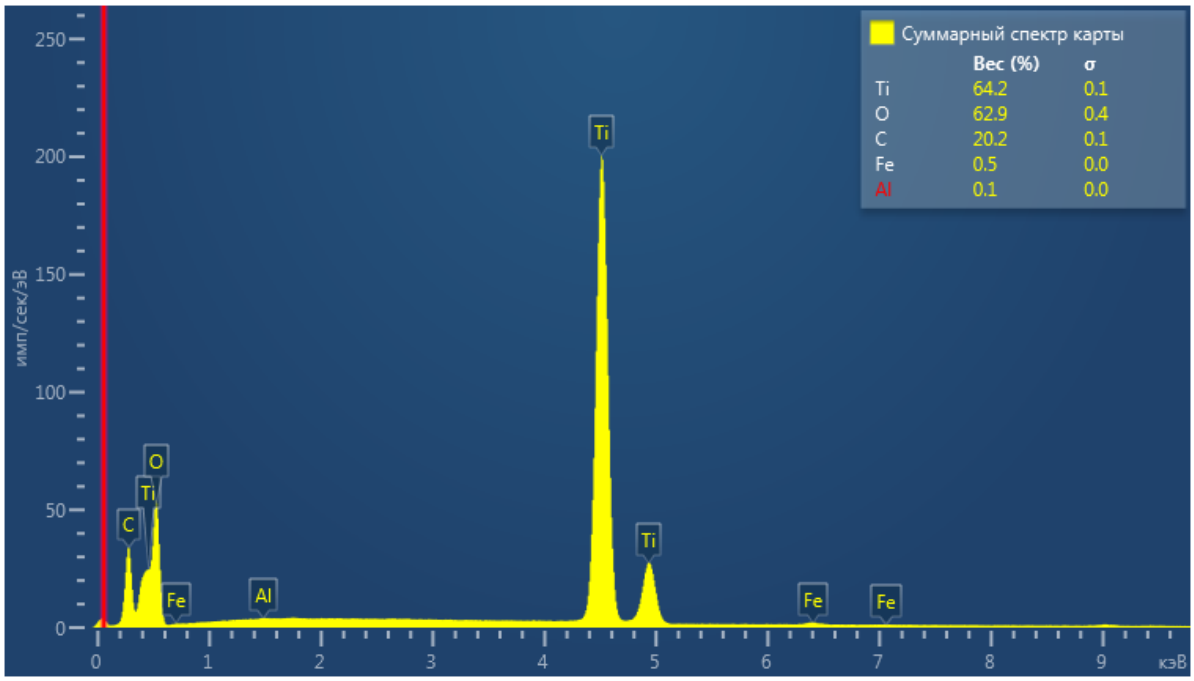
Суммарный спектр карты
Вес (%) σ
Ti 64.2 0.1
O 62.9 0.4
C 20.2 0.1
Fe 0.5 0.0
Al 0.1 0.0
имп/сек/эВ
кэВ
C
O
Ti
Fe
Al
Ti
Ti
Fe
Fe

Figure B.10: EDS mapping of SEM analysis of fresh Fe-TiO_2 (2%)

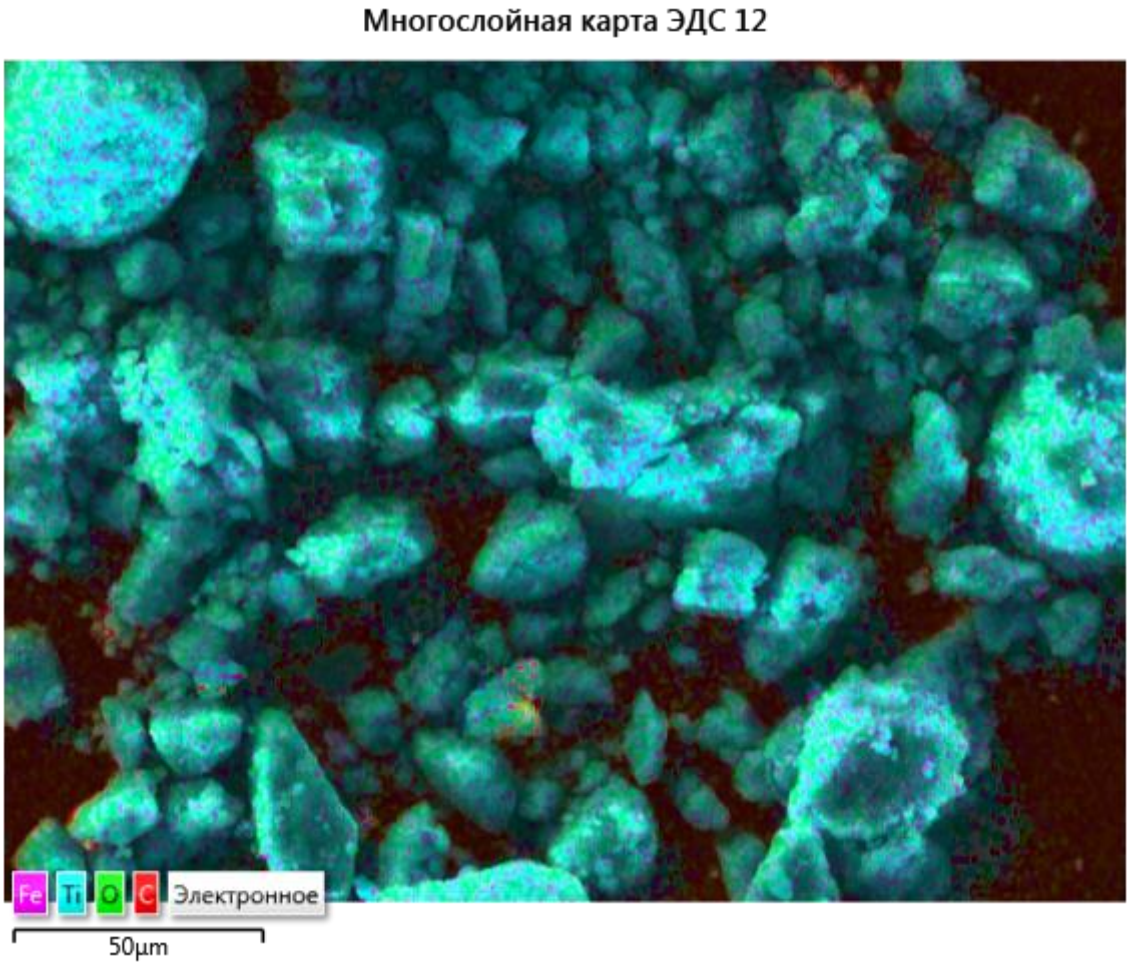

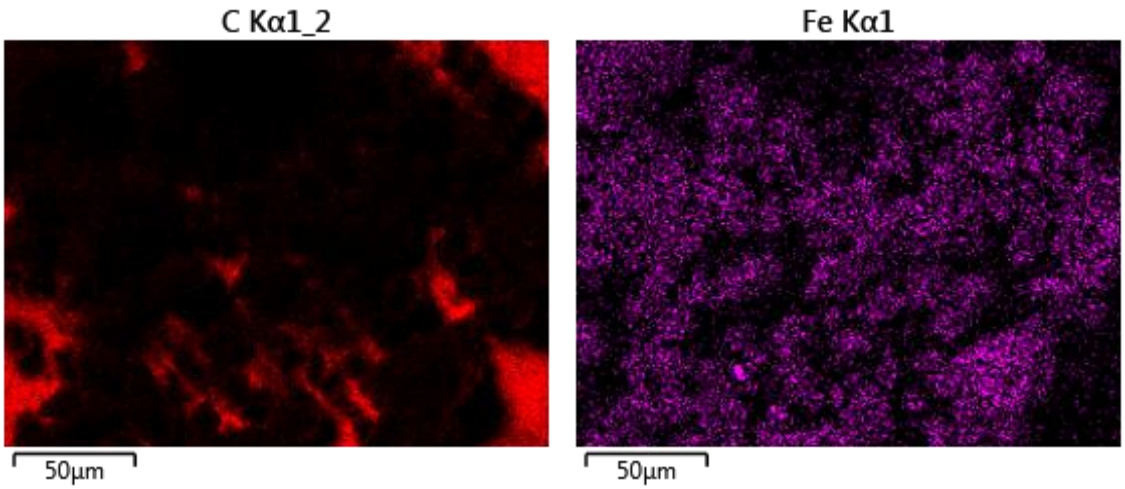
C Kα1_2
Fe Kα1
50µm
50µm

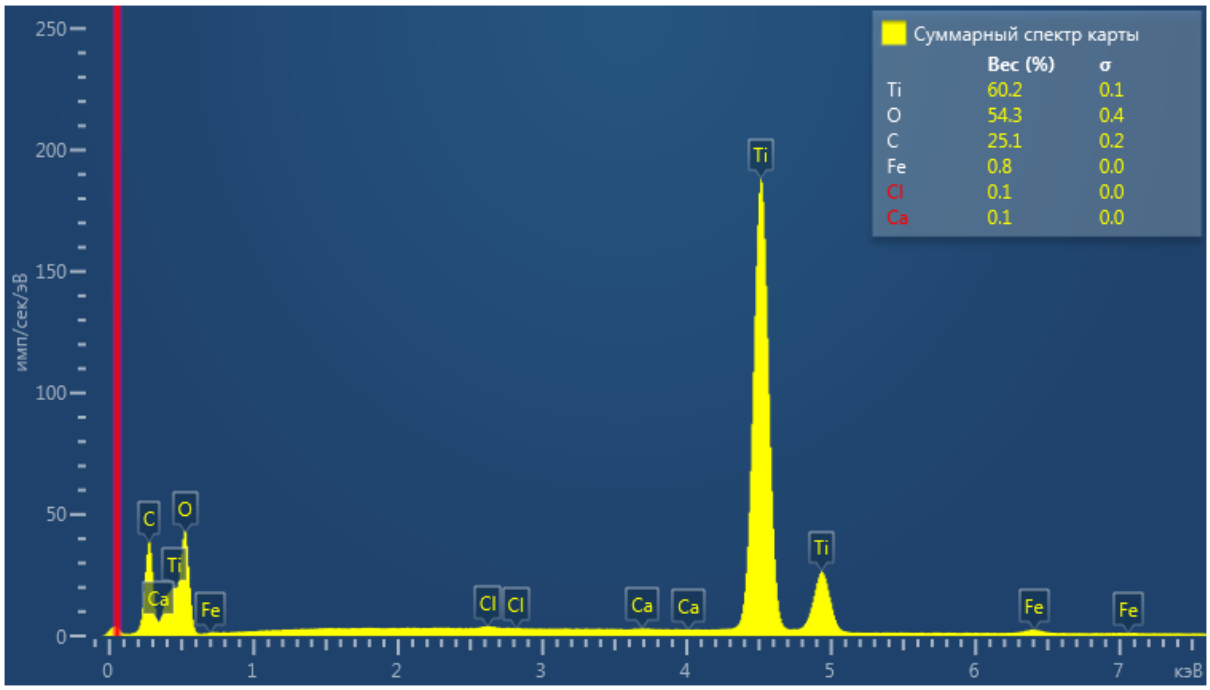
Суммарный спектр карты
Вес (%) σ
Ti 60.2 0.1
O 54.3 0.4
C 25.1 0.2
Fe 0.8 0.0
Cl 0.1 0.0
Ca 0.1 0.0
имп/сек/эВ
кэВ
C
O
Ti
Ca
Fe
Cl
Cl
Ca
Ca
Ti
Ti
Fe
Fe

Figure B.11: EDS mapping of SEM analysis of used Fe-TiO_2 (2%) after UV/Fe-TiO_2 (2%)

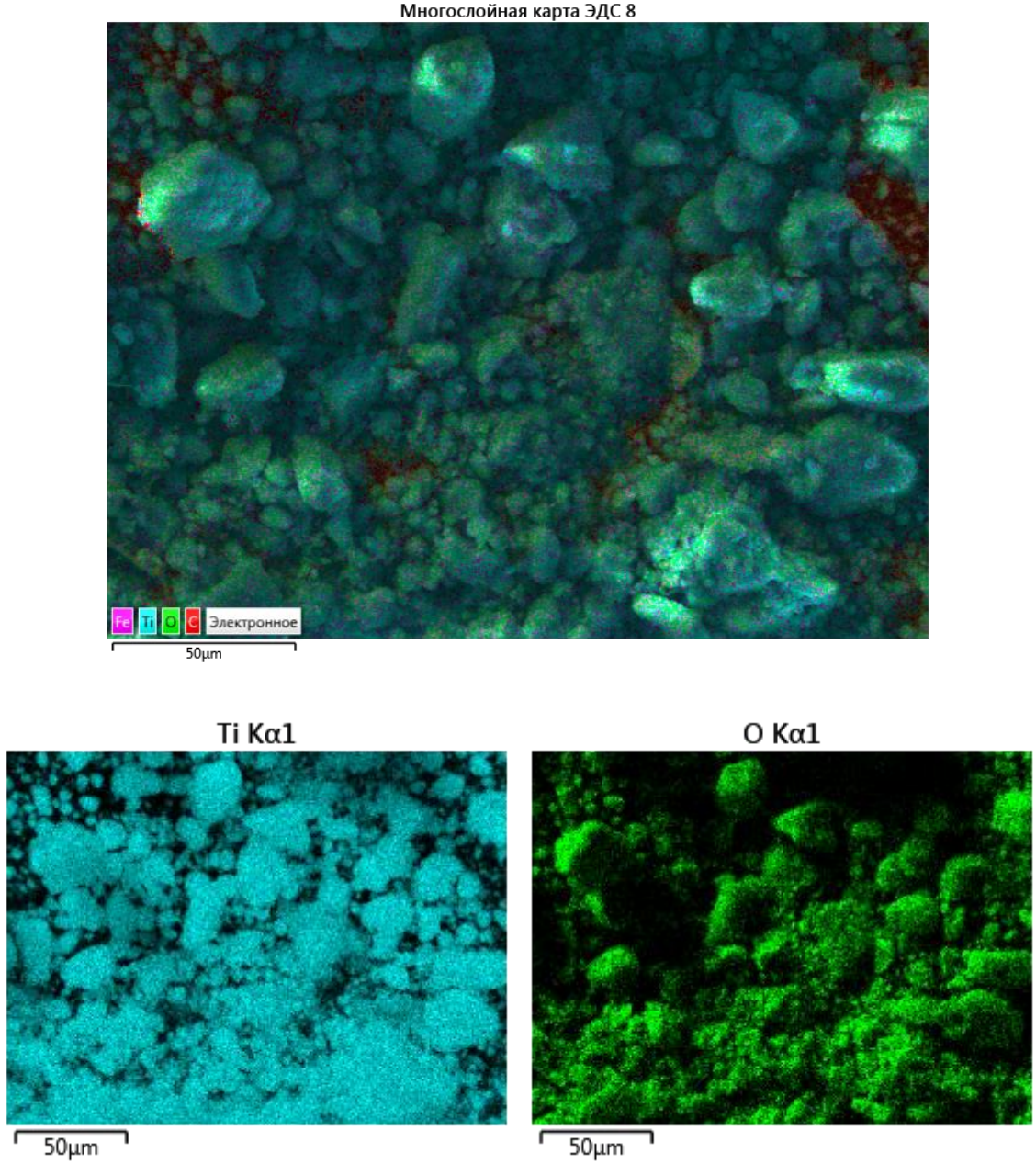

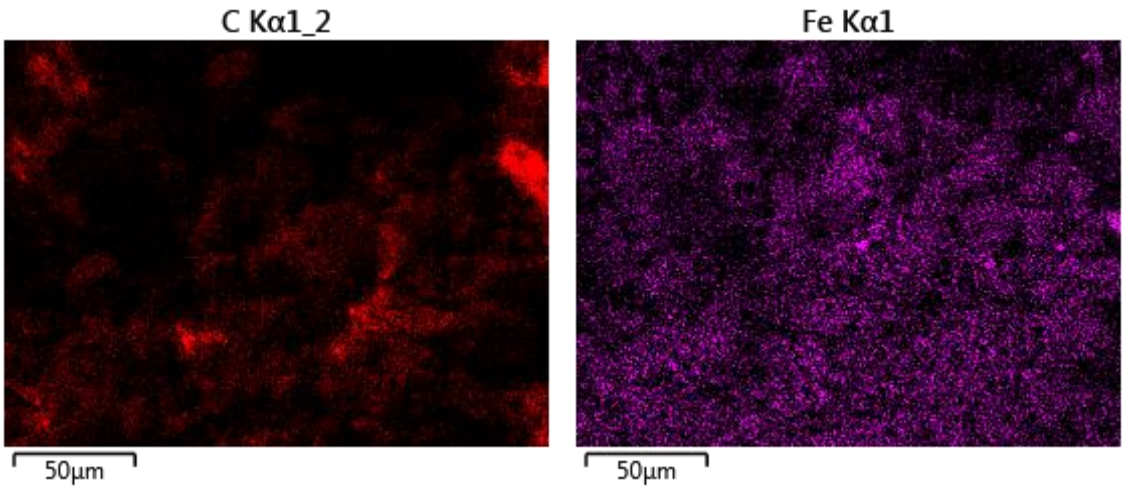
C Kα1_2
Fe Kα1
50µm
50µm

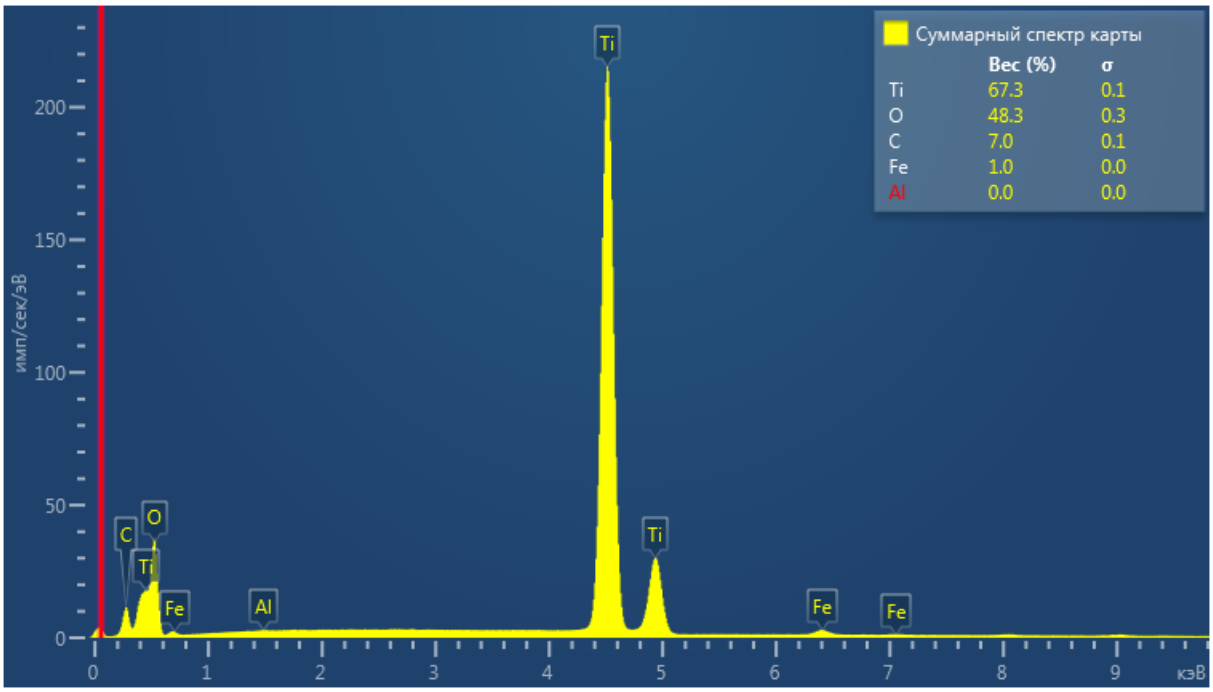
Суммарный спектр карты
Вес (%) σ
Ti 67.3 0.1
O 48.3 0.3
C 7.0 0.1
Fe 1.0 0.0
Al 0.0 0.0
имп/сек/эВ
кэВ
C
O
Ti
Fe
Al
Ti
Ti
Fe
Fe

Figure B.12: EDS mapping of SEM analysis of used Fe-TiO_2 (2%) after UV/H_2O_2/Fe-TiO_2 (2%)

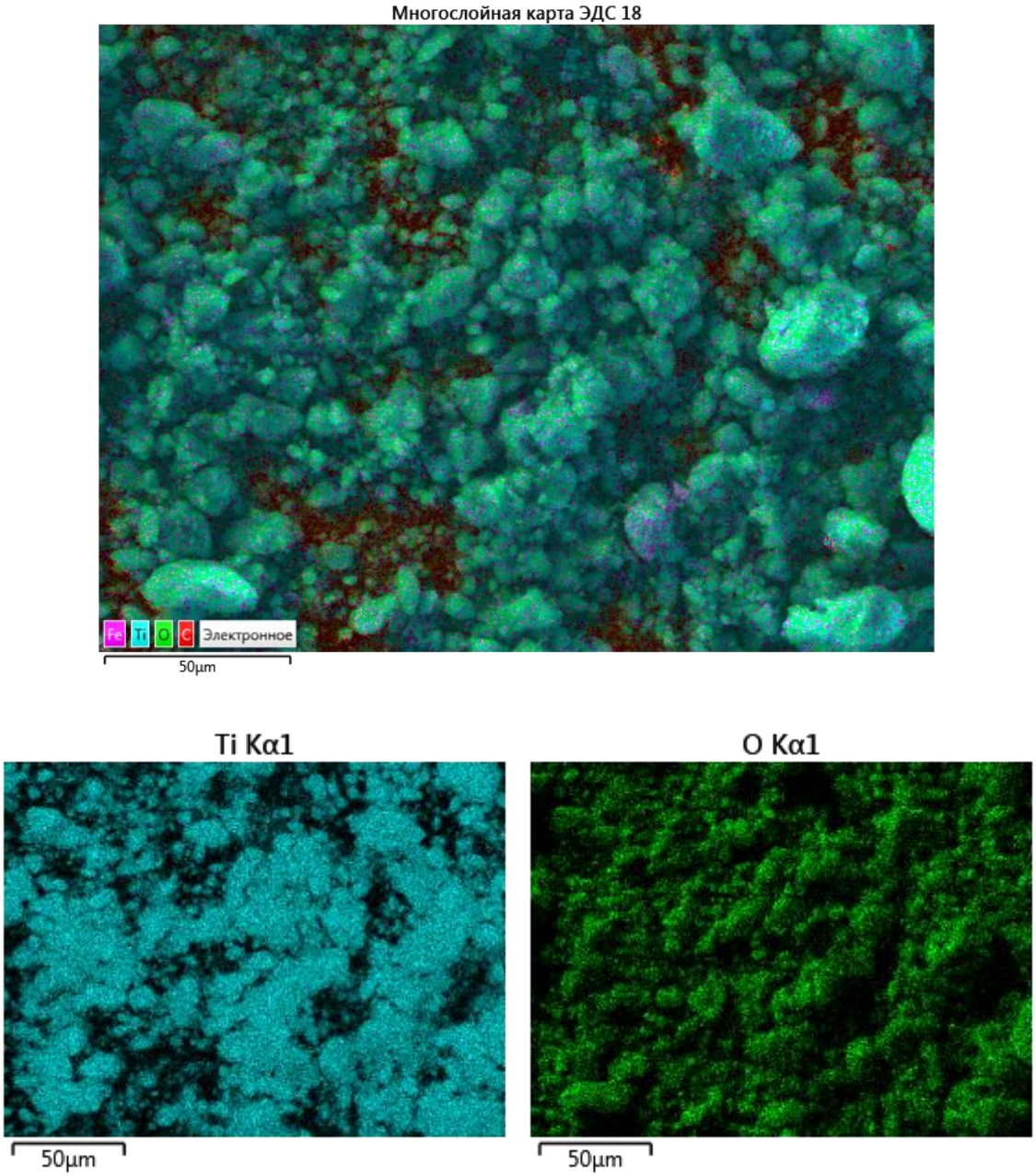

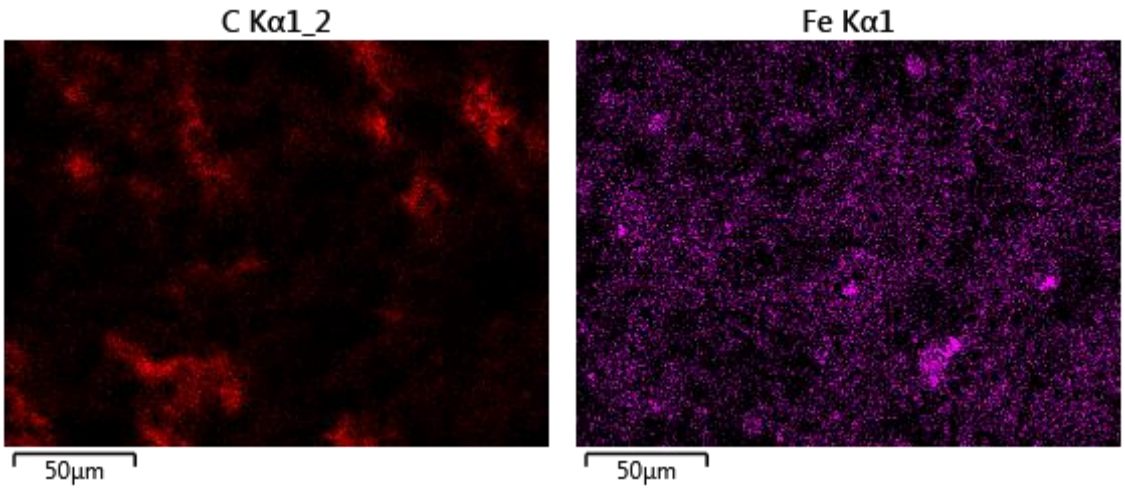
C Kα1_2
Fe Kα1
50µm
50µm

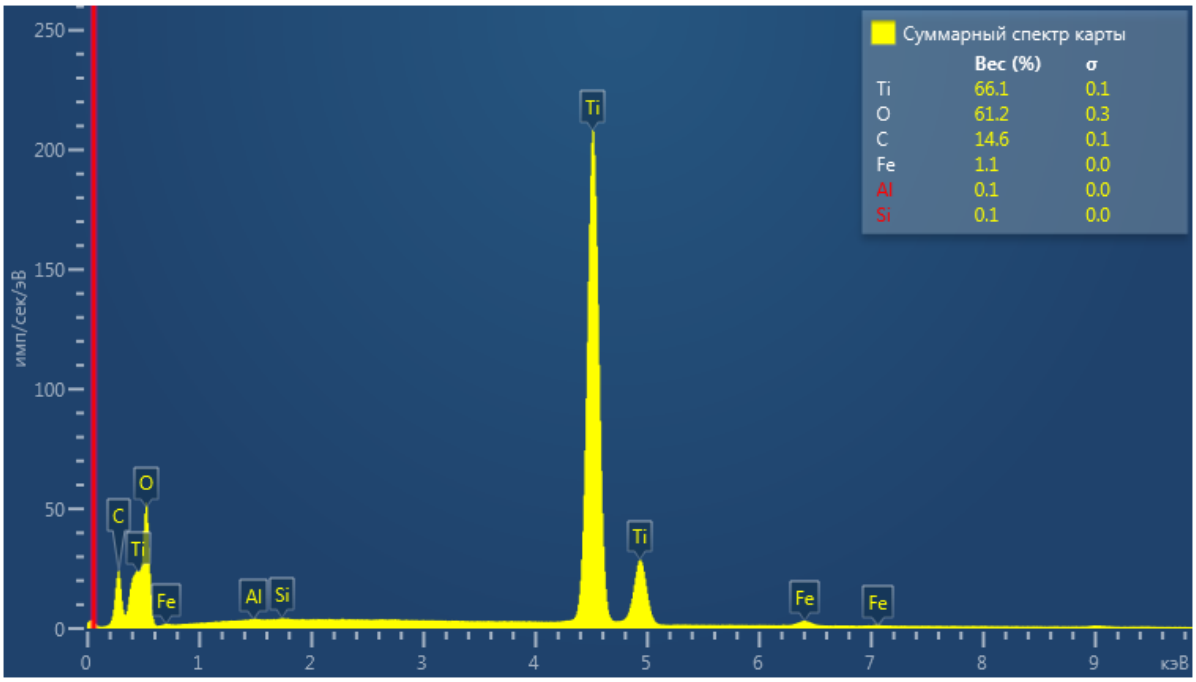
Суммарный спектр карты
Вес (%) σ
Ti 66.1 0.1
O 61.2 0.3
C 14.6 0.1
Fe 1.1 0.0
Al 0.1 0.0
Si 0.1 0.0
имп/сек/эВ
кэВ
Ti
O
C
Ti
Fe
Al
Si
Ti
Fe
Fe

Figure B.13: EDS mapping of SEM analysis of fresh Fe-TiO_2 (4%)

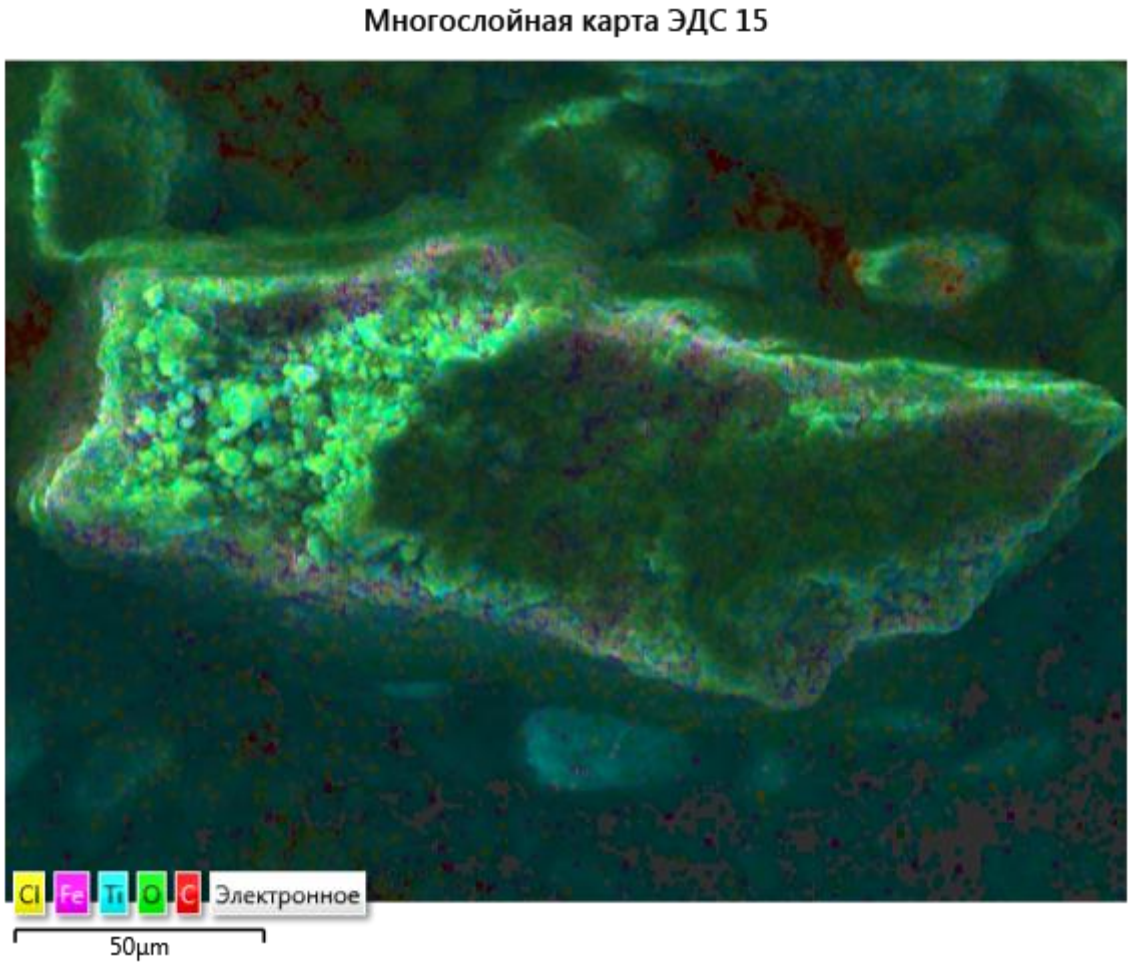

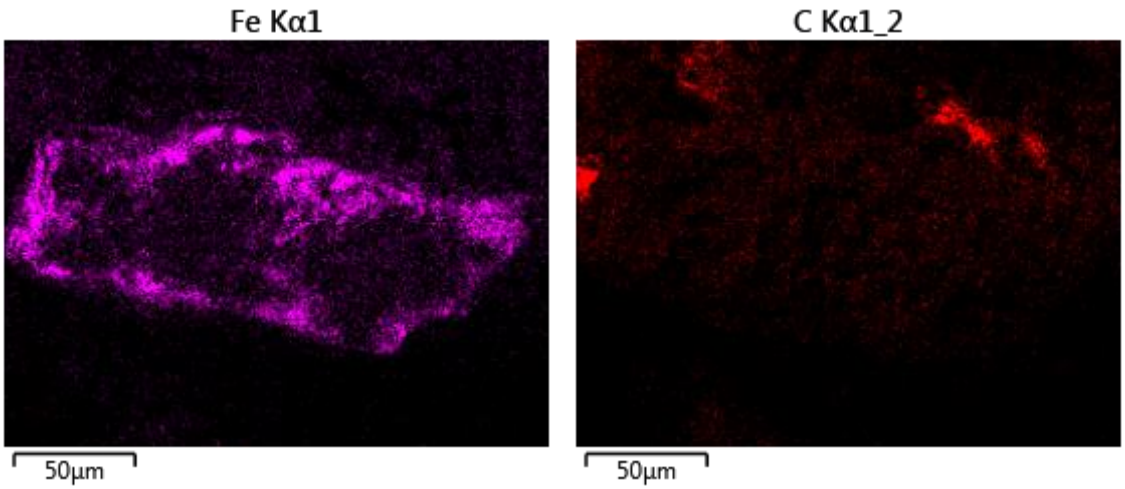
Fe Kα1
C Kα1_2
50µm
50µm

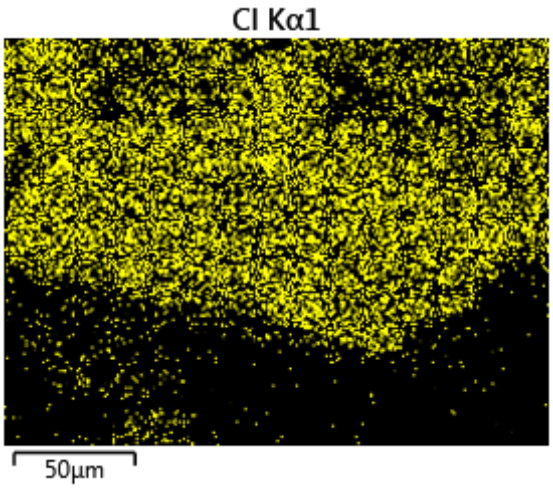
Cl Kα1
50µm

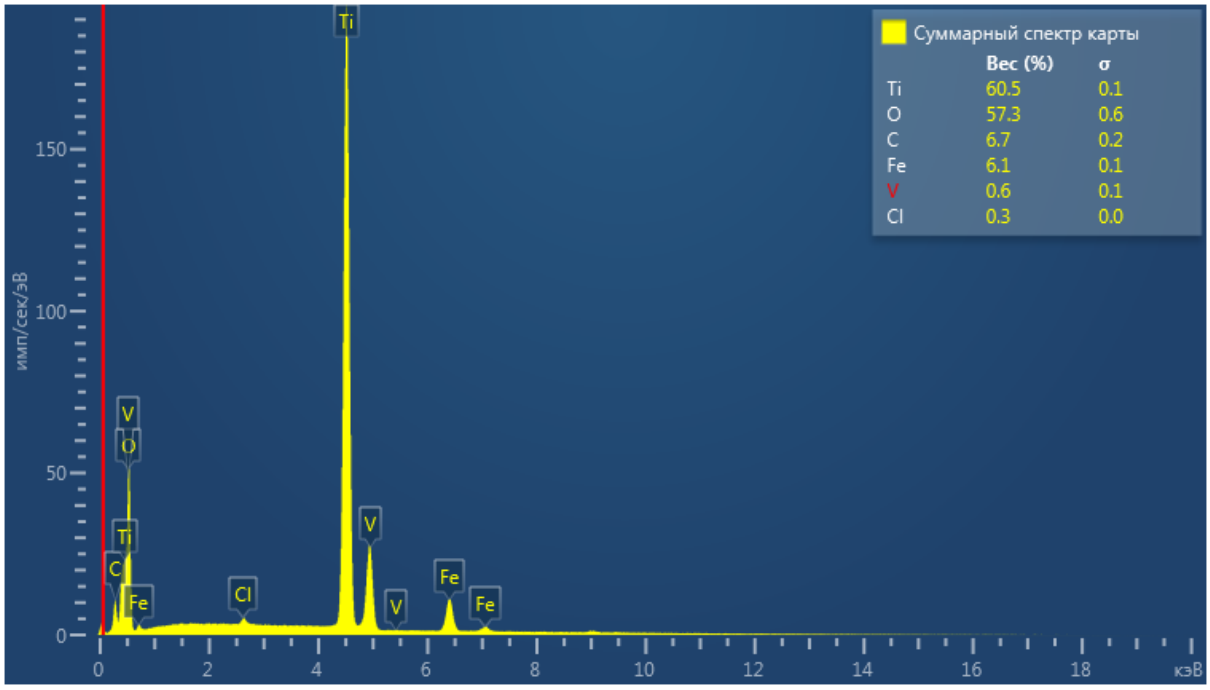
Суммарный спектр карты
Вес (%) σ
Ti 60.5 0.1
O 57.3 0.6
C 6.7 0.2
Fe 6.1 0.1
V 0.6 0.1
Cl 0.3 0.0
имп/сек/эВ
кэВ
Ti
V
O
Ti
C
Fe
Cl
V
V
Fe
Fe

Figure B.14: EDS mapping of SEM analysis of used Fe-TiO_2 (4%) after UV/Fe-TiO_2 (4%)

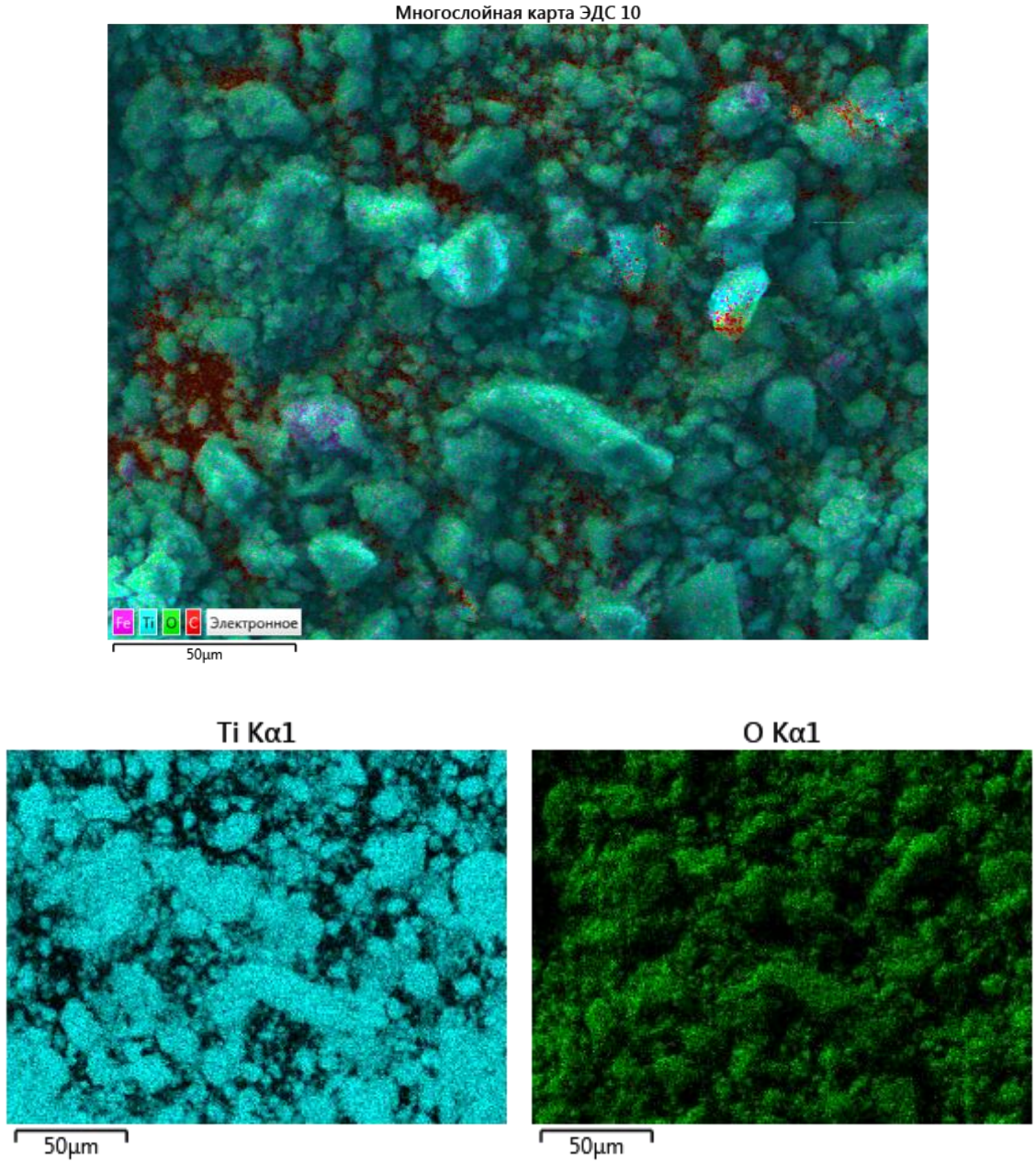

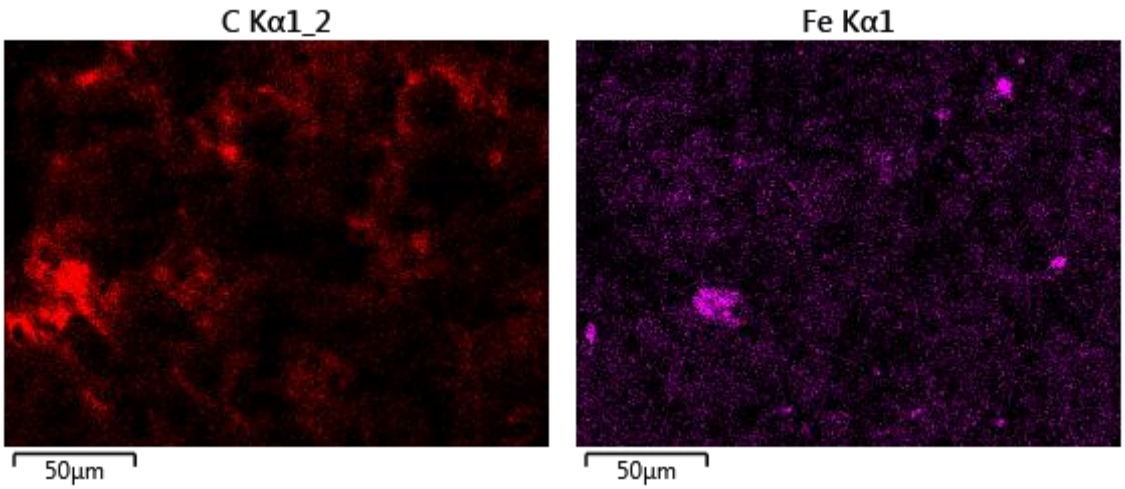
C Kα1_2
Fe Kα1
50µm
50µm

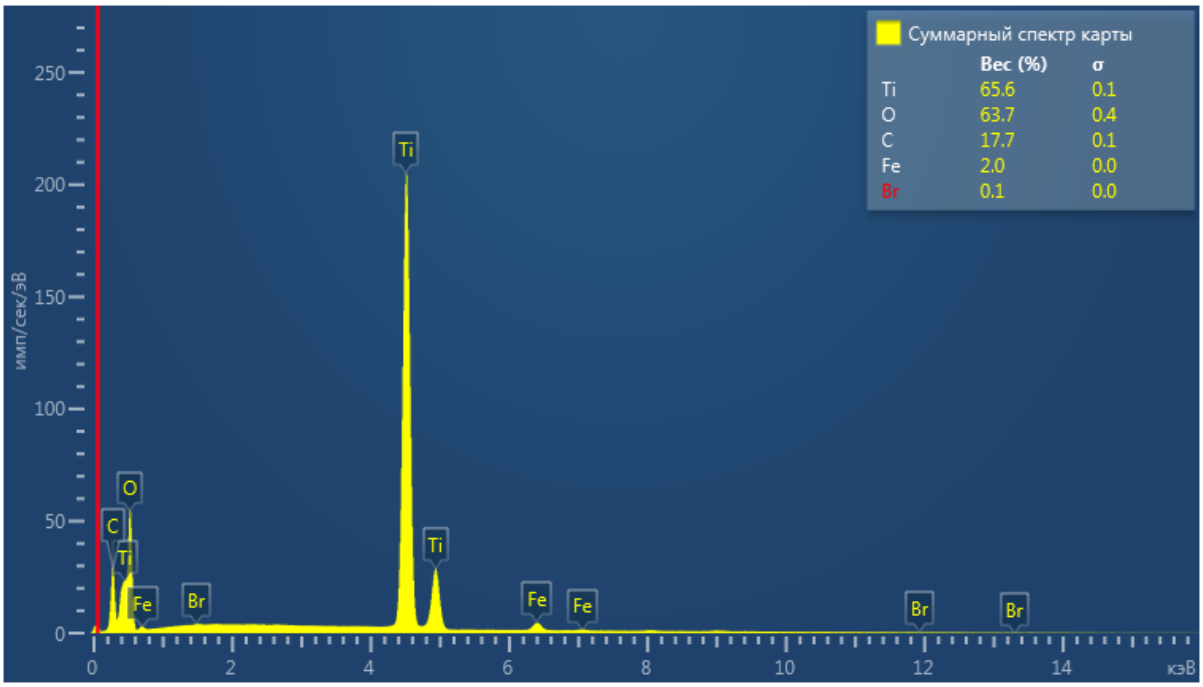
Суммарный спектр карты
Вес (%) σ
Ti 65.6 0.1
O 63.7 0.4
C 17.7 0.1
Fe 2.0 0.0
Br 0.1 0.0
имп/сек/эВ
кэВ
O
C
Ti
Fe
Br
Ti
Ti
Fe
Fe
Br
Br

Figure B.15: EDS mapping of SEM analysis of used Fe-TiO_2 (4%) after UV/H_2O_2/Fe-TiO_2 (4%)

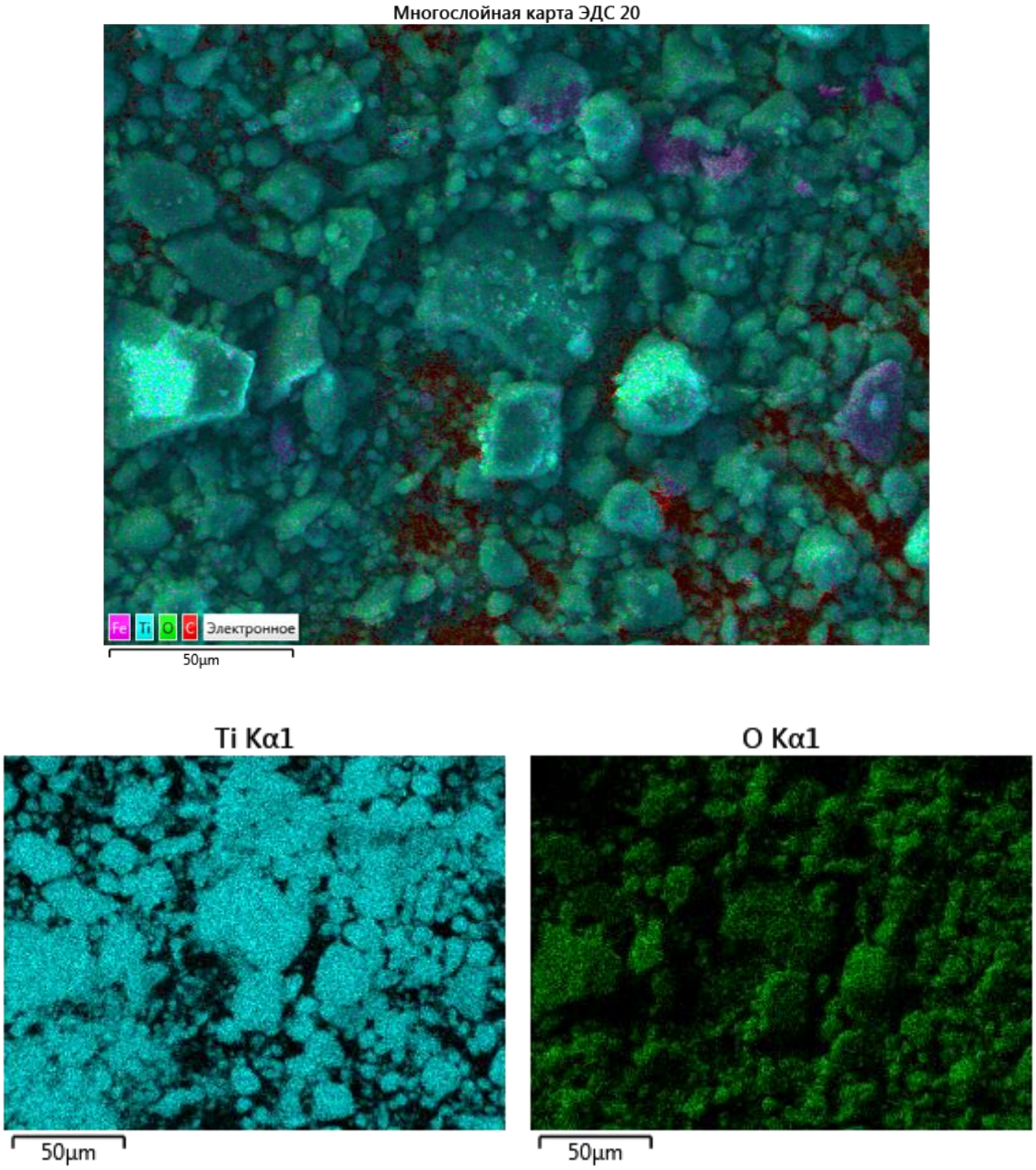

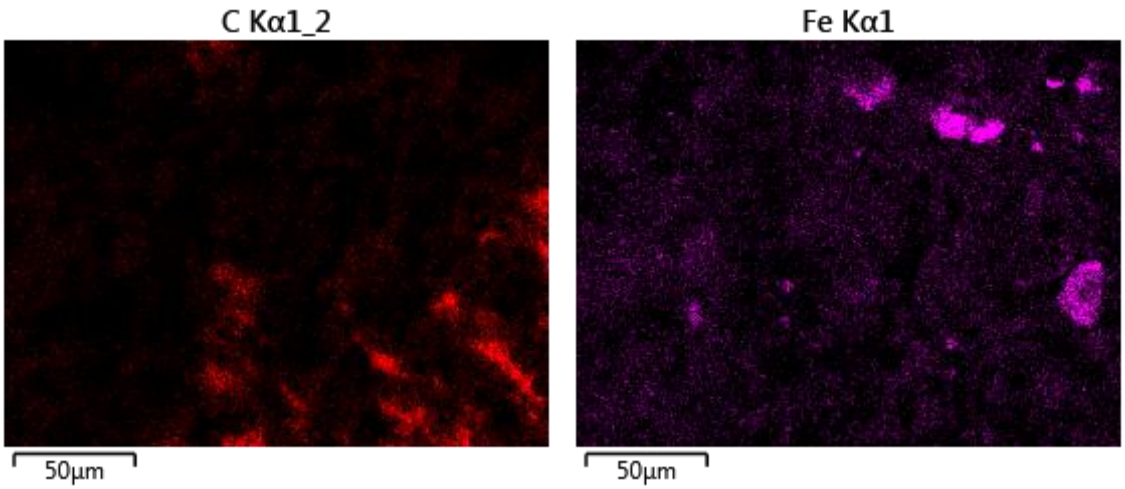
C Kα1_2
Fe Kα1
50µm
50µm

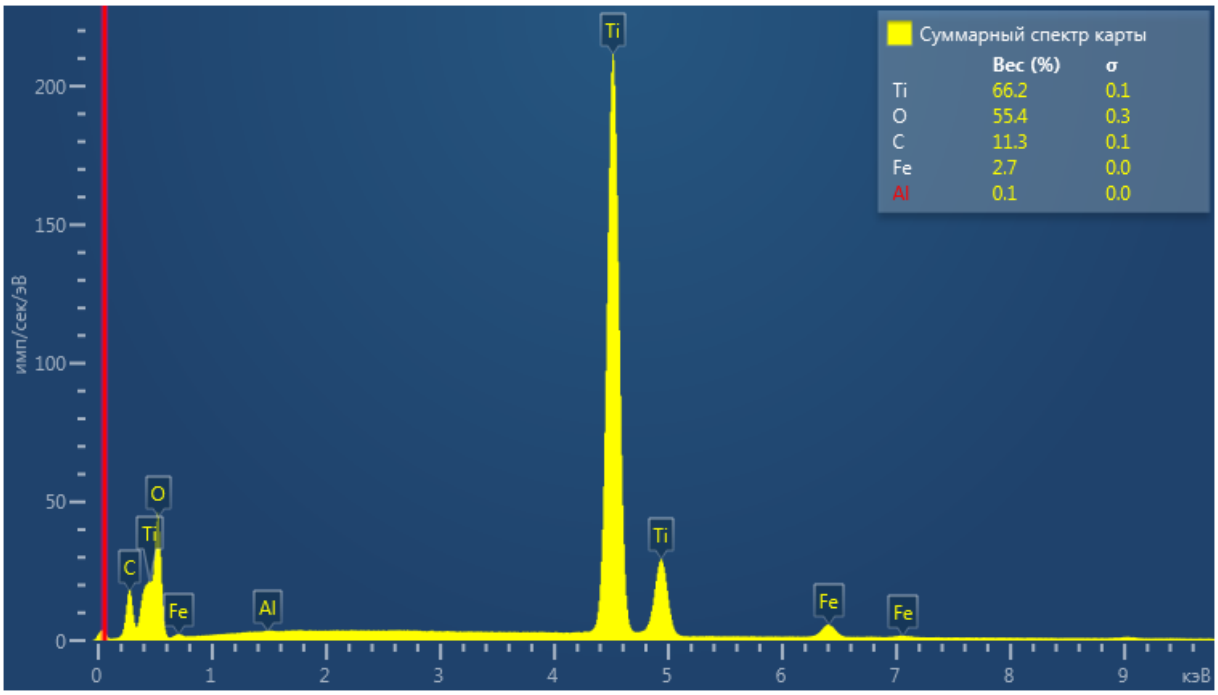
Суммарный спектр карты
Вес (%) σ
Ti 66.2 0.1
O 55.4 0.3
C 11.3 0.1
Fe 2.7 0.0
Al 0.1 0.0
имп/сек/эВ
кэВ
Ti
O
Ti
C
Fe
Al
Ti
Fe
Fe